Microcontrolled injectable stimulators based on electronic rectification of high frequency current bursts

Laura Becerra Fajardo

TESI DOCTORAL UPF / 2016

Director: Dr. Antoni Ivorra Cano

Department of Information and Communication Technologies
Universitat Pompeu Fabra

This work was carried out in the Department of Information and Communication Technologies (DTIC) at Universitat Pompeu Fabra (UPF), Barcelona, Spain. This work was supported by a fellowship from the DTIC - UPF.

Abstract

Neuroprostheses based on dense networks of wireless microstimulators have been proposed in the past for restoring movement in paralysis patients. Yet existing implantable microstimulators are too bulky and invasive for implementing such networks because of the powering approaches they employ.

To overcome this limitation, it was recently proposed an innovative electrical stimulation method incorporating electronic implants. The method consist in delivering, by means of superficial textile electrodes, high frequency current bursts which innocuously flow through tissues by galvanic coupling and which are rectified by the implants, thereby transforming these bursts into low frequency currents capable of performing local stimulation. Since the implants lack bulky components for powering, such as coils and batteries, the method will enable miniaturization levels without precedents for microstimulators.

The method was first demonstrated with very simple implants that could not be controlled externally, impeding independent stimulation of different target muscles. This thesis demonstrates that the method allows the development of digitally addressable microstimulators. In particular, this thesis describes the development, characterization and *in vivo* assay of addressable stimulators made of off-the-shelf electronic components. The developed microcontrolled and wireless stimulators are semi-rigid and can be easily implanted by injection thanks to their elongated shape (2 mm thick and almost 49 mm long). They perform charge-balanced neuromuscular stimulation in response to commands modulated in high frequency current bursts which meet safety standards. This thesis paves the way to future ultrathin stimulators based on a custom integrated circuit.

Resumen

En el pasado se propusieron neuroprótesis basadas en densas redes de microestimuladores inalámbricos para restablecer el movimiento en pacientes con parálisis. Aún así, los microestimuladores implantables existentes en la actualidad son demasiado voluminosos e invasivos como para implementar dichas redes debido a los métodos de alimentación eléctrica que utilizan.

Para superar esta limitación, recientemente se propuso un método de estimulación eléctrica innovador que incorpora implantes electrónicos. El método consiste en aplicar mediante electrodos textiles superficiales, corrientes de alta frecuencia que fluyen inofensivamente por los tejidos por medio de acople galvánico, y que son rectificadas por los implantes. De esta forma las ráfagas se transforman en corrientes de baja frecuencia que pueden estimular localmente. Debido a que los implantes no contienen componentes voluminosos como bobinas y baterías para alimentarse eléctricamente, el método permitirá niveles de miniaturización sin precedentes para microestimuladores.

El método fue demostrado por primera vez con implantes muy simples que no podían ser controlados externamente, impidiendo la estimulación independiente de diferentes músculos objetivo. Esta tesis demuestra que el método permite el desarrollo de microestimuladores direccionables digitalmente. En particular, esta tesis describe el desarrollo, caracterización y ensayos *in vivo* de estimuladores direccionables basados en componentes electrónicos comerciales. Los estimuladores inalámbricos desarrollados son semirrígidos y pueden ser fácilmente implantados por medio de inyección gracias a su forma alargada (2 mm de diámetro y casi 49 mm de largo). Los dispositivos realizan estimulación neuromuscular con balance de carga en respuesta a comandos modulados en las ráfagas de corriente de alta frecuencia. Dichas ráfagas de corriente cumplen con estándares de seguridad. Esta tesis abre el camino hacia futuros estimuladores ultrafinos basados en circuitos integrados diseñados para este propósito.

Contents

List of Figures

List of Tables

Abbreviations and symbols

A: Amplitude
σ: Conductivity
Ø: Diameter
F: Frequency of stimulation
ε_r: Relative permittivity
ρ: Tissue density
ac: Alternating current
AP: Action potential
ASIC: Application-specific integrated circuit
ASK: Amplitude-shift keying
BION: BIOnic Neurons
BGA: Ball grid array
Ca^{2+}: Calcium ion
Cl^-: Chloride ion
CNS: Central nervous system
CS: Control signal
CU: Control unit
DAQ: Data acquisition
dc: Direct current
DTIC: Department of Information and Communication Technologies
EMG: Electromyography
FDA: Food and Drug Administration
FEM: Finite element method
FES: Functional electrical stimulation
GA: Gastrocnemius muscle
HF: High frequency
IBC: Intrabody communication
IC: Integrated circuit
ICNIRP: International Commission on Non-Ionizing Radiation Protection
IEEE: Institute of Electrical and Electronics Engineers
I_r: Rheobase current
K^+: Potassium ion
LF: Low frequency
LPF: Low-pass filter
Na^+: Sodium ion
NaCl: Sodium chloride
NIH: National Institutes of Health
PCB: Printed circuit board
PD: Pulse duration
RF: Radiofrequency
RMS: Root mean square
SAR: Specific absorption rate

SAT: Subcutaneous adipose tissue
SCI: Spinal cord injury
SPICE: Simulation program with integrated circuit emphasis
TA: Tibialis anterior muscle
T_c: Chronaxie
UPF: Universitat Pompeu Fabra

Al abuelo

CHAPTER 1

Introduction

Part of the contents of this chapter is adapted from the following publication:

L. Becerra-Fajardo and A. Ivorra, “In Vivo Demonstration of Addressable Microstimulators Powered by Rectification of Epidermically Applied Currents for Miniaturized Neuroprostheses,” PLoS One, vol. 10, no. 7, p. e0131666, Jul. 2015.

1.1. Paralysis

Paralysis is a medical disorder characterized by the impossibility or difficulty to perform muscle functions. It can result in loss or difficulty to move the upper and/or lower extremity, and to control basic body functions such as urinating or coughing. Among other reasons, it can be acquired with different medical conditions or injuries that disrupt the flow of nervous impulses, including spinal cord injury (SCI), stroke, multiple sclerosis and cerebral palsy. By 2015 it was estimated that every year 795,000 people suffer stroke in the United States, which makes it the leading cause of disability in the country [1]. Additionally, it has been estimated that every year between 250,000 and 500,000 people suffer SCI worldwide [2].

Several options for paralysis patients have been clinically explored, including physical therapy, assistive technologies (e.g. orthotics, wheelchairs), restorative therapies such as body weight supported treadmill training, and surgical interventions (e.g. nerve and tendon transfers [3], [4]) [5]. Even though these options provide a degree of functional gain, the patient remains with important functional loss that limits independence.

For several years it has been proposed to bypass the disrupted nervous path to restore function by using electrical stimulation. This technique artificially triggers nervous impulses in the nerves. The nervous impulses are known as action potentials (APs) and correspond to rapid changes in the membrane potential that propagate through the nerve fiber membrane.

Electrical stimulation has been extensively used to restore lost sensory functions. For example, cochlear implants that stimulate the auditory nerves are an important success case in electrical stimulation [6]. According to the National Institute of Health of United States (NIH), in 2010 it was estimated that 188,000 people worldwide had a cochlear implant, and only in the United States more than 41,000 adults had one [7]. As described by the NIH, cochlear implants are “one of the more groundbreaking biomedical achievements in the last thirty years”. Recently, retinal prostheses have been successfully evaluated [8]. One example is the Argus II, a device designed for patients with photoreceptors dysfunction caused by retinitis pigmentosa, and approved by the Food and Drug Administration (FDA) [9] [10]. This degree of success for sensory prostheses based on electrical stimulation is not met in the case of motor prostheses based also on electrical stimulation.

1.2. Functional electrical stimulation

The term Functional Electrical Stimulation (FES) is used to define a set of techniques that elicit APs to restore function in neurologically impaired individuals. These artificially triggered APs received by the muscle fibers are virtually the same as those generated naturally by the nervous

system [11]. The devices that perform FES are known as neuroprostheses [12]. There are two types of FES systems: sensory FES (e.g. cochlear implants, retinal prostheses) and motor FES [12]. However, most researchers only refer to FES in the context of neuromuscular electrical stimulation.

Nowadays, there are few electrical stimulation systems for paralysis patients. These include devices that control bladder function [13], implantable stimulators for foot drop [14], and phrenic pacing systems for respiratory function [15], [16]. Electrical stimulation systems for standing and transfers have been clinically tested [5]. However, in spite of several research efforts, it has not been possible to design practical stimulators to restore complex movement such as gait.

The reason systems for gait restoration have not been successful is attributed to the lack of selectivity in current stimulation technologies. That is, existing systems are not able to activate a chosen set of nerve cells without activating the nerve cells nearby [17]. In this sense, neuroprostheses cannot activate specific muscles that perform a controlled movement, promoting fatigue: a condition in which the force exerted by muscle fibers decreases. Developed FES systems for gait restoration require more energy expenditure than natural gate [18].

In essence, electrical stimulation systems consist of two types of components: a pulse generator and a set of electrodes (active and return electrodes). FES systems can be coarsely classified into three categories according to the location of these components: surface, percutaneous and implanted (Figure 1.1) [12]. In surface systems, the pulse generator is external and the electrodes are attached to the patient's skin. This configuration offers the least level of invasiveness but has three major disadvantages: it lacks spatial selectivity, it causes activation of subcutaneous pain receptors and it is difficult to don and doff [12] [19]. Spatial selectivity is obtained in percutaneous systems [20]. In this configuration, electrodes anchored to excitable tissues are connected to the external generator using wires that pierce the skin. However, percutaneous systems are almost exclusively used for clinical diagnosis and research purposes because they cause infections and imply cosmetic issues.

Nowadays, when spatial selectivity is required, fully implantable systems are largely preferred over the two other configurations. In this case, both the pulse generator and the electrodes are implanted within the patient's body, avoiding risk of infections due to skin piercing.

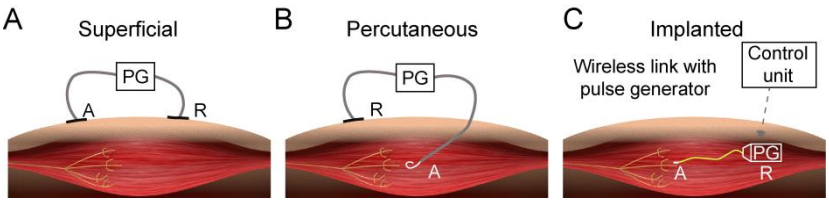

Figure 1.1. Configuration of FES systems. A pulse generator (PG) delivers monophasic or biphasic pulses to the motor nerve using a pair of electrodes. A is the active electrode and R is the return electrode. A) Both electrodes are attached to the skin. B) The active electrode is pierced through the skin and anchored to the target tissue. C) The electrodes and the pulse generator are deployed in tissues, accomplishing much better selectivity. An external control unit sends control signals, and in some cases power, to the PG wirelessly. Adapted from [21] [12].

The implantable configuration is the least disadvantageous option in many clinically relevant scenarios. However, implantable neuroprosthetic systems consisting of a central unit wired to stimulation electrodes require complex implantation surgeries. Additionally, the long leads that connect the stimulation electrodes to the central unit are prone to mechanical failure, to cause mechanical damage to tissues and to promote infections [22], [23]. As a consequence, since more leads imply more failure factors, implantable central units have less stimulation channels than desirable, limiting stimulation selectivity. Therefore, a constraint of centralized systems is that they are not suitable for managing a large number of stimulation points (i.e. channels) over large and mobile body parts. An obvious consequence is that the number of muscles that can be controlled is limited thus narrowing the range of movements.

1.3. Wireless networks of microstimulators

As an alternative to central stimulation units, in the 1990s it was proposed the development of addressable single-channel wireless microstimulators to be deployed by injection into the muscles to be stimulated [24]. These microstimulators were meant to form a dense network to be activated by an external automated controller so that fine movement restoration would be achievable.

According to that paradigm, the microstimulators would be deployed close to small peripheral nerves corresponding to a few motor units [23]. This would greatly improve selectivity because the microstimulator would not act on a whole muscle but over a few muscle fibers.

A motor unit consists of the somatic motor neuron and the muscle fibers that are innervated by the neuron’s terminals (Figure 1.2-B). The motor nerves essentially consist of bundles of motor neurons' axons, which are long (up to 1 m) projections of the neurons in which AP transmission occur. The point where the motor neuron’s axons (a long

projection of the nerve cell that conducts the APs) contacts the muscle fiber is called neuromuscular junction. In here, APs coming from the spinal cord (or which are artificially generated by electrical stimulation) trigger the secretion of acetylcholine, a neurotransmitter [25], [26]. This in turn starts an AP in the muscle membrane, and the subsequent starting attractive forces between myosin and actin protein filaments that generate a muscle contraction (Figure 1.2-A).

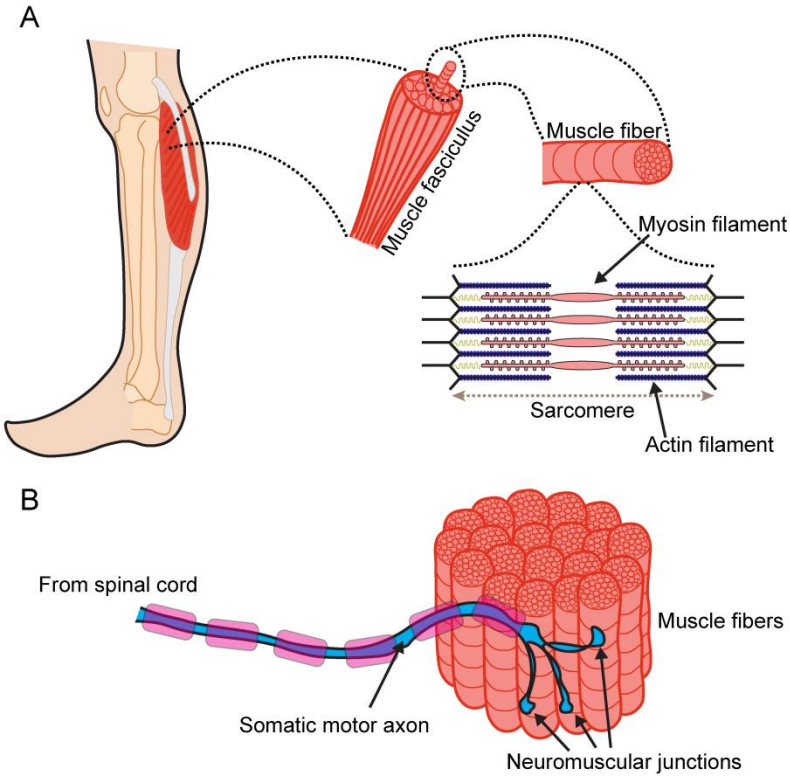

Figure 1.2. Organization of the skeletal muscle to perform muscle contraction. A) The muscle is composed of muscle fasciculus which are made up of muscle fibers. Each muscle fiber has myofibrils composed of actin and myosin protein filaments, which are responsible for contraction. B) Motor unit, composed of a motor neuron and the muscle fibers stimulated by that motor axon. To generate muscle contraction, the information travelling from the spinal cord through the somatic nervous system is transmitted to muscle fibers in the neuromuscular junction. Adapted from [21].

As mentioned above, the force exerted by muscle fibers decreases after prolonged and intense periods of muscular contraction. This condition, known as fatigue, is of primary concern in electrical stimulation. When muscle contraction occurs naturally, the organism tries

to minimize fatigue by activating first slow twitch fibers, which are fatigue-resistant and, only when strong muscle contraction is required, fast twitch fibers are activated. Yet, when muscular contraction is triggered with electrical stimulation, so-called inverse recruitment occurs: fast twitch muscle fibers, which are powerful but prone to fatigue, are somehow predominantly activated by electrical stimulation over the slow twitch muscle fibers which, although less powerful, can work for long periods of time because they sustain aerobic activity. This causes rapid muscle fatigue. The causes for the rapid onset of muscle fatigue are not completely elucidated. The most cited hypotheses for explaining inverse recruitment is that, because of their diameter, axons of motor neurons innervating fast twitch muscle fibers are more electrically excitable than axons innervating slow twitch muscle fibers [27]. There are alternative explanations based on anatomical differences regarding the distribution of the nerves or the fibers types within the muscles [28]. In principle, regardless of its ultimate cause, inverse recruitment could be avoided if motor neurons could be individually stimulated by using massive arrays of ultrathin electrodes able to independently stimulate each motor neuron – an utopia with current, an mid-term envisioned, technologies. In recent times, however, it has been suggested an alternative feasible solution: to perform interleaved multisite stimulation for reducing fatigue. This approach has been tried with a reduced number of electrodes on animal muscles [29] and transcutaneously on human muscles [30] with very promising outcomes. Results from these studies, and from others in which interleaved stimulation is performed at the nerves [31][32], strongly indicate that if a significant amount of muscle sites could be individually stimulated (i.e. minor motor points corresponding to a few motor units) not only finer movement control could be achieved but also the fatigue issue would be avoided or greatly minimized. Therefore since the dense network of microstimulators would accomplish better selectivity, the miniaturized devices could more easily mimic the natural processes of the body, promoting fatigue-resistant electrical stimulation.

Until now, the microstimulators aimed to form this network of addressable wireless devices are considerably bulky and stiff ($Ø \geq 2$ mm; lengths $\geq$ 16 mm). This implies that the implants are quite invasive, impeding their dense deployment. Therefore, these microstimulators do not exploit the full potential of the network concept for treating paralysis.

Miniaturization of electronic implants, and of stimulators in particular, has been hampered by the available methods for powering them.

1.3.1. Powering implantable electrical stimulators

Implantable electrical stimulators are active devices, therefore they require a power source [33]. Their power requirements depend on the specific application of the medical device. For example, pacemakers

require at most 100 μW, while neurostimulators need more than 500 μW, and cochlear implants can require almost 10 mW [34].

According to their powering approach, electronic implants can be classified into *self-powered systems* in which no external device is required, and *remotely powered systems* in which the implants depend on an external unit that wirelessly transfers power to them.

Self-powered systems

Independent power supplies are applicable in electrical stimulators that require low power. Since the introduction of pacemakers in the 1970s, battery powered implantable devices have been extensively used. This powering approach has benefited from important developments in battery technology, resulting in batteries with high volumetric energy density such as those based on lithium-ion (density > 400 Wh/l [35]) [34]. However, some stimulation applications require miniaturized devices that can deliver enough power for stimulation (e.g. neuromuscular stimulators), hampering the use batteries, as they take up between 25 and 60% of the volume of an implantable device [36].

Flexible and biodegradable batteries, and super capacitors have been explored in the last few years to power implantable medical devices. For flexible batteries, it has been proposed to add battery chemistries onto flexible substrates, flexible nanofribrous cathodes and paper-based batteries using laser ablation techniques [37]. However, these flexible batteries show short lifetime for long-term applications, and high cost. Supercapacitors have accomplished higher power densities compared to batteries. Nevertheless, they are incapable of storing this energy for long time periods. Different solid-state and nanotechnology techniques have improved this feature, but much more development is required as energy densities are too low to provide power for neuromuscular stimulators [37]. Some researchers have proposed to recharge the supercapacitors with radiofrequency (RF) links, which, as discussed below, requires a coil that increases the volume of the implantable device [38]. Therefore, this approach is not optimal if miniaturization is a must.

Biofuel cells have also been explored to power implantable medical devices. These elements transform biochemical energy into electricity by electrochemical reactions that involve biochemical pathways [34]. Some proof-of-concept artificial hearts used biofuel cells in the 1960s [39]. During the 1970s other implantable medical devices powered by biofuel cells were explored. Some used glucose as fuel and oxygen as oxidizer. Since then, implantable medical device researchers have been looking for different ways to provide biocatalysts for long periods of time. However, microbial biofuel cells provide power in the order of the microwatts, hampering their application in neuromuscular stimulators [34]; and the

instability and denaturalization of enzymes used for enzymatic biofuel cells impedes their application in long-term implantable devices [35].

Another type of independent powering approach is the nuclear batteries technology. They were used commercially in pacemakers in the 1970s, and were discontinued in the 1980s because of potential risks, including the need to track the radioactive material, and the risk posed to the patient if hermeticity was not guaranteed [34]. Their greatest advantage was their longevity (> 15 years), and the stability of their output energy. Multiple pacemakers were developed in the 1970s using this powering approach [40]. However, lithium batteries replaced nuclear batteries as they were much safer and accomplished acceptable longevity (~10 years).

A very attractive powering approach for implantable medical devices would consist in the use of so-called energy scavengers, as their operating lifetime is in theory unlimited [37]. These devices accumulate existing energy from the background, that otherwise would not have been used. For instance, piezoelectric energy harvesters generate an electric potential using kinetic energy of the body (e.g. muscular movement) [41]. Other energy scavengers use natural processes of the body such as electric potentials of the inner ear [42]. Even though these "unlimited" power sources have had important improvements, their invasiveness and low power capabilities are inadequate for neuromuscular stimulation [34], [37].

Remotely powered systems

Remote wireless powering approaches rely on external units that deliver energy to be used by the implantable devices. In some cases, these external units also use the energy signal to generate a communication link between the wireless devices and the external controller. The external unit usually has to be close or in contact to the human body.

The most prevalent remote wireless powering method is inductive coupling. In this approach, the external system powers the implantable devices using near-field magnetic power transmission. It relies on Faraday's law of induction: the external unit has a coil (i.e. primary coil) that couples with a coil located in the implantable device (i.e. secondary coil). As a varying magnetic field is generated in the external coil, alternating current (ac) is induced in the implanted coil. The induced electromotive force ε (i.e. the induced voltage in the second coil) can be mathematically expressed as:

$$\varepsilon = -\frac{d\phi_B}{dt} \tag{1.1}$$

where ϕ_B is the magnetic flux.

The magnetic flux through a coil of area A and number of turns N depends on the angle θ between the normal to the coil and the magnetic field. This can be expressed as:

$$\phi_B = \mathrm{N}\,\vec{\boldsymbol{B}}\cdot\,\hat{\boldsymbol{n}}\mathrm{A} = \mathrm{N}\,B\,\mathrm{A}\,\cos\theta \tag{1.2}$$

where *B* is the magnetic field magnitude. Then, the induced electromotive force between two coils can be rewritten as:

$$\varepsilon = -\mathrm{N}\,\mathrm{A}\,\cos\theta\,\frac{d(B)}{dt} \tag{1.3}$$

Eq. 1.3 indicates that the induced voltage in the implantable device is proportional to its coil diameter and the number of turns. Therefore, the implanted coil must have a minimum diameter (i.e. area A) to accomplish a significant voltage capable of powering the electronics and perform stimulation. This constraint hampers the miniaturization of neuromuscular stimulators based on inductive coupling. It was numerically shown that implants with diameters of less than 1 mm would not be able to power such a stimulator [43]. Additionally, Eq. 1.3 also implies that the electromotive force is affected by coupling misalignment. Therefore, a key restriction in inductive coupling is that the external and implanted coils must be aligned to induce enough voltage to power the implantable device and perform stimulation.

Despite these limitations, injectable neuromuscular stimulators based on inductive coupling have been developed and clinically tested [44]–[47]. Currently, the most remarkable development is the BION (BIOnic Neurons), which will be described in section 1.3.2. BION implants have accomplished important technological advances in terms of miniaturized implantable medical devices, developing addressable and injectable implants of 2 mm diameter. Another important development based on inductive coupling is the Networked Neuroprosthetic System developed by Peckham et al. at the Cleveland FES Center [48]. It consists of an implantable central unit with rechargeable battery to be charged by inductive coupling. This central unit is wired to small stimulation modules. Each module processes information and controls electrical stimulation, which is delivered using electrodes connected to leads. The modules are scalable in order to restore different body functions. The biggest drawback of this technology, as explained above, is the use of leads in large and mobile body parts. This can imply long and difficult surgical procedures, risk of infection, tendency to fail because of mechanical stress, and can be considered cosmetically unacceptable for some patients [47].

Another significant disadvantage of inductive coupling is its incapability to power deep seated implants [49]. This limitation has been partially addressed recently by Poon et al. by confining electromagnetic energy transport through propagating modes in tissue (mid-field) [50] [51]. However, this electromagnetic induction method also relies in the diameter of the receiving coil. They have demonstrated that, with a frequency of 1.7 GHz, a 2 mm diameter coil would receive only 100 μW [50]. Therefore, both inductive coupling methods based on near-field and mid-field do not avoid the need for an implant coil with a diameter above 1 mm.

Another electrical approach for wirelessly transferring power is the use of electromagnetic propagation (far-field) and, in particular of microwaves as they allow miniaturized antennas. Researchers have reported injectable devices that act as dipole antennas that capture 915 MHz microwaves, accomplishing electrical stimulation in rats [52]. However, this powering approach is only suitable for superficial implants in humans as the skin effect impedes the penetration of high frequency electromagnetic radiation in tissues. For instance, the skin depth penetration of 900 MHz electromagnetic fields in human tissues is only of about 1 cm and at a depth of 3 cm the power reduces to 1% [53].

Highly energy efficient wireless power transfer can be accomplished with ultrasound. This is possible because ultrasound energy can be focused into tight beams using acoustic lenses [54]. However, power transfer methods based on ultrasounds present two important disadvantages: 1- ultrasound can unacceptably raise the temperature in bone as it is strongly absorbed by this tissue at MHz frequencies; and 2- the location of the ultrasound exciter must be close enough to the implant for efficient power transfer. Two implantable devices that are powered with this method have been demonstrated. Larson et al. proposed a nerve cuff stimulator consisting on a piezoelectric receiver, a diode and a capacitor [55] which does not include addressability capabilities. Yet they proposed a method to locate the implant on the body by detecting on the skin the signals emitted by the implants [56], [57]; and a telemetry system for bioelectric events [58]. Charthad et al. proposed an implantable device that also included RF data transmission, but its form factor (7.8 mm long × 4 mm wide) hampers its deployment by injection, and it drives only 100 μW, which is not enough for neuromuscular stimulation [59]. However, it must be noted that recently leadless pacemakers based on ultrasound were successfully demonstrated in heart failure patients [60].

Near-infrared (wavelength between 760 – 1500 nm) has also been explored for wireless power transfer. Two sorts of energy receivers have been proposed: pyroelectric generators and photodiodes. Liu et al. reported in [61] an implant consisting on a pyroelectric generator: a

device that can generate an electric potential when it is cooled or heated. This wireless device absorbs light and induces temperature fluctuations in the pyroelectric generator, generating at most 200 nA, which is too low for neuromuscular stimulation. Additionally, as the pyroelectric current generated by the implant is proportional to the effective area of the device [61], its size (20 mm × 20 mm × 0.2 mm) is too large to be deployed by injection. Much thinner devices have been also developed, which are based on photodiode implants that are wirelessly powered by laser sources [62], [63]. These floating-light-activated micro-electrical stimulators (coined "FLAMES") can be independently activated using wavelength selectivity [64], but deliver low current (< 120 μA) that is only applicable in intraspinal microstimulation, where the threshold of stimulation is lower than that needed for neuromuscular stimulation. Additionally, a fiber optic close to the central nervous system (CNS) must be implanted to drive the microstimulators [65], increasing surgical complexity and safety concerns.

1.3.2. The BION case

By the end of the 1980s, G. Loeb proposed to electrically power a wireless neuromuscular stimulator by inductive coupling using a 1.5 mm diameter and 3 mm long coil [47], and W.J. Heetderks numerically demonstrated that this was feasible [43]. This is the basis for the development of a general-purpose injectable single channel wireless stimulator coined BION. BIONs were meant to accomplish the dense network of wireless microstimulators described above.

Two powering approaches based on inductive coupling were explored for the BIONs: 1- to power the implant directly from this power transfer, and 2- to recharge an implantable lithium-ion battery that could power the implant's electronics without the need to have an external power transfer system constantly [47]. Figure 1.3 shows three different generations of BION implants: 1- the BION 1 AMI, designed by the Alfred Mann Institute, which has glass housing and is powered only by inductive coupling; 2- the BION 1 AMF, designed by the Alfred Mann Foundation, which is also powered by inductive coupling but consists on a ceramic housing; and 3- the BION 3 developed by Advanced Bionics Corp., which includes a lithium-ion rechargeable battery.

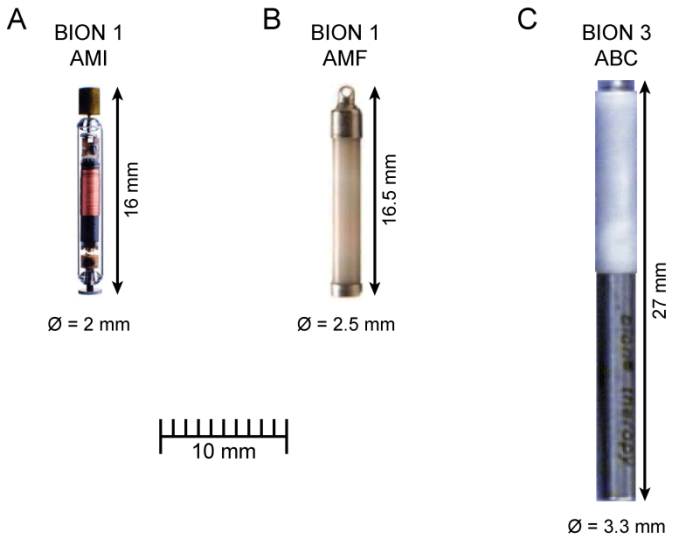

Figure 1.3. Three different generations of BION implants. A) Glass housed implant powered by inductive coupling. Extracted from [66]. B) Ceramic housed implant powered by inductive coupling. Extracted from [47]. C) Implant powered by a lithium-ion rechargeable battery. Extracted from [47].

Several developments can be highlighted from these microstimulators. First, they were conceived as general-purpose neurostimulators, therefore they were meant to be used to restore function in a wide range of clinical disorders [67]. Second, the microstimulators were designed to avoid leads using integrated electrodes. The leads complicate the implantation procedure and tend to fail. The BION implants were then understood as implants made up of a single body that could be easily deployed by injection, improving surgical procedures while minimizing possible foreign body response. A surgical kit was designed by the BION team to perform this procedure [68]. Third, as the implants were to be massively deployed in tissues, they required addressability capabilities. This implied that a receiver coil would be needed to receive information. Then, the BION implants used the energy coupling coil also as receiver coil, and bidirectional communications were developed not only to control de implants but to extract information from them (i.e. telemetry features were included). Fourth, the design avoided the use of bulky crystals to generate a stable clock signal. Instead, it used the external RF magnetic field as a primary clock signal. Fifth, the BIONs included a custom wirebond method to attach the application specific integrated circuit (ASIC) die to the rest of the assembly [69]. This was critical to ensure that the packaging and interconnect modules were smaller than the ASIC. Sixth, a capacitor-electrode design was implemented to combine in a single

component energy storage, blocking capacitor (for passive charge-balance), and electrode functions [22]. Seventh, several hermetic packaging designs and housing materials such as glass and ceramic were evaluated. Different mechanical tests were performed, evidencing the need to avoid weak mechanical parts that tend to fail in real clinical scenarios [66], providing evidence of critical design factors for intramuscular implantable devices. In short, BION microstimulators are a major case of study in neuroprosthetics, as they boosted research and advances on bidirectional communications, packaging hermeticity, electrodes, implantation tools, and especially in the implant's form factor. Furthermore, the researchers involved in the project have reported the design evolution in detail [22], which is an important contribution for the design of implantable devices.

Advanced Bionics Corp., developer of the BION microstimulators, was purchased by Boston Scientific Corp. in 2004 [70]. By 2011, it was said that Boston Scientific, the Alfred Mann Foundation and other research institutes worldwide were developing clinical and technical research on the BIONs [22]. Nowadays there is no information about the development of BION microstimulators. However, the knowledge acquired from its development in the University of Southern California (where the Alfred Mann Institute is established) gave rise to other technologies, as a percutaneously implantable fetal pacemaker [71], [72].

Even though BION microstimulators have accomplished high miniaturization levels, the implants are still too stiff and bulky as to be massively implanted in tissues, hampering the development of a network of wireless microstimulators. Then, questions arise in terms of how to develop thinner and less rigid devices that can accomplish miniaturization levels without precedents for microstimulators. This thesis will address this important issue.

1.4. The eAXON method

In [73] Ivorra proposed a heterodox method for developing implantable microstimulators that avoids the use of inductive coupling or electrochemical batteries. Briefly: 1- innocuous high frequency (HF) current bursts ($\geq$ 1 MHz) are conductively supplied by external electrodes across the tissues where the implants are located (Figure 1.4); 2- The implants act as rectifiers of these HF current bursts, generating locally low frequency (LF) currents capable of stimulating excitable tissues.

The proposed method requires a minimum voltage drop between the two implant electrodes to power up the microstimulator and to generate the stimulating LF currents. This implies a minimum separation distance (in the order of a very few centimeters [74]) between the two implant electrodes to avoid the need of excessively large HF currents which would significantly heat the tissues. To ensure this, we conceive the implants as

elongated bodies consisting of flexible and stretchable materials. Their mechanical properties match those of the tissue in which they are implanted. Because of such characteristic and their intended functionality, Ivorra named these implants "Electronic Axons" (eAXONs). The electrical stimulation and powering method is referred to in this thesis as the "eAXON method".

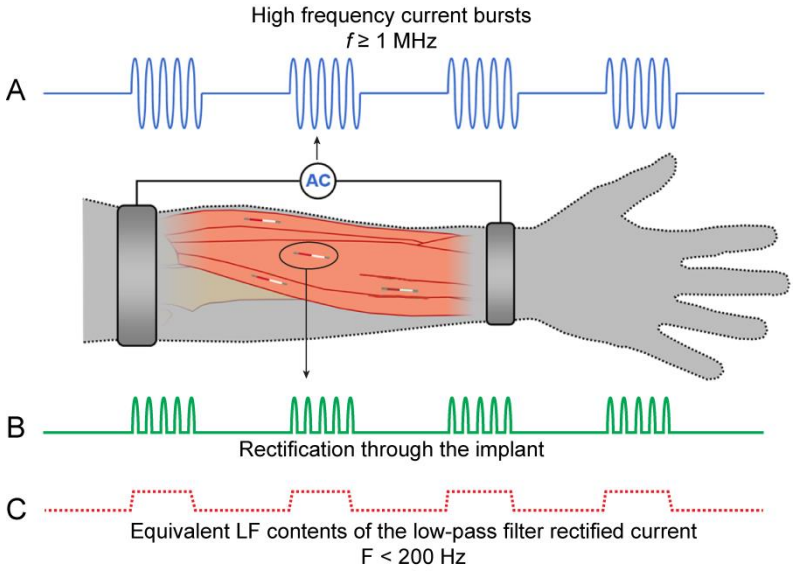

Figure 1.4. The eAXON method. Two external electrodes deliver innocuous high frequency current bursts that flow through the tissues by galvanic coupling (A). The implants pick up this current and rectify it (B). Due to the passive dielectric properties of cells, these bursts of rectified current cause voltages across the cell membrane which are low-pass filtered and perceived as rectangular pulses capable of causing membrane depolarization. If strong enough, this depolarization is capable of electrical stimulation. (C). Adapted from [73].

1.4.1. Background

In essence, the cell membrane consists of a lipid bilayer which embeds some structures across it made of proteins. Few substances move through the lipid bilayer by diffusion, and most substances move between the intracellular and extracellular fluid compartments using channel and carrier transport proteins. One of those carriers is the sodium-potassium pump. It pumps three Na^+ ions outward through the cell membrane, while pumping two K^+ ions into the cell [21]. This maintains a charge imbalance across the membrane which causes a negative potential inside the cell membrane with respect to the outside. Other transmembrane protein structures activate with changes in the membrane potential (e.g. sodium

and potassium voltage-gated ion channels), and have a key role in the generation of nerve impulses [26].

The cell can be modeled as an electrical circuit made up of resistances and a capacitance (Figure 1.5). Due to the insulating characteristics of the lipid bilayer, the cell membrane is modeled as a capacitance (C_m). The intracellular and extracellular media of the cell are modeled as resistors (R_i and R_e respectively) [75].

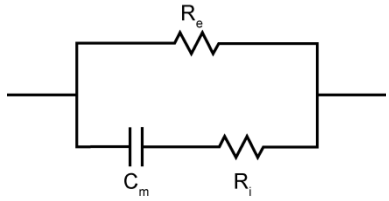

Figure 1.5. Circuit model for the cell consisting of the combination of a capacitor C_m (capacitance of the cell membrane due to its insulating characteristics), resistor R_i (resistance of the intracellular space), and R_e (resistance of the extracellular space).

When currents are applied to excitable tissues, APs are initiated if the variation of voltage across the membrane (i.e. across C_m in the circuit model) overcomes a threshold (i.e. if the membrane is sufficiently depolarized). Therefore, since the membrane and the intracellular and extracellular media form a first order low-pass filter (f_c of a few kHz [76]), it will be much harder to cause stimulation by injecting HF currents (e.g. 100 kHz) than by injecting LF currents (e.g. 100 Hz).

The above paragraph corresponds to the biophysical explanation of the key fact that makes the eAXON feasible: the strong dependence of excitation thresholds on the frequency of alternating electric fields [77]. To artificially trigger APs, higher electric field magnitudes are required at HF than at LF. HF currents are safer than LF currents for preventing unwanted electrostimulation (explained in depth in Chapter 6). In the eAXON method, the external electrodes deliver HF current for powering the implantable devices ($\geq$ 1 MHz) without eliciting electrical stimulation. The implants rectify these HF currents causing bursts of rectified current with LF and HF components. Due to the low-pass filter behavior of the cell membrane, these bursts of rectified current are perceived as rectangular pulses capable of causing membrane depolarization.

1.4.2. Features of the electrical stimulation and powering method

The HF current bursts delivered by the external system are picked-up by two peripheral electrodes (hereinafter “implant electrodes”), and rectified by the implant circuitry to electrically feed the device. This rectification

process is based purely on electronics, while in inductive coupling and independent powering approaches the implants require additional components that usually take up a large volume (e.g. coils and batteries). The implant electrodes are also used for performing electrical stimulation, and all the necessary electronic components can be integrated into a tiny hybrid microcircuit or an ASIC. These features allow the development of very thin implants, accomplishing unprecedented levels of miniaturization for implantable neuromuscular electrical stimulators.

The first demonstrations of the electrical stimulation method were performed using an implant consisting of a single diode [78]. Such simple configuration is not adequate for clinical purposes because direct currents (dc) are generated through the implant and can electrochemically damage both the tissues and the electrodes (section 1.5.4). Hence we developed and demonstrated implants capable of overcoming that drawback whose electronics consists of a diode, a capacitor and a resistor (described in section 1.6) [79]. However, these devices are only suitable for single target stimulation and this is not sufficient for movement restoration in paralysis patients. We envision neuroprosthetic systems in which eAXONs will be deployed forming a dense network of microstimulators that will be individually controlled by an autonomous external unit. This unit will deliver the required innocuous HF current bursts and will individually command each microstimulator. The implantable devices will perform complex stimulation patterns in a number of muscles or in segments of a muscle, as those required for fine movement restoration in patients suffering from paralysis [80]. Additionally, the dense network of miniaturized implantable devices will include bidirectional communications that enable device monitoring, patient follow-up and real-time stimulation control [33].

Another remarkable feature of the eAXON method is that the network of wireless microstimulators located in a certain body region can be powered and controlled by only two external electrodes connected to a portable external HF current generator. Essentially because these currents are of HF, the electrodes can be made of conductive fabric, which can be easily included in garment. This increases comfort, as no bulky external connections are required, as those needed for inductive coupling.

It must be noted that the concept of electronic rectification of HF current for stimulation, which we independently envisioned in [73], was in fact first proposed in the 1960s by at least two independent research teams in two infrequently cited studies [81][82]. However, to the best of our knowledge, neither advanced rectifiers with communication capabilities nor simple rectifiers capable of blocking dc current have been proposed until now. In historical perspective it is easy to understand such neglect: at the time microelectronics was at its infancy and, therefore, the coils and batteries were not the miniaturization bottleneck but the electronics.

1.4.3. Galvanic coupling as means for HF current conduction

The eAXON method uses galvanic coupling to conduct HF current bursts from an external system to the implantable devices. Figure 1.6 illustrates the HF current flow through the body extremities using this mean for HF current conduction.

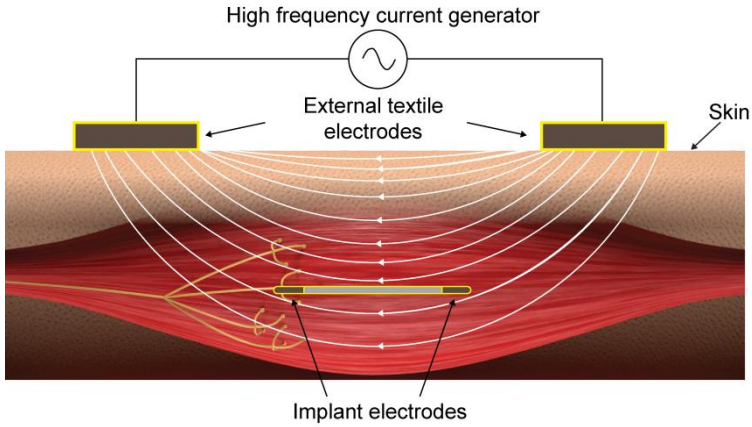

Figure 1.6. Current flow in the eAXON method due to galvanic coupling. The external electrodes are in contact with the skin (strapped around the limb), and the implant is located near the motor unit of the target muscle.

Galvanic coupling has been extensively studied for using the human body as a communication path [83] [84] [85], [86]. This approach, known as intrabody communication (IBC), has been proposed as an alternative to RF technology in body area networks. Two drawbacks faced with RF are overcome with galvanic coupling: electromagnetic interference and security issues [87].

Very few studies have been found in which galvanic coupling is used to power implants. As an example of those it can be indicated that Tang et al. proposed in [88] the use of galvanic coupling as means to recharge an implantable ion coin battery (Ø ~ 19 mm) [89].

Another group of researchers has proposed to use passive implantable leads that pick up currents delivered by external electrodes and that flow through the tissues by galvanic coupling. These leads route the currents to the vicinity of the target excitable tissue to perform electrical stimulation [90]. This approach, known as *stimulus router system*, avoids the use of implanted electronics to control the stimulation, with the drawback of implanting the leads for stimulation. The technology, developed in the University of Alberta, was tested in 2012 as an implantable forearm stimulator for a tetraplegic man with bilateral hand paralysis [91]. Cuff electrodes that control hand opening and grasp were implanted in the patient. The passive leads from the cuff terminated under

the skin, underneath an external wristlet that contained the pulse generator attached to moistened pad electrodes. These external device delivered electrical pulses through the skin and to the leads [90]. Bioness Corp. acquired the technology in the 2010s and focused its application in chronic pain of peripheral nerve origin, earning the FDA clearance in 2015. Even though the stimulus router system uses galvanic coupling as a mean to perform electrical stimulation, it cannot be considered that galvanic coupling is being used as a powering approach.

Galvanic coupling has certain limitations when used as a powering approach for implantable electronic devices. First, the voltage drop across the implant electrodes depends on the orientation of the implant with respect to the electric field. As the electronics require a minimum voltage for operation, the orientation of the device can become critical to ensure this electric potential difference. Second, the energy efficiency of the approach is very low, as most of the power is lost as Joule heating. This issue is studied in Chapter 6 to ensure that tissue heating does not exceed the limits established in safety standards.

1.5. Constraints for neuromuscular microstimulators

1.5.1. Strength-duration and spatial relationships in electrical stimulation

Pulse amplitude, duration and frequency determine muscle contraction in electrical stimulation [12]. The so-called rheobase current I_r is the minimum current needed to stimulate an excitable tissue with an infinite duration pulse. It obviously largely depends on the distance between the electrode and the target excitable tissue [26]. The chronaxie T_c is the pulse duration needed to stimulate an excitable tissue with an amplitude that is two times de rheobase current I_r. This parameter depends on the tissue: in neural tissues $T_c < 1$ ms, while in skeletal muscle $T_c > 10$ ms [26].

Weiss equation can be used to describe the *strength-duration relationship* experimentally observed for electrical stimulation (Eq. 1.4). The minimum stimulus amplitude needed to stimulate a nerve (I_{th}) increases as the duration of the stimulus (pulse duration *PD*) decreases.

$$I_{th} = I_r \left(1 + \frac{T_c}{PD}\right) \tag{1.4}$$

The *charge-duration relationship* defines the amount of charge necessary to accomplish stimulation. It is determined from the *strength-duration relationship*, and can be expressed as:

$$Q_{th} = I_r(PD + T_c) \tag{1.5}$$

As the pulse duration of the stimulation decreases, the charge needed to perform this stimulation decreases too [25]. Both the *strength-duration* and *charge-duration relationships* for neural tissues are shown in Figure 1.7. The rheobase current I_r and chronaxie T_c are indicated in the graphs. Even though short stimulation pulses require more current for stimulation, they are more efficient at generating excitation [25]. This is explained as shorter pulses need less charge, therefore they reduce the power requirements for stimulation [17]. Additionally, shorter pulses increase the spatial selectivity as they increase the threshold difference between nerve fibers that are located at different distances from the stimulating electrode [17] [92].

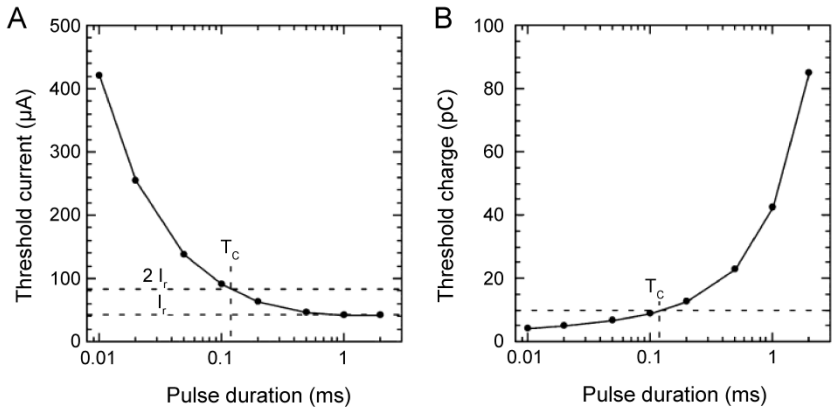

Figure 1.7. Duration of stimulus for a nerve fiber (Ø = 10 μm). A) *Strength-duration relationship*. As the pulse duration increases, the threshold current needed for stimulation decreases. B) *Charge-duration relationship*. As the pulse duration increases, more charge is required to generate an AP. Extracted from [26].

Figure 1.8 shows the *spatial relationship* between the threshold current for electrical stimulation, and both the distance from the electrode to the nerve fiber and the diameter of the fiber. When an electrode is close to the nerve fiber, the current delivered by the stimulator generates a larger transmembrane potential than if it was located farther away from the nerve (Figure 1.8-A). Therefore, less current is needed to trigger an AP [25].

Under normal conditions, nerve fibers with larger diameter have larger spacings between nodes of Ranvier (gaps in myelin sheaths that cover the myelinated axon of a nerve cell, and where the cell membrane is exposed to extracellular space). These larger spacings translate into larger transmembrane potential changes [25]. This makes it easier for the stimulator to trigger an AP in larger nerve fibers than in smaller ones

(Figure 1.8-B). In other words, current thresholds vary inversely to the fiber diameter for a specific pulse width [26][93].

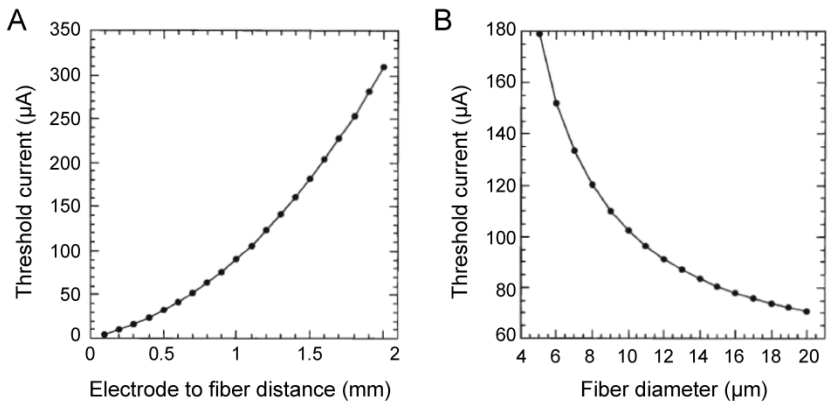

Figure 1.8. *Spatial relationship* between the threshold current and the nerve fiber for a pulse width of 100 μs. A) *Current-distance relationship*. As the distance between the stimulating electrode and the nerve fiber increases, the stimulator has to deliver more electric current to trigger an AP. B) *Current-fiber diameter relationship*. It is easier to trigger an AP in large nerve fibers than in smaller ones due to larger transmembrane potential changes. Adapted from [94].

1.5.2. Physiological conditions to accomplish electrical stimulation

Neuromuscular electrical stimulators are capable of eliciting muscle contractions if the motor nerves are intact [95]. This is due mainly because the stimulus magnitude needed to stimulate a muscle is almost 100 times larger than that needed to stimulate a nerve [96]. Such a large magnitude could damage tissue if applied multiple times, as much more electrochemical reactions are generated in the electrode-tissue interface (explained below), compared to those generated when stimulating nerve. Then, it is essential for FES that the entire lower motor neuron, including the neuromuscular junction, is preserved.

1.5.3. Electrode-tissue interface

Electrodes have a crucial role in electrical stimulation and can determine the long-term viability of a neuroprosthetic device [26]. Inside the body, most of the electric current is carried by ions [97], while the electric current delivered by the electrical stimulators is composed of electrons. This implies that electrochemical reactions may occur at the electrode-tissue interface in order to transform electronic current into ionic current [98], and the charge and current density of the applied electrical stimulus is determined by the area of this interface [26].

In the electrode-tissue interface, the metallic surface of the electrode is in contact with an electrolyte (basically Na^+ and Cl^-). In equilibrium, when no current flows through the interface, a distribution of negative charges along the metallic surface, and a distribution of positive charges along the electrolyte is established. This forms the so-called double-layer capacitance [99]. When the interface voltage is modified, for instance, when stimulation is performed, electricity can flow to the electrolyte in two ways: capacitively (i.e. involving displacement currents) or faradically (i.e. involving electrochemical redox reactions). In the capacitive path, there is no electron transfer, but a redistribution of charges of the ions in the electrolyte [100]. This mechanism does not produce chemical reactions that can damage the electrode or the tissue. Yet, in faradaic reactions (reversible and irreversible), electrons are transferred in the electrode-tissue interface, resulting in reduction or oxidation processes in the electrolyte. In reversible faradaic reactions, the products remain bounded or close to the electrode surface, and this can be reverted by forcing a current in the opposite direction of the current that generated the reaction. In irreversible faradaic processes, the products diffuse away from it, spreading through the tissues.

The electrode-tissue interface can be electrically modeled according to the above. The first model (Figure 1.9-A) corresponds to the case in which only the capacitive path is significant because the voltage across the interface is not sufficient to generate the faradic reactions. It is composed of the parallel combination of a capacitor C_{DL} (corresponding to the double-layer capacitance) and a resistor R_F (corresponding to the faradaic impedance), connected in series with a resistor R_{ES}, which models the resistance of the electrolyte solution [101]. The values of C_{DL} and R_F depend on the geometry of the electrode. The second model (Figure 1.9-B) accounts for faradaic reactions. The faradaic impedance R_F is replaced with the series combination of a resistor R_{RF} and a capacitor C_{RF} to model the reversible reactions, while the irreversible faradaic processes are modeled with the combination of a diode and a resistor, as those reactions occur from a certain voltage threshold (forward voltage of diodes) [102].

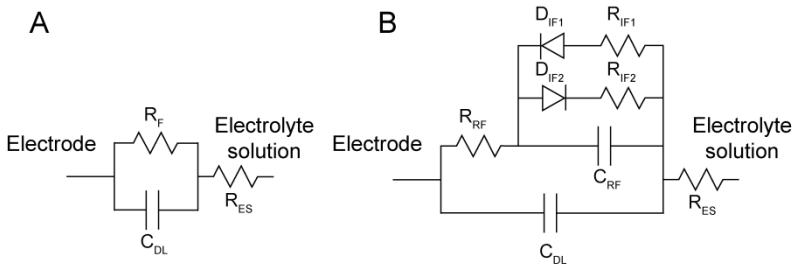

Figure 1.9. Equivalent circuit models of the electrode-tissue interface. A) Electrode-tissue interface circuit model corresponding to the double-layer capacitance C_{DL}, faradaic impedance R_F and electrolyte solution resistance R_{ES}. B) Electrode-tissue interface circuit model including the reversible (R_{RF}, C_{RF}) and irreversible (D_{IF}, R_{IF}) faradaic reactions, which are produced from a certain threshold voltage. Adapted from [102].

As explained above, electrical stimulation depends on the electric field magnitude that develops in tissues [17]. Therefore, neuronal excitation can be controlled by controlling the delivered electric field during electrical stimulation. The circuits used to deliver electrical stimulation in neuroprostheses are usually composed of regulated current or voltage sources (Figure 1.10-A and B respectively). Regardless of the electrode-tissue interface impedance, current-controlled stimulation generates the same current flow through the tissue, and consequently, the same electric field. In contrast, voltage-controlled stimulators depend on the load impedance [33].

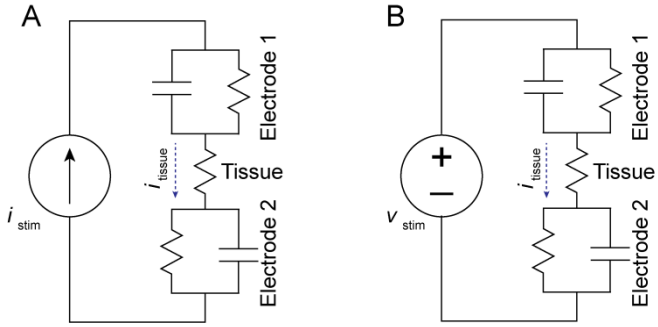

Figure 1.10. Typical electrical stimulation modes. A) Current-controlled and B) voltage-controlled stimulation, including the electrode-tissue interface, and the tissue resistance. Adapted from [17].

In some specific cases, voltage-controlled stimulators are preferred over current-controlled. For example, when the electrodes are placed over the skin (i.e. superficial configuration), they can easily detach, increasing the interface impedance. In this case, since the current-controlled stimulator is not affected by this impedance, the current density can

rapidly increase, causing pain or skin damage [17]. Voltage-controlled stimulators avoid this undesirable effect as the generated field depends on this impedance. It must be noted that, nowadays, good quality current-controlled stimulators have feedback control. This feature automatically powers down the stimulator if the interface impedance exceeds a defined threshold, avoiding unpredictable function and increasing its safety [19]. Other cases in which voltage-controlled stimulators are preferred are those in which high-current stimulation is needed (e.g. pacemakers). In those cases, voltage-controlled stimulators are preferred because they are capable of stimulating with voltages close to their supply level, therefore they achieve higher efficiency, which translates into longer battery lifetime [103].

1.5.4. Damages in the electrode-tissue interface

Tissues can be damaged by the presence of the electrode [17]. This is usually known as *passive tissue damage*, and it can be due to mechanical and surgical trauma and to biocompatibility issues related to the chemistry of the materials or their surface structure.

In the case of percutaneous and implantable configuration systems in which the electrodes are implanted (section 1.2), it has been demonstrated that mechanical trauma can be minimized by decreasing the diameter of the electrodes and beveling the electrode tip [17].

Foreign body response can be minimized by using biocompatible materials [104]. Implantable stimulators preferably use gold, platinum, iridium and platinum/iridium electrodes as they are highly resistant to corrosion; and stainless steel electrodes as they are stable to it [105].

Active tissue damage corresponds to the damage generated by the flow of electrons in the electrode-tissue interface. As explained above, this damage may arise from the products of the electrochemical reactions. The type and rate of electrochemical reactions depend to some extend on the charge density delivered during electrical stimulation [17]. For most metallic electrodes, above 20 $\mu F/cm^2$ a significant portion of the electrical current is faradic [102]. A typical electrochemical reaction in the electrode-tissue interface is the electrolysis of water. This generates pH changes and gas formation. Other effects are electrode dissolution (typical of platinum electrodes), transpassive corrosion (typical of stainless steel electrodes), oxidation of organics (e.g. tyrosine and glucose), and oxygen reduction [106].

Reversible faradaic reactions can be reverted by forcing a current in the opposite direction of the current that generated the reaction. To do so, the pulse generators frequently perform charge balance. This can be done with monophasic pulses followed by a charge recovery mechanism or by using biphasic waveforms [12]. Figure 1.11 shows three typical stimulus waveforms used in electrical stimulation. When monophasic pulses are

used, the current is forced to flow through a capacitor. The waveform consists of a unidirectional pulse (generally cathodic – electron flow from the electrode to the tissue [106] – as it is sought to depolarize the membrane with the least possible stimulus amplitude), followed by a charge stage created by allowing the capacitor to discharge through the tissue and the generator. In biphasic pulses, the waveform consists of a pulse that has two phases, generally a cathodic phase followed by an anodic phase. The first phase elicits the AP for stimulation, while the second phase reverses the electrochemical processes that occur during the first phase [99], and the electrode potential is shifted towards the direction of the original potential [17].

Typically, biphasic waveforms are symmetric or asymmetric (Figure 1.11-B and C). The first type uses a negative (cathodic) and a positive (anodic) pulse with the same duration and magnitude. Biphasic asymmetric waveforms consist of pulses that have different magnitudes. As the objective is to balance the charge delivered by the biphasic waveform, and the charge can be expressed as the time integral of current, the duration of the anodic pulse is adjusted to match the charge delivered in the first phase of the waveform.

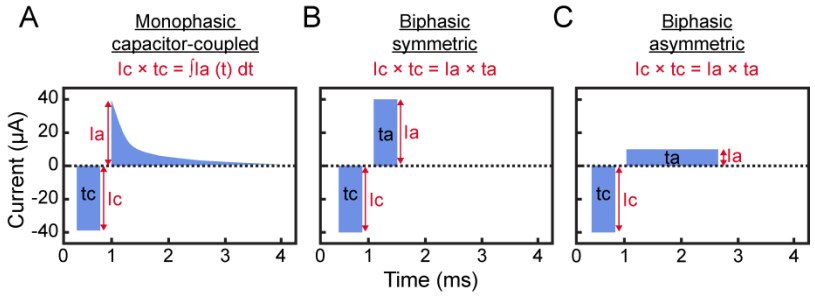

Figure 1.11. Types of waveforms in electrical stimulation for charge balance. A) Monophasic capacitor-coupled waveform. B) Biphasic symmetric waveform. The cathodic and anodic pulses have the same pulse duration and magnitude. C) Biphasic asymmetric waveform. The cathodic and anodic pulses have different magnitudes and durations, but the total charge delivered in the first pulse is recovered during the second phase. Adapted from [106].

It must be noted, however, that the faradaic reactions are only reversible if the current and charge densities are limited to a certain level [106]. Therefore, the above strategies based on performing charge balance only avoid electrochemical damage if the delivered currents are not excessive. To develop materials and processes that allow to safely inject larger stimuli with small electrodes is an active field of research [106].

1.5.5. Selectivity, fatigue, and force modulation

One of the most important challenges in electrical stimulation is to achieve the maximum possible selectivity.

In addition to the reasons pointed out above for selectivity regarding motor control, it must be noted that selectivity will also be crucial to minimize one of the most adverse effects of electrical stimulation: muscle fatigue. First the body naturally activates the small motor units (i.e. stimulates small muscle fibers), and if more force is required, it activates larger motor units, therefore larger muscle fibers. However, when artificial electrical stimulation is performed, it first activates the large fibers and then the smaller ones, due to their lower activation threshold (as shown by the *spatial relationship* illustrated in Figure 1.8-B). This means that neuroprostheses first recruit the fatigable muscle fibers [27]. This phenomenon is known as inverse recruitment, and is an enormous challenge as it hinders the control of movement in electrical stimulation and promotes fatigue.

One approach to avoid fatigue is performing *interleaved stimulation*: to stimulate excitable tissue by multiplexing the stimulus through different electrodes [107]. In this way, different muscle fibers can promote the muscle contraction by alternating their activation [108] [109] [110]. This can only be accomplished with high spatial selectivity. Then, neuroprostheses that could individually stimulate few motor units and that could be addressed to have a temporal and spatial control of the stimulation, could minimize fatigue while obtaining better muscle recruitment.

When it is not possible to achieve sufficient selectivity and the whole muscle or group of muscles is simultaneously stimulated, a way to encourage fatigue-resistant electrical stimulation is by adequately defining the parameters of stimulation. For example, higher frequencies produce stronger muscle contractions up to the maximum possible force generated by the muscle. However, as frequency increases, the rate of muscle fatigue does too [17] [12]. Then, the frequency of stimulation should be defined high enough to accomplish summation of muscle twitches, but low enough to avoid fatigue. Electrical stimulation exercise regime may also help solve this issue, increasing contraction time and fatigue resistance [96].

The force induced by electrical stimulation can be modulated by varying the frequency of stimulation or the recruitment (i.e. number of motor units simultaneously stimulated). However, as mentioned above, high frequencies tend to promote muscle fatigue, therefore frequency should be defined as low as possible. Then, it is desirable to modulate force by controlling recruitment (i.e. controlling the stimulus intensity by varying the pulse duration or magnitude). The *charge-duration relationship* (Figure 1.7-B) suggests that shorter pulse durations make

electrical stimulation more efficient, therefore it is recommended to use the shortest pulse duration that the stimulator can support (e.g. PD $\leq T_c$) [26]. Consequently, it is proposed to control the stimulation intensity to modulate the force induced by electrical stimulation, generating a more gradual recruitment of nerve fibers [93].

1.6. Simple charge-balanced rectifier based on the eAXON method

Simple non-addressable rectifiers based on electronic rectification of HF current bursts could be used in clinical scenarios in which only one target must be stimulated. In [79] we proposed a simple electronic architecture capable of performing charge-balance consisting of a diode, a capacitor and a resistor (Figure 1.12-A). This simple electronic circuit was embedded in a 3 cm long silicone tube with two electrodes at opposite ends. The implants weighted 40.5 mg and had a diameter of 0.94 mm (Figure 1.12-B). In a recent study, the implants were deployed by injection into the gastrocnemius or tibialis anterior muscles of four anesthetized rabbits using a 14 G catheter [111]. The implants were able to rectify HF current bursts and generate charge-balanced current waveforms for stimulation. The forces recorded in one stimulation assay are shown in Figure 1.12-C.

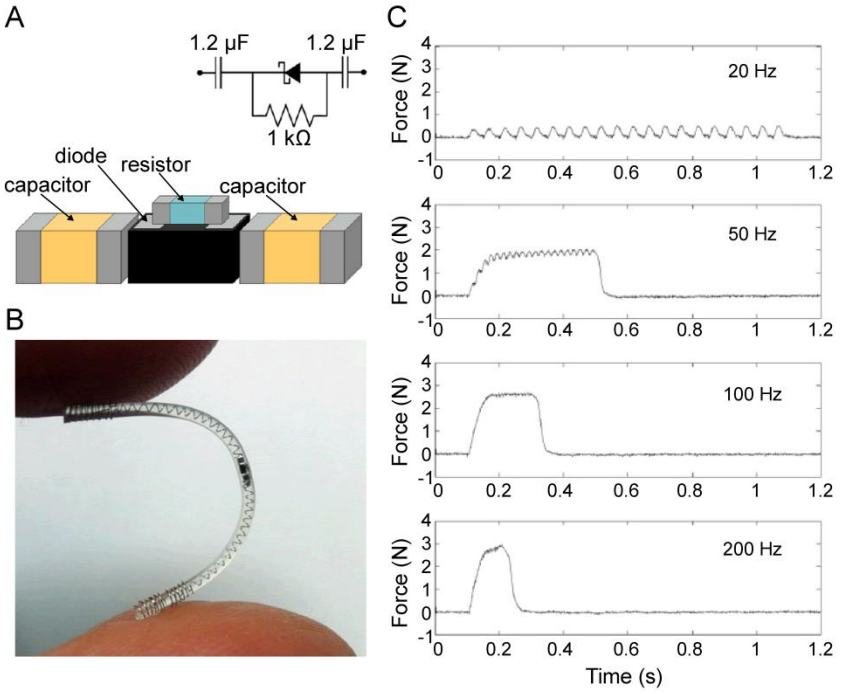

Figure 1.12. Non-addressable charge-balance rectifier based on the eAXON method. A) Circuit architecture and B) injectable version developed using commercial components (Ø = 0.94 mm) [79]. C) Force recordings during stimulation of the tibialis anterior muscle. Adapted from [111].

1.7. Comparison of the eAXON method with other technologies

As explained in section 1.2, FES systems can be classified into three configurations: superficial, percutaneous and implantable systems. Section 1.3 described different powering approaches for implantable neuroprostheses. Table 1-1 compares superficial, percutaneous and implantable FES configurations in terms of surgical simplicity, selectivity, safety, usability and ability to perform neuromuscular stimulation. Superficial and percutaneous configurations are not appropriate for fine muscle recruitment in long-term applications, as superficial systems lack selectivity, and percutaneous systems present low safety and usability levels [12]. Implantable central units wired to electrodes are able to accomplish high selectivity [48], but they entail surgical complexity and are not adequate for stimulation in large and mobile body parts due to leads that run through the tissues [47]. Implantable single-channel wireless microstimulators offer high selectivity as they can be located near motor points (e.g. inductive coupling, batteries, microwave, ultrasound or eAXON method), or near the neural tissue (e.g. near-infrared). However,

some of these powering approaches do not provide enough electrical energy for neuromuscular stimulation.

The ultrathin implants based on the eAXON method could present high levels of surgical simplicity and usability as their deployment would be much simpler than that offered by implants based on inductive coupling or batteries. In terms of usability, in Chapter 6 we demonstrate that the external system can be powered with portable batteries [74][112]. Additionally, external textile electrodes can be easily added to garments. This is an advantage over systems powered by inductive coupling: whereas in the eAXON method the energy for the implants will be delivered through textile electrodes integrated in garments, systems based on inductive coupling require the use of cumbersome coils.

A few months ago, *Nature* published an article that proposes to control electrical stimulation with signals acquired directly from the brain. Bouton et al. demonstrated in [113] that intracortically recorded signals can be linked in real-time to multichannel stimulators for muscle activation. The neuronal activity was decoded using machine-learning algorithms, and this information was used to control the forearm muscles of a patient using a high-resolution superficial neuromuscular electrode array. Figure 1.13 shows how the proposed system was capable of restoring multiple functions of the hand to, for example, play *Guitar Hero* (music rhythm game in which the player simulates playing a guitar by pressing buttons in a guitar-shaped game controller). Bouton and colleagues suggested that it was the first time a paralyzed patient could restore a motor function using the natural neural signals that used to control this body movement before the patient's lesion.

Even though the system proposed by Bouton et al. represents a major achievement in the field of neuroprosthetics, it must be noted that the performance of the system was greatly diminished because of the use of surface stimulation. As Robert Kirsch (Case Western Reserve University) criticizes in [114]: "the performance of implanted systems is an order of magnitude better than surface stimulation. We moved away from surface stimulation about 40 years ago". Superficial FES presents three important disadvantages for the proposed system: 1- the configuration lacks selectivity, 2- it requires much more power than other stimulation configurations, and 3- it could affect the integrity of the signals recorded intracortically because of this high voltage [114]. Therefore, the real-time decoded signals demonstrated by Bouton et al. [113] could be complemented with a network of single-channel wireless microstimulators that could be easily deployed by injection in the target tissues. The eAXON method has the potential to provide such ultrathin devices.

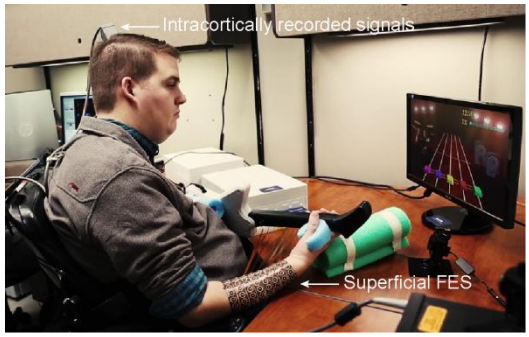

Figure 1.13. Patient playing *Guitar Hero* by controlling a superficial neuromuscular stimulator using real-time intracortically recorded signals. This system could be greatly improved using a network of wireless implantable microstimulators. Extracted from [113].

Table 1-1. Comparison of configurations for FES systems

System configuration	Surgical simplicity	Selectivity	Safety	Usability (ease to don and doff)	Ability to perform stimulation in muscle
Superficial (external pulse generator connected to skin electrodes)	+++++ (no surgery needed)	+ (hard to do isolated contractions and deep muscle activation; may activate pain fibers [12])	++++ (skin electrodes are driven by external system)	++ (every use implies don and doff; difficult to position for adequate stimulation [12])	+++++
Percutaneous (external pulse generator; the skin is pierced by leads)	+ (skin piercing and electrode anchoring)	+++ (electrodes can displace due to traction forces in the leads)	+ (possible infections due to skin piercing)	+ (used on research and clinical diagnosis [12])	+++++
Wired implants Central unit (leads connect electrodes to the implantable pulse generator -powered using rechargeable batteries- [48])	++ (implantation of generator and leads that run through tissues; electrode anchoring)	+++++ (electrodes are placed near motor points)	++ (possible infections due to leads that run through tissues [47])	++++ (only one anatomical point is required for programming using RF. This is also used for battery recharging)	+++++

Continues in next page.

Coming from previous page.

System configuration	Surgical simplicity	Selectivity	Safety	Usability (ease to don and doff)	Ability to perform stimulation in muscle
Wireless inductive microstimulators (ø 2 mm) [67]	++++ (deployment using thick catheter)	+++++ (microstimulators are placed near motor points)	+++ (possible foreign body response)	++ (external and implanted coils have to be coupled)	+++++
Wireless battery powered microstimulators (ø 3.15 mm) [47]	++++ (deployment using thick catheter)	+++++ (microstimulators are placed near motor points)	+++ (possible foreign body response)	+++ (radiofrequency used for battery recharge of each microstimulator)	+++++
Wireless near-infrared microstimulators (optical fibers used to power microstimulators in CNS.) (ø ≤ 0.2 mm) [62]	++ (implantation in CNS; optical fibers must be anchored close to microstimulators)	+++++ (microstimulators are placed in neural tissue for intraspinal stimulation)	++ (possible infections in optical fibers)	++++ (only one RF link is used for powering and programming implantable central unit)	+ (not enough current, only for intraspinal stimulation (≤ 120 μA))
Wireless eAXON microstimulators (ø ≤ 0.6 mm)	+++++ (deployment using **thin** catheter)	+++++ (microstimulators are placed near motor points)	+++ (possible foreign body response)	+++ (external electrodes added to clothes; portable external system [74])	+++++

Meaning of qualifiers: + stands for poor, whereas +++++ stands for excellent.

1.8. Available neuroprostheses for motor control

The applications of FES systems can be classified by the function restored and the type of configuration used. The examples below refer to technologies that are commercially available or that are awaiting for regulatory agencies approval such as the American FDA and the European CE mark.

1.8.1. Lower extremity

Superficial stimulators

The Parastep was developed by Graupe and colleagues between 1980 and 1994, and was the first superficial FES walking system that gained FDA approval and coverage from US Medicare and Medicaid [115]. It is a six-channel superficial stimulator that is used with a walker, and which is controlled using hand switches. This FES system is still available, however, the patient faces rapid fatigue [19].

Nowadays neuroprostheses used for lower extremity function are mostly applied to ensure ground clearance. This is done with foot drop stimulators. In the case of superficial stimulators, they are generally made in the form of cuffs that are worn below the knee. MyGait by Otto Bock, L300 by Bioness [116], and ODFS Leg Cuff by Odstock Medical use a sensor that triggers the stimulation of the peroneal nerve. This sensor is worn on the ankle or under the heel, and transmits the information wirelessly. An additional feature of MyGait is that it can stimulate two muscle groups as it has two channels for stimulation, improving gait. WalkAide by Innovative Neutronics avoids the use of sensors inside the shoe by including a tilt sensor in the cuff. The ODFS Pace is another foot drop stimulator from Odstock Medical, which uses superficial electrodes wired to a portable stimulator that can be stored in a pocket. This avoids the use of a big device under the knee that does not feel cosmetically appealing when using thin clothes and dresses. The L300 by Bioness is now complemented with a thigh cuff (L300 plus) that improves bending and straightening of the knee [117].

Implantable stimulators

Most of the lower extremity implantable stimulators are also intended for foot drop. This is probably because of simplicity and market reasons. Nowadays there are two implantable foot drop stimulators that are commercially available in Europe: the STIMuSTEP by Finetech Medical, and the ActiGait, by Otto Bock [14]. They are triggered from a sensor located under the heel. The Neurostep is a closed-loop stimulator that is fully implantable [118]. It consists of cuff electrodes and a pulse generator that is implanted in an inner thigh pocket. The technology was developed by the spin-off Neurostream Technologies and was acquired by Otto Bock in 2011.

Several applications are still under clinical evaluation since restoring gait is a more complex task than that accomplished with a foot drop stimulator [19].

1.8.2. Upper extremity

Superficial stimulators

Two commercially available neuroprostheses that provide functional improvement to the upper extremity are the H200 and the Bionic Glove. The Wireless H200 by Bioness is a superficial stimulator and orthosis that includes a control unit that can be carried in a pocket, bag or purse. The orthosis fits over the hand and forearm. The Bionic Glove, which started to be commercialized by Rehabtronics Inc. in 2015, is another superficial stimulator. The electrodes are located in the inner surface of a wristlet, and the stimulation is triggered by a wireless earpiece that detects toothclicks [119] or headnods [19]. A superficial FES called MyndMove is also commercially available, but has only therapeutic purposes [120].

Implantable stimulators

In terms of implantable neuroprostheses for the upper extremity, few devices are available. The Case Western Reserve University developed between the 1980s and the 1990s the Freehand system. It consisted in an implantable stimulator with leads that connected to 8 epimysial or intramuscular electrodes that provided lateral and palmar grasp [12]. The pulse generator was inductively powered using an external system. The device got the FDA approval in 1997, but it was discontinued in 2002.

Different devices are still under clinical trials, as the STIMuGRIP by Finetech Medical [121]. It uses epimysial electrodes wired to an implantable pulse generator. The device stimulates motor points in the forearm, by receiving commands from an external unit that is inductively coupled to the pulse generator.

1.9. Hypothesis and objectives

In this thesis we start with the hypothesis that it is feasible to implement addressable implants capable of performing neuromuscular stimulation based on rectification of HF current bursts. These HF currents that flow through the tissues by galvanic coupling could power up the implant. Since no coils, batteries or any bulky electronic component would be required to operate the implants, they could be integrated into a hybrid microcircuit or an ASIC, accomplishing miniaturization levels without precedents for electrical stimulators. This powering and electrical stimulation method (coined "eAXON method") would be an alternative to existing electrical stimulation methods.

The aim of this thesis is to demonstrate the hypothesis by developing and assaying implantable proof-of-concept prototypes which are made only of commercial off-the-shelf components. These implants are able to generate locally LF currents capable of stimulating excitable tissue. To accomplish this objective, the following contributions are proposed:

1. Design a microcontrolled implantable stimulator based on the proposed electrical stimulation method.
    - The electronic architecture should be capable of rectifying HF current to power up the electronics of the implantable device, and of reading information modulated on this HF current.
    - The device should include two matched current limiters for electrical stimulation.
    - The device should apply biphasic current waveforms and should include a charge-balance approach to avoid tissue damage in the electrode-tissue interface.
    - The implant must avoid passive tissue damage. To do so, the stimulator should be thin enough to be deployed in tissues by injection, and should be semi-rigid to settle down gently in tissues. Additionally, the device should include biocompatible materials that prevent corrosion and foreign body response.
2. Develop a communication system to power up and address the implants using the HF current bursts.
    - Design a communication protocol to address the implants, demonstrating that the eAXON method could not only power but also control a network of wireless microstimulators.
    - Explore the possibility of bidirectional communications to send information to the external system for closed-loop control.
    - Demonstrate that the proposed HF current bursts used for powering and communications are safe in terms of tissue heating and unwanted electrostimulation.

3. Demonstrate the feasibility of the proposed injectable stimulators *in vitro* and *in vivo*.
    - Demonstrate the capability of the system to power up wireless devices implanted in tissue using only galvanic coupling.
    - Demonstrate that the implantable devices can be addressed by the external system.
    - Demonstrate that the implants are able to stimulate excitable tissue, and that the delivered LF currents are charge-balanced.

This thesis will be limited to the development of an injectable device based only on commercially available electronic components. It defines the fundamentals for the future development of an ultrathin eAXON based on ASIC technology. The contributions of this thesis have been divided as follows:

- Chapter 2 describes the basic electronic architecture of the addressable neuromuscular stimulators, including the protocol used for downlink communication.
- Chapter 3 describes an add-on consisting of an active charge-balance approach.
- Chapter 4 describes an add-on for uplink communications, essential for the development of closed-loop controlled neuroprostheses.
- Chapter 5 describes the development of the addressable and injectable stimulator. The chapter reports the results obtained in *in vitro* and *in vivo* evaluations, demonstrating that the implants power up by galvanic coupling and perform controlled neuromuscular stimulation.
- Chapter 6 numerically demonstrates that the HF current bursts are safe in terms of unwanted electrostimulation and tissue heating. The chapter also includes finite element method simulations using high-resolution anatomical models to demonstrate that the external system can be portable.

CHAPTER 2

Basic electronic architecture

Abstract – The eAXON method is a powering and electrical stimulation method for miniaturized implantable stimulators. It proposes the use of implants as rectifiers of high frequency (HF) current bursts that are supplied by skin electrodes and flow through the tissues where the implants are located by means of galvanic coupling. This results in an unprecedented level of miniaturization since no bulky parts such as coils or batteries are included in the implant. It was previously demonstrated a charge-balance rectifier that performed electrical stimulation. However, this implantable rectifier could not be controlled externally, impeding independent stimulation of different target muscles. In here it is described a more complex system composed of addressable stimulators based on the eAXON method. We demonstrate that such addressable stimulators are feasible by developing and assaying circuit prototypes suitable for implantation. The main goal of this chapter is to describe the architecture of these prototypes. The electronic architecture was first evaluated in a simulation software. The results obtained showed that the circuit could be electrically powered by the rectification of HF current bursts and could passively balance the low frequency (LF) currents delivered for stimulation using a dc-blocking capacitor. After implementation with off-the-shelf components, the proof-of-concept circuit was *in vitro* evaluated by deploying one probe connected to a prototype into a 0.9% NaCl agar cylinder. The circuit was able to decode commands that were amplitude modulated on the HF (1 MHz) auxiliary current. Additionally, the rectified voltage obtained by the prototype circuit was enough to power all its electronics ($\geq$ 1.8 V). To evaluate the architecture's ability to perform electrical stimulation, two probes were percutaneously implanted in antagonist muscles of an anesthetized rabbit. The devices were capable of independently stimulating the target tissues by delivering charge-balanced LF current (~2 mA), accomplishing controlled dorsiflexion and plantarflexion joint movements. In short, it was demonstrated that addressable rectifiers based on the eAXON method are feasible.

Part of the contents of this chapter is adapted from the following publication:

L. Becerra-Fajardo and A. Ivorra, "In Vivo Demonstration of Addressable Microstimulators Powered by Rectification of Epidermically Applied Currents for Miniaturized Neuroprostheses," PLoS One, vol. 10, no. 7, p. e0131666, Jul. 2015.

2.1. Introduction

Nowadays, most implantable microstimulators rely on powering approaches that require bulky components such as coils and batteries, resulting in too stiff and bulky implants (Chapter 1, section 1.3). This hampers miniaturization, and impedes exploiting the full potential of the envisioned dense networks of microstimulators for treating paralysis. The eAXON method, a powering and electrical stimulation method that avoids the use of these bulky components, was proposed in [73]. It consists in the electronic rectification of high frequency (HF) current bursts that flow through the tissues by galvanic coupling (Chapter 1, section 1.4). To demonstrate the method, very simple implants were initially developed and *in vivo* tested [79] [111]. However, since the implant did not include any communications and control capabilities, the external system could not address them independently. This impeded their use in a network of single-channel microstimulators.

At first, a basic electronic architecture was proposed to accomplish these advanced addressable rectifiers [122]. In essence, it consisted of a bridge rectifier and a control unit that governed two current generators. This basic architecture was the starting point for this thesis. From here, different electronic and software architectures were developed and improved, including current limiters, a charge-balance approach, and communication capabilities [123] [124]. A final electronic architecture for addressable stimulators made of commercially available electronic components was proposed.

The aim of this chapter is to describe and evaluate these addressable circuit prototypes that rectify epidermically applied HF (1 MHz) current bursts for neuromuscular stimulation. These proof-of-concept prototypes are able to decode commands that are amplitude modulated on these innocuous HF bursts. The chapter includes a description of the basic electronic architecture of the stimulators, and *in vitro* and *in vivo* testing. For these evaluations, we have developed external proof-of-concept prototypes connected to a bipolar flexible probe which can be percutaneously implanted at the target of interest for experimentation.

2.2. Methods

The architecture of the circuit prototypes consists of five main blocks: 1- a demodulator for the communication system, 2- a regulation circuit, 3- a digital control unit (microcontroller), 4- two current limiters for electrical stimulation, 5- a Schmitt trigger that wakes up the control unit during stimulating bursts and 6- a switch that disconnects the bridge rectifier from the rest of the circuits.

Figure 2.1 shows the sign convention used here to define the voltage across the two stimulator terminals and the current flowing through it. This corresponds to the so-called *passive sign convention*. In here, the

cathodic current is defined as the current flowing from the negative to the positive terminal (i.e. opposite direction to the $I_{implant}$ current).

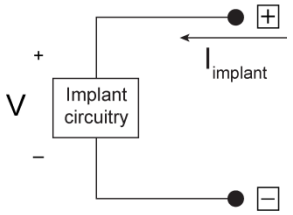

Figure 2.1. Sign convention used for the electronic architecture, based on the *passive sign convention*. Implant electrode 1 (Figure 2.3) is the positive terminal, while implant electrode 2 is the negative terminal. The current flowing through the implant enters by the positive terminal ($I_{implant}$).

2.2.1. Communications scheme

Amplitude-shift keying (ASK) is used to send data modulated on the HF auxiliary current. In particular, Manchester coding was selected in order to guarantee a constant average amplitude (as required by the ASK demodulator described below) and for self-clocking.

The modulated 1 MHz signals consist of three distinguishable active stages (Figure 2.2) of specific relative amplitudes to minimize tissue heating (explained in depth in Chapter 6). First, an 85 ms low amplitude unmodulated signal is used for the *Power up* stage. That is, for guaranteeing power up and stabilization of the whole circuitry and, in particular, of the microcontroller. The *Power up* stage is followed by a 600 μs *Synch&Data* stage in which the control unit synchronizes and reads the information sent on the HF current. This stage is composed of a sequence of 3 rising-edge transitions for synchronizing the decoder to the modulated signal and a 9 bit data stream (8 address bits and 1 parity bit). Bits are received at a baud rate of 25 kBd. After the *Synch&Data* stage, a 200 μs zero-amplitude slot is included for processing purposes. Processing tasks comprise decoding the information sent in the *Synch&Data* stage, checking parity bit, and comparing the decoded address with the programmed address to activate the device for stimulation. At last, an unmodulated signal of maximum amplitude is used for the *Stimulation burst* stage. It is during these bursts when LF currents (i.e. half-wave rectified ac current) flow through the circuit and neuromuscular stimulation is performed. The duration of these bursts (450 μs) is fixed in this study. The first 20 μs are employed for preprocessing purposes (control unit wake-up and power supply unit stabilization). Then, for 200 μs, rectified current flows through the circuit from the '-' terminal to the '+' terminal and, after a brief slot of 30 μs in which no rectified current flows through the circuit, rectified current flows from the '+'

terminal to the '-' terminal for 200 μs. Therefore, a biphasic symmetric pulse of 200 + 200 μs is applied to tissues with an interphase dwell of 30 μs. This interphase dwell is a short time delay typically used in electrical stimulation between the cathodic and anodic pulse that allows the propagation of the AP away from the stimulation site before the injected charge is recovered by the electrode [125].

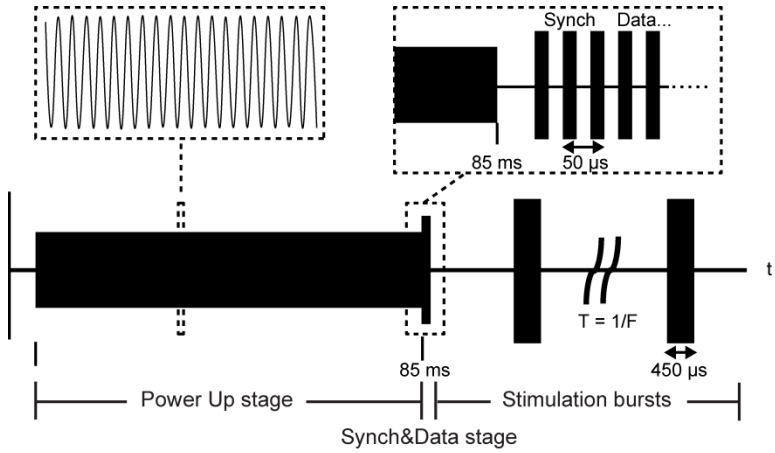

Figure 2.2. Representation of the ASK modulated voltage signal delivered by the external system and employed both for communications and for powering the circuit prototypes. It consists of three active stages: A) *Power up*, B) *Synchronization and Data*, in which a specific circuit prototype is addressed and thereby activated; and C) *Stimulation bursts* in which, for each burst, the activated circuit prototype delivers to tissues a biphasic symmetrical pulse of 200 + 200 μs with an interphase dwell of 30 μs.

It is only necessary to perform the *Power up* stage when initialization of the circuits is required. This is possible because the circuit enters a low power consumption mode (sleep mode) in-between *Stimulation bursts* and power is maintained by an internal capacitor (hereinafter 'sleep capacitor'). As a result, once initial power up has been performed at the beginning of a stimulation session, no further *Power up* stages are required if *Stimulation bursts* are continuously delivered at a sufficient frequency (F > 20 Hz). Similarly, the *Synch&Data* stage only needs to be performed each time a different circuit must be activated for stimulation. That is, once a specific circuit prototype has been activated (i.e. selected by means of the address contained in the *Synch&Data*) no further *Synch&Data* stages are required until another circuit must be activated or an initialization is required for all circuits (*Power up*). This strategy is crucial to minimize the amount of HF current flowing through living

tissues, therefore minimizing Joule heating and meeting safety standards (explained in depth in Chapter 6).

2.2.2. Electronic circuitry

The circuit prototypes were implemented using off-the-shelf components mounted on a pair of stacked rigid printed circuit board (PCB) breadboards (40 × 40 mm). The full electronic circuitry is explained below and is shown in Figure 2.3.

Power supply

A full-bridge rectifier implemented with Schottky diodes (MCL103B-TR by Vishay Intertechnology, Inc.) provides full-wave rectification of the ac voltage picked up by the implant electrodes. It is followed by a simple dc voltage regulation circuit consisting of a smoothing capacitor, a resistor and a zener diode. In-between *Stimulation bursts* the microcontroller, in sleep mode, is powered using a 47 µF capacitor (sleep capacitor).

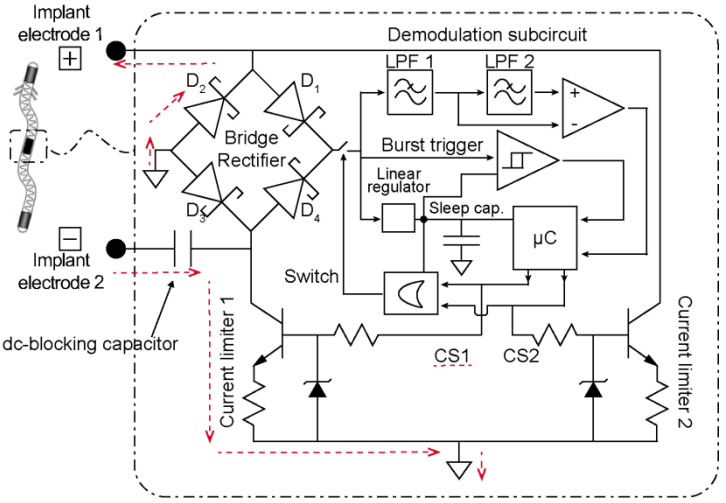

Figure 2.3. Architecture of the developed circuit prototypes for the stimulators. The dashed red line represents the flow of stimulating (half-wave) rectified current when control signal 1 (CS1) activates current limiter 1. If no current limiter is active, the bridge switch closes and the alternating current picked-up by the implant electrodes flows through the linear regulator to power up the rest of the electronics. A demodulation circuit is used to extract information from the HF bursts, and a burst trigger is used to wake up the control unit when it is asleep in-between *Stimulation bursts*.

Demodulation circuit

The demodulation circuitry consists of two RC low-pass filters (series combination of a resistor and a capacitor) and a comparator that process

the full-wave rectified signal from the implant electrodes (Figure 2.4). Low-pass filter 2 (cutoff frequency f_{C2} = 100.2 Hz) sets a threshold (amplitude average) that is compared to the signal filtered by the first low-pass filter (f_{C1} = 120.8 kHz > f_{C2}). The output of the comparator (single-supply amplifier AD8605 by Analog Devices, Inc.) is then digitally processed in the microcontroller for Manchester decoding.

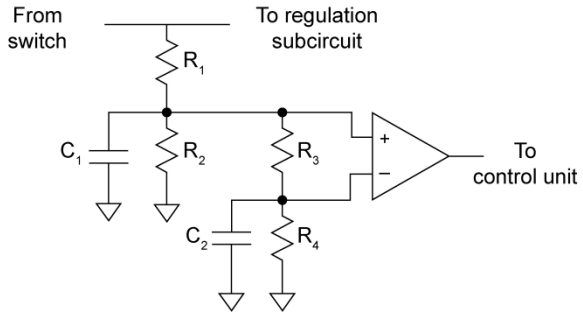

Figure 2.4. Demodulation circuit based on two low-pass filters. The combination of R_1, R_2 and C_1 (cutoff frequency = 120.8 kHz) generates a signal that is compared to a threshold established by the combination of R_3, R_4 and C_2 (cutoff frequency = 100.2 Hz). These two signals are compared using a precision, low noise operational amplifier.

Digital control system

Aiming miniaturization for implantation, a control system based on one of the smallest programmable devices was pursued. It was selected what nowadays appears to be the smallest commercially available programmable microcontroller: the ATtiny20 (Atmel Corp.). This integrated circuit is an 8 bit reduced instruction set computing (RISC) low-power microcontroller. One of its packaging options measures only 1.555 × 1.403 mm. It includes 10 input/output lines and software selectable power saving modes.

As depicted in Figure 2.3, two digital output lines of the microcontroller are used as control signals to switch on and off the two current limiters and serve as inputs for an OR gate (SN74LVC1G32 by Texas Instruments, Inc.) that enables/disables the bridge switch. A digital input is used as an external interrupt trigger to wake up the microcontroller when a new burst arrives. Another input is used for ASK demodulation.

The microcontroller of each stimulator circuit is programmed with a specific address of 8 bits. That is, only when the address received in the *Synch&Data* stream coincides with the programmed address, the prototype becomes active and stimulation is initiated.

Current limiters

As explained in Chapter 1, the delivery of current pulses in order to perform electrical stimulation may elicit electrochemical damage both to the electrodes and to the tissue [106]. To avoid this, most implantable stimulators use magnitude-limited biphasic waveforms that perform zero net-charge injection (i.e. the net dc component of the delivered current is zero). This has also been implemented here: the developed circuit prototypes include two independent current limiters that generate complementary cathodic and anodic pulses (i.e. biphasic symmetric waveform).

Each current limiter includes a zener diode that fixes a voltage in the base of a NPN transistor (Figure 2.3). This in turn fixes a voltage in the emitter of the transistor, defining a current flowing from the emitter to the resistor and ground. The circuit acts as a peak current limiter for the half-rectified HF current.

Bridge switch

During the stimulation stage, the full-bridge rectifier is disconnected from the rest of the circuits using a switch to ensure that the generated LF current (half-wave rectified HF current) flows through the tissues rather than into the circuit (Figure 2.3). The bridge switch architecture is shown in Figure 2.5. It is made up of one NPN transistor (Q_1) connected through its base to the collector of a second NPN transistor (Q_2). When the control unit enables the current limiters to deliver LF current for stimulation, it sends a digital signal to open the switch. This signal in R_2 (2 kΩ) polarizes transistor Q_2, forcing the current to flow through R_1 (10 kΩ), the collector and emitter of Q_2, the zener diode, ground, and back to the bridge rectifier and the implant electrode. The opened switch minimizes the flow of current through the bridge rectifier in the other half of the ac cycle, making the implant behave as a half-wave rectifier. When the control unit disables the current limiters, a digital ‘low’ in the switch control signal forces Q_2 to operate in the cut-off region. Therefore a small current flowing through R_1 forces Q_1 to operate in the forward-active region, and the full-wave rectified current from the bridge rectifier flows from the collector to the emitter of Q_1 to electrically power the circuits.

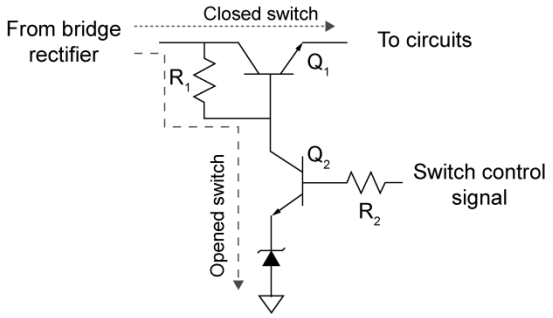

Figure 2.5. Electronic architecture of the bridge switch used to disconnect the implant circuits from the bridge rectifier during stimulation. When the control signals for stimulation are disabled, the switch closes, and the circuits receive the full-wave rectified current from the bridge rectifier. When the control unit enables the control signals to deliver LF current for stimulation, the switch opens, making the electronic prototype behave as a half-wave rectifier with current limiter.

Passive charge-balance approach

Since component tolerances, and in particular NPN transistors beta differences, can degrade matching between the two current limiters, some degree of unbalanced charge injection could appear. Because of this, a dc-blocking capacitor was included to perform passive charge-balance of the unbalanced currents delivered by the electronic prototypes. The cathodic phase of the biphasic waveform charges the capacitor in one direction. When the anodic phase is enabled, it forces the dc-blocking capacitor's discharge. If the injected charge of the first phase does not match the injected charge of the second phase, the remaining charge in the capacitor discharges passively through the implant and the tissues, compensating the injected misbalanced charge.

Wake up signal

To minimize the amount of average HF current that flows through tissues, the microcontroller is programmed so that it enters a power-down sleep mode in-between *Stimulation bursts*. For waking-up the device, the electronic architecture includes a custom Schmitt Trigger based on a low power comparator (NCX2200 by NXP Semiconductors) that triggers an interrupt whenever a *Stimulation burst* is delivered by the external generator.

2.2.3. Simulations

The circuit shown in Figure 2.6 was implemented to study and illustrate the behavior of the bridge switch, the dc-blocking capacitor and the voltage compliance of the electrical stimulator, using a SPICE simulator

freeware (LTspice IV, by Linear Technology Corp.). The stimulator circuit and a low-pass filter for LF current recording (explained below) are drawn in black, and a simplified circuit of the rest of the system (i.e. external generator and tissue impedances) is represented in gray. The electrodes of the circuit are represented with nodes '+' and '-', and their impedances are neglected for simplicity. The resistances were chosen to coarsely represent muscle tissue impedances for a 3 cm long implant according to finite element method simulations (not reported here).

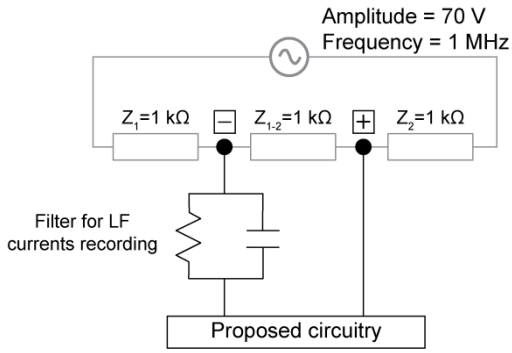

Figure 2.6. Setup used for SPICE simulations. The proposed circuit and a low-pass filter used for recording the low frequency components of the current delivered by the implant are shown in black, and a simplified circuit for the external generator and the tissue impedances is drawn in gray.

The LF components of the electric current flowing through the simulated circuit were obtained by recording the current flowing through an RC low-pass filter (Figure 2.6) connected in series with the proposed circuit. The simulated filter consisted of a 10 Ω resistance and a 2.2 μF capacitance (cutoff frequency = 7.2 kHz). This simulated filter corresponds to the actual filter later used in *in vitro* and *in vivo* tests.

2.2.4. External system

The external system used for the *in vitro* and *in vivo* evaluations consisted of three main concatenated parts: 1- a computer that generated the modulating signal in response to the commands and specifications indicated by the user on a graphic interface, 2- a carrier generator and modulator, and 3- a high voltage amplifier (Figures 2.7 and 2.8). The user interface was implemented as a LabVIEW (National Instruments Corp.) virtual instrument running in a PC. It encoded the information defined by the user and generated a Manchester coded data stream that was sent to a modulator via a data acquisition (DAQ) board (NI-USB6216 by National Instruments Corp.). This signal modulated a 1 MHz sinusoidal voltage carrier using a function generator (AFG3022 by Tektronix, Inc.). The

amplitude-modulated signal was amplified using a high voltage amplifier (WMA 300 by Falco Systems).

2.2.5. *In vitro* evaluation

Figure 2.7 shows the *in vitro* setup used to evaluate the electronic circuit described above. One bipolar probe was inserted in a 0.9% NaCl agar cylinder (A7002 by Sigma-Aldrich Corp.), and was connected to a circuit prototype. Two 15 mm wide aluminum foils separated 110 mm were strapped around the edges of the cylinder, and were connected to the external generator that delivered the amplitude modulated HF signal.

The bipolar probe consisted of a 1.17 mm diameter coaxial cable (Filotex ET087059 by Nexans S.A.) whose core conductor (silver plated copper covered steel wire of 0.17 mm diameter) was exposed for 3 mm at its distal tip. A 3 mm wide stainless steel ring of 1.3 mm in diameter was placed in contact with the shield conductor at a distance of 4.3 cm from the tip. This formed a probe made up of two electrodes at a distance of 4.3 cm on a flexible shaft. The proximal tip of the coaxial cable (~ 50 cm) was soldered to a bipolar jack connector that could be plugged into circuit prototypes. The distal electrode (at the tip) acted as the stimulation electrode whereas the proximal one, which is thicker, acted as the return electrode.

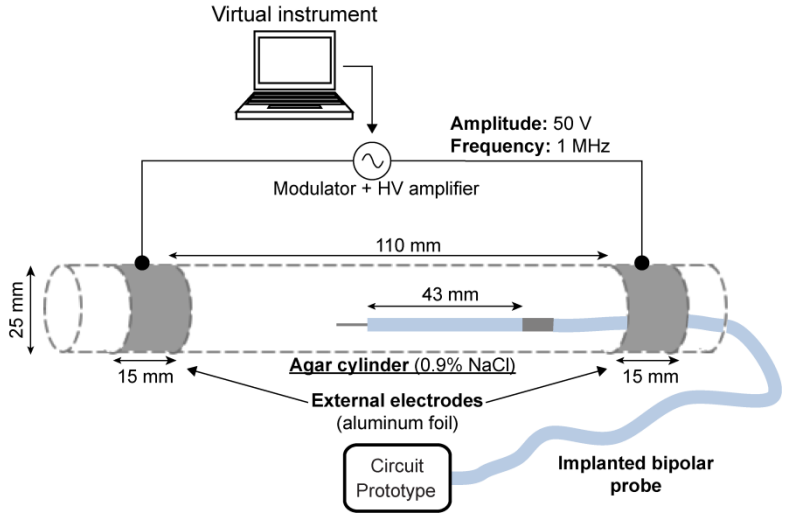

Figure 2.7. *In vitro* setup. One bipolar probe (Ø = 1.17 mm) was inserted into a 0.9% NaCl agar cylinder, and was connected to a circuit prototype. Two external electrodes strapped around the edges of the cylinder were connected to the external system delivering HF current. Electrical signals obtained with the circuit prototype were recorded using an oscilloscope.

A digital oscilloscope (TPS2014 by Tektronix, Inc.) with fully isolated and floating channels, and an isolated external trigger was used to record the voltage output of the regulation circuit (i.e. the dc current to power the digital electronic components), the output of the demodulator and the output of the wake-up trigger. The modulating signal generated by the external system was used for triggering acquisition.

2.2.6. *In vivo* evaluation

Animal handling

The animal procedure was approved by the Ethical Committee for Animal Research of the Barcelona Biomedical Research Park (CEEA—PRBB), application number: JMC 14–1606. One New Zealand White male rabbit weighting 4 kg was employed in this study.

For sedation and initial anesthesia Dexmedetomidine (0.9 ml), Butorfanol (0.45 ml) and Ketamine (0.45 ml) were intramuscularly administered. Then, prior to probe implantation and stimulation assays (later described), the left hind limb of the animal was shaved, from the head of the femur to the mid tarsus. During implantation and stimulation assays, anesthesia was induced by delivering Sevofluorane using an oxygen mask, Ringer's lactate was administered intravenously, a heating pad was employed, and the animal was constantly monitored with a capnograph and pulse oximeter.

Implantation procedure and experimental setup

In order to test the circuit prototypes *in vivo*, the motor point of the tibialis anterior (TA) and gastrocnemius (GA) muscles were located. The strategy is similar to the one proposed for the BION implants [47]. At first, the TA muscle was identified by palpation and the approximate site for deploying the implant (i.e. motor point) was located using anatomical cues Then, a 14 G intravenous catheter (Angiocath by Becton, Dickinson and Co.) was longitudinally introduced from a location close to the hock, up to the proximal end of the TA muscle. The stainless steel introducer needle of the catheter was used as an exploration electrode, and an Ag/AgCl gel electrode (model 2228 by 3M Co.) located on the thigh of the animal was employed as the return electrode. A custom made generator was used to generate conventional electrical stimulation with 2 to 5 V bipolar square pulses of 200 μs + 200 μs (cathodic first, no interphase dwell time) at 50 Hz. If the movement was considered not strong enough or did not match the expected dorsiflexion joint movement, the catheter was repositioned by pulling out or pushing in the catheter a few millimeters. Once the adequate motor point was located, the introducer needle was withdrawn. The same process was performed to locate the motor point of the GA muscle. Afterwards, two custom made bipolar probes were inserted in these catheters assuring that the distal tip (where the

stimulation electrode is located) was placed at the tip of the catheter. Finally, the catheters were pulled out and the probes were fixed to the skin using a hypoallergenic fabric bandage to avoid dislocation. Each one of these two probes was then connected to one of the circuit prototypes. The distance between the electrodes of these bipolar probes was fixed to 3 cm, as shown in Figure 2.8 B.

Figure 2.8-A shows the *in vivo* setup. The amplitude modulated HF current bursts generated by the external system was delivered across a pair of 3 cm wide textile electrodes made of silver-based stretchable conductive fabric (MedTex P-180 by Statex) strapped around the rabbit's hind limb where the bipolar probes were implanted. The signal amplitude was 50 V.

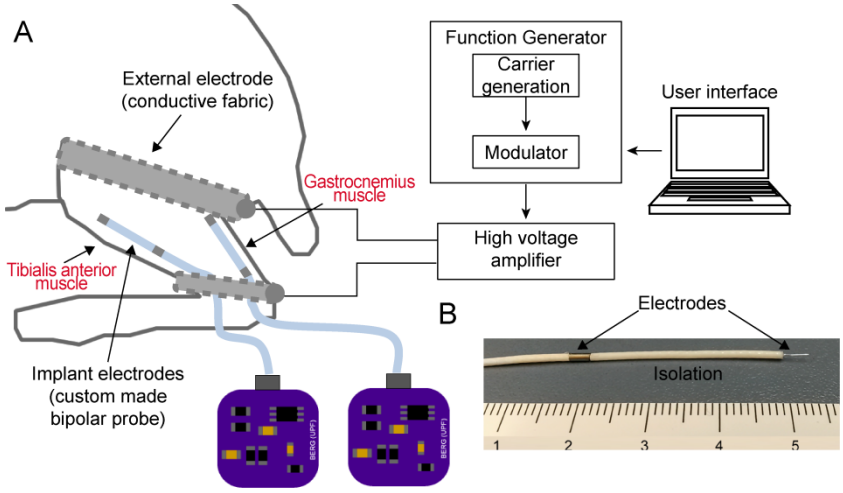

Figure 2.8. *In vivo* setup. A) External system consisting of PC, function generator and modulator, high voltage amplifier and textile electrodes; and two prototypes connected to two bipolar probes implanted in the tibialis anterior and the gastrocnemius muscles. The prototypes were capable of independently performing electrical stimulation of either muscle in response to the commands defined in the user interface. B) Picture of bipolar probe tip.

The LF components of the electric current flowing through a circuit prototype were obtained by recording with an oscilloscope (TPS2014 by Tektronix, Inc.) the voltage drop across the parallel combination of a 10 Ω resistor and a 2.2 µF capacitor (low-pass filter, cutoff frequency = 7.2 kHz) in series with the bipolar probe.

During stimulation assays, the number of *Stimulation bursts* and their frequency F was determined with the user interface of the external system. Isometric plantarflexion and dorsiflexion forces were recorded using a load cell (STC- 10kgAL-S by Vishay Precision Group, Inc.) mounted on a

custom-made acrylic board (Figure 2.9). The animal was positioned sideways, and using atraumatic padded clamps, its ankle was fixed to the board and its hind foot was tied to the load cell. This setup was inspired by the torque measurement setup developed by Riso et al. in [126]. A LabVIEW virtual instrument recorded the load cell signal at a rate of 10 kHz by means of a DAQ board (NI USB-6211, by National Instruments Corp.) through a custom developed signal conditioning electronics which included a first order low-pass filter with a cutoff frequency of 500 Hz.

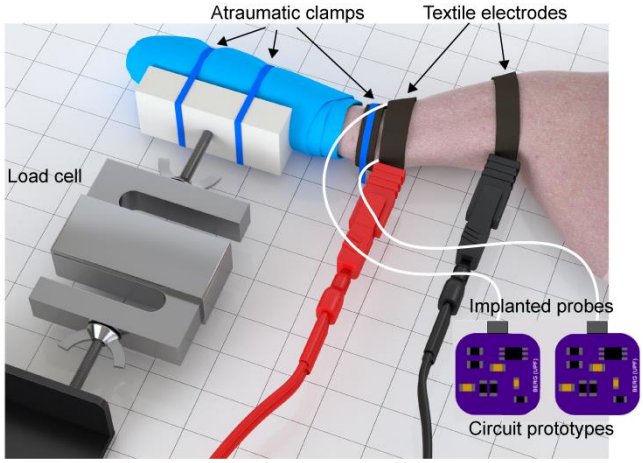

Figure 2.9. Force acquisition setup. The ankle of the animal was fixed to a horizontal surface and the foot was fixed to a load cell. Two textile electrodes strapped around the limb were connected to the high voltage amplifier in order to supply high frequency current to the tissues.

2.3. Results

2.3.1. Simulations

The microcontroller delivers two control signals (CS1 and CS2) to control the two current limiters and the bridge switch. These signals have a 'high' logic level that is equivalent to the operating voltage of the microcontroller. According to this, the results show that the voltage magnitude (Vcc) obtained by the regulation circuit is more than enough to operate the proposed microcontroller (Vcc = 3 V), the current limiters and the switch (Figure 2.10-C).

Figure 2.10 compares the behavior of the circuit when the bridge switch is operated. When control signal 1 (CS1 in Figure 2.3) is enabled, it forces the flow of one semi-cycle of the ac current through current limiter 1, ground, diode D_2 and electrode 1. However, since the control signal opens the switch during stimulation, the switch disconnects the cathode of D_1 from the rest of the circuits. This forces the current of the

other semi-cycle to flow through D_1, ground, D_3 and electrode 2. This makes the implant circuit behave as a peak current limiter for the half-rectified HF current (Figure 2.10-B).

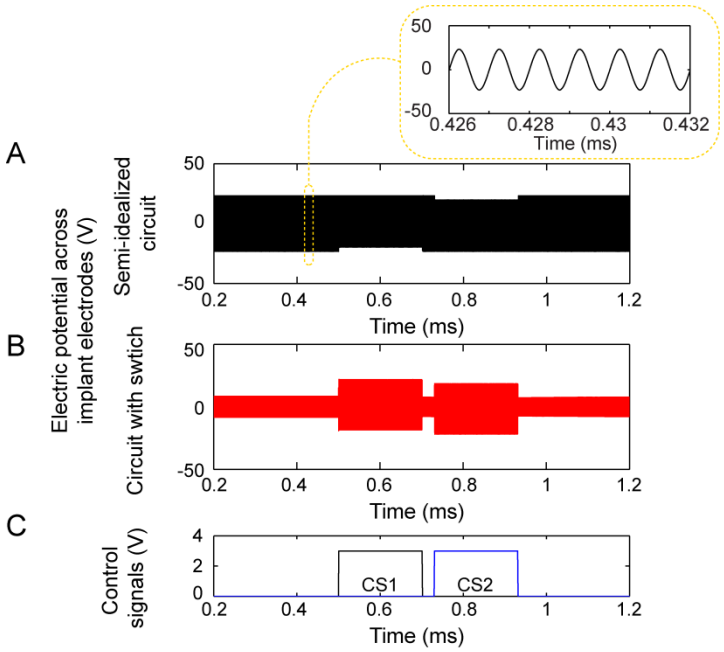

Figure 2.10. Effect of the bridge switch in the behavior of the stimulator according to simulations. A) Voltage across the implant electrodes in a semi-idealized circuit (only full-bridge rectifier, and current limiters). B) Voltage across implant electrodes in the complete electronic circuit proposed. The bridge switch makes the circuit act as a peak current limiter for the half-rectified HF current. C) Control signals delivered by the simulated control unit to open/close the bridge switch and perform stimulation.

Figure 2.11 compares the LF current for stimulation delivered by a circuit that lacks bridge switch, and one that does have it. The circuits are compared using the same ac input amplitude, and the same current limiters' configuration. Since the bridge switch makes the implant behave as a peak current limiter for the half-rectified HF current, the stimulator is much more effective delivering LF currents for stimulation.

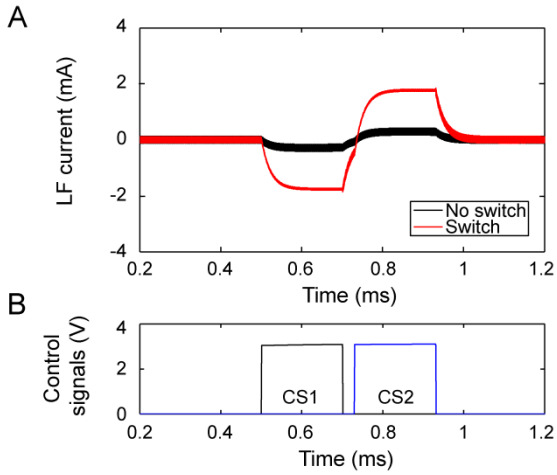

Figure 2.11. LF current injected by the circuit for electrical stimulation. A) The bridge switch makes the circuit behave as a peak current limiter for the half-rectified HF current, improving the efficiency of the stimulation. B) Control signals generated by the control unit.

As explained above, the electronic architecture proposed uses two current limiters to perform electrical stimulation. To test the ability of the circuit to behave as a peak current limiter for the half-rectified HF current, it was measured the maximum electric potential across the implant electrodes, and the average LF current delivered by the circuit during an anodic pulse. Figure 2.12-A shows the I-V characteristics obtained while varying the tissue load. As reported in [127], the circuit requires minimum 7.35 V across the implant electrodes for operation. From this amplitude, the I-V characteristics show that the current limiters will deliver LF currents with magnitudes between 1.8 and 2.3 mA. Figure 2.12-B shows the practical I-V characteristics of the current limiter when 9.3 V were measured across the implant electrodes.

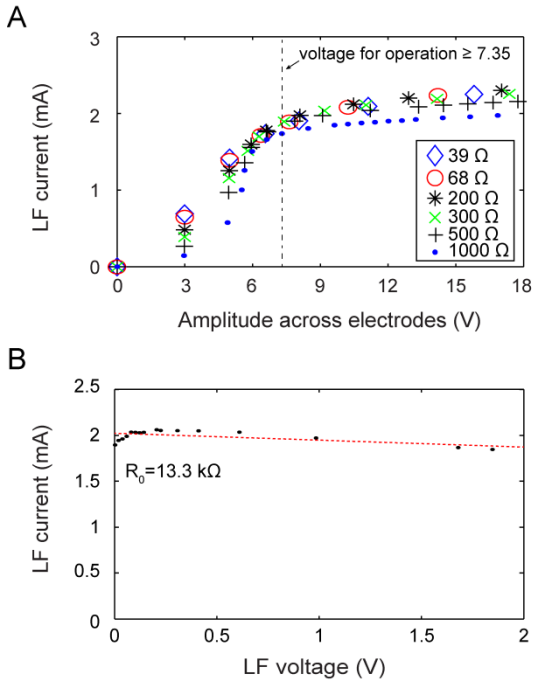

Figure 2.12. Behavior of current limiters. A) I-V characteristics of the current limiter for different tissue loads. B) Practical I-V characteristics for the current limiters when a HF voltage of 9.3 V is measured across the implant electrodes.

Since the dc-blocking capacitor is connected in series with the stimulation electrodes, and the circuit delivers biphasic waveforms, the capacitor charges in one direction during the first phase of the stimulation, and discharges in the other direction during the second phase of the stimulation. If the current limiters were matched, these two phases would accumulate zero net charge in the capacitor. However, if there is a mismatch between them, a certain amount of charge would be stored in the capacitor after the biphasic pulse. To accomplish charge-balance, this residual charge passively flows through the circuit and the tissues immediately after the biphasic pulse, when the external system is delivering HF current and the diodes of the bridge rectifier are forward-biased.

The first prototype included a dc-blocking capacitor of 10 µF to ensure voltage compliance. However, the time constant of the capacitor's discharge limited the frequency of stimulation and could promote tissue heating due to the long duration of the HF bursts that generates stimulation and allows the dc-blocking capacitor's discharge. Thereby, the dc-blocking capacitor was replaced with a 100 nF capacitor, improving the discharge speed while blocking dc current injection.

Figure 2.13 shows the results obtained by purposely mismatching the current limiters in three different simulations. When CS1 enabled the current limiter to deliver a cathodic pulse, a net charge accumulated in the capacitor (~ 0.4 μC). During the anodal phase, this charge was partly recovered (Figure 2.13-C). However, as the anodic current magnitude was larger than that of the cathodic current, the dc-blocking capacitor remained charged. Immediately after the anodal phase, the dc-blocking capacitor discharged through the circuit and the tissue. Figure 2.13-A shows the voltage across the dc-blocking capacitor during the stimulation, and its passive discharge. A time constant τ of approximately 103 μs was obtained for this circuit configuration. Figure 2.13-B and C show the delivered LF currents during stimulation and their calculated charge injection. The charge waveforms demonstrate that the dc-blocking capacitor is capable of passively balance the charge delivered during electrical stimulation.

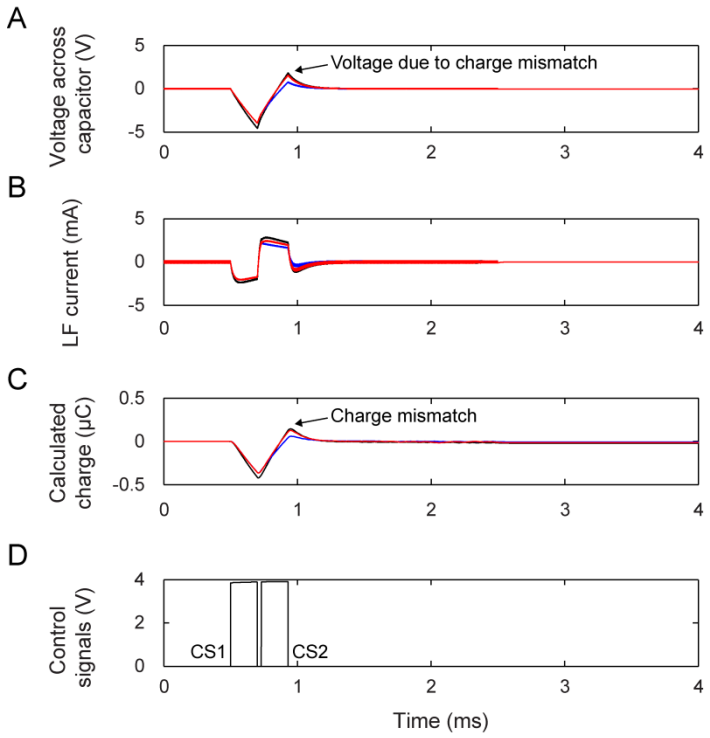

Figure 2.13. Simulated passive charge-balance using dc-blocking capacitor and three different current limiters' mismatches. A) Voltage across the capacitor during cathodic and anodic phases of the stimulation. The charge mismatch is compensated by the capacitor. B) LF current delivered for stimulation. C) Calculated charge injection. D) Control signals that enable the current limiters.

2.3.2. *In vitro* evaluation

Figure 2.14 shows the modulating signal generated by the external system, and the signal obtained by the demodulation circuit of the electronic prototype. The output of the demodulation circuit clearly shows the three stages of the communication protocol. The control unit was capable of reading the rising and falling edges of the *Synch&Data* stage. It synchronized the reading process using the 3 synchronization bits of the incoming data stream, and decoded the 9 bit data that included information about the circuit address and parity bit check.

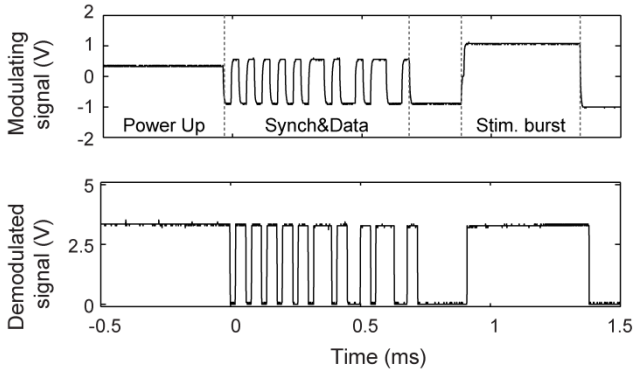

Figure 2.14. Results of the high frequency current modulation. Modulating signal (top) generated by the user interface through a DAQ, and its corresponding demodulated signal (bottom) obtained by the demodulation circuit of the electronic prototype. The three stages of the communication protocol are indicated.

After the reading process, the microcontroller used 200 μs for processing purposes. During the *Stimulation bursts* stage, the bursts trigger was able to wake up the microcontroller to start the stimulation. One biphasic symmetric current waveform was delivered in each stimulation burst.

Figure 2.15 shows the voltage across the sleep capacitor (i.e. input voltage of the control unit) when the "power down" sleep mode of the microcontroller was enabled or disabled in-between *Stimulation bursts*. The sleep capacitor fully charged during the *Power up* stage. It also charged during part of the bursts, in specific time frames in which the current limiters were not enabled and the switch was closed.

In-between bursts, the microcontroller and the wake-up trigger electrically fed from the component. If the microcontroller did not go to its "power down" mode (i.e. the sleep was 'off'), there was high power consumption, and the sleep capacitor discharged faster. This reduced the time that the device remained active, since the minimum operating voltage of the microcontroller is 1.8 V. In the particular case shown in Figure 2.15

(F = 100 Hz, pulse width = 200 μs), the microcontroller that did not enter to the "power down" mode would only stimulate in the first three bursts of the stimulation sequence. When the microcontroller was programmed to enter the "power down" mode, the power consumption was much lower, making the sleep capacitor discharge more slowly.

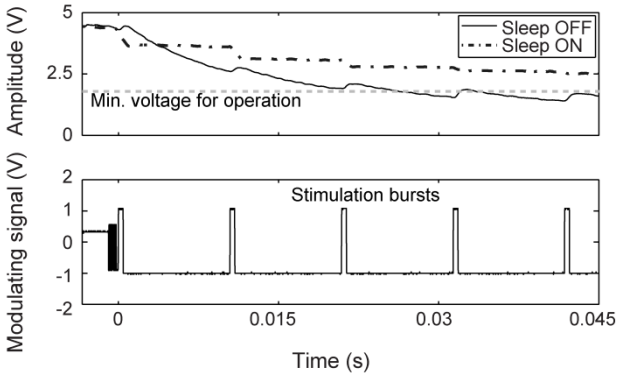

Figure 2.15. Regulated voltage obtained for powering the microcontroller during the *Stimulation bursts*, disabling/enabling the sleep mode of the programmable device (F = 100 . In-between bursts, the power consumption is reduced to keep the input voltage above the minimum operating voltage of the microcontroller (A = 1.8 V).

2.3.3.*In vivo* evaluation

Figure 2.16 shows a stimulation biphasic pulse as recorded *in vivo* using the low-pass filter described in section 2.2.3, and the injected charge as calculated by integration. It can be observed that the circuit was able to apply pulses with an amplitude of 2 mA. The control signals CS generated by the microcontroller are also depicted for reference. A slight charge mismatch was present at the end of the biphasic pulse, which was later passively balanced by the dc-blocking capacitor.

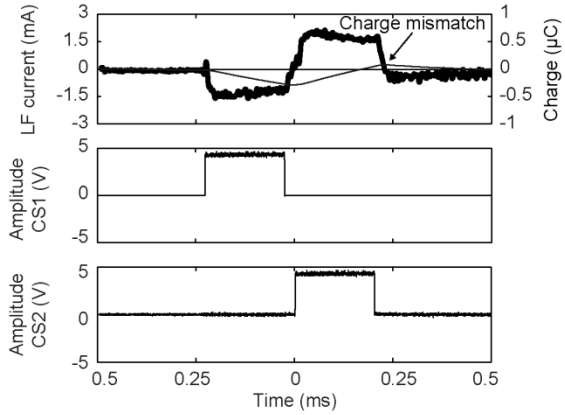

Figure 2.16. Low frequency current applied *in vivo* by a circuit prototype. Cathodic (negative) current was generated when control signal CS1 was activated whereas anodic (positive) current was generated when control signal CS2 was activated. A slight charge mismatch was present at the end of the biphasic pulse which was later passively balanced by the dc-blocking capacitor.

We were able to induce either plantarflexion or dorsiflexion forces at will by clicking one or another button on the user interface that governed the HF signal modulation. Figure 2.17-A shows a stimulation assay (F = 100 Hz, 30 bursts). First the circuit prototype connected to the bipolar probe implanted in the GA muscle was addressed and this generated a 1.9 N plantarflexion force on the load cell. Three seconds later, the second circuit prototype was addressed causing electrical stimulation of the TA muscle, and generating a 1.1 N dorsiflexion force. No force was exerted by the rabbit before, in-between or after triggered stimulations. This confirms that the circuits were capable of controlling the LF current for stimulation and that the system was able to address each circuit at a time.

Figure 2.17-B shows two trials in which the frequency of the *Stimulation bursts* (F) was increased from 40 Hz to 100 Hz while the duration of the biphasic pulse was kept constant. It can be observed that the force exerted by the foot on the load cell increased with the frequency of the bursts. That is, force modulation was not only possible by varying the amplitude of the pulses or their duration (results not shown here), but also by varying the repetition rate of the *Stimulation bursts*. This is a common observation in neuromuscular electrical stimulation when regular LF pulses are employed [128]. Therefore, this seems to indicate that the outcome of the currents generated by the devices (rectified HF current bursts) was equivalent to that of regular current pulses.

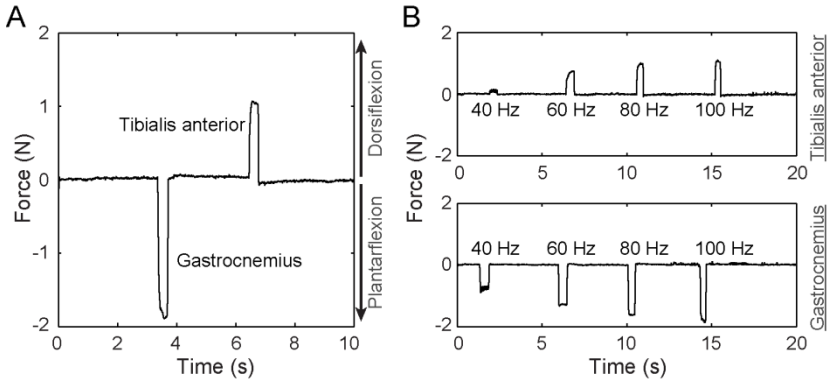

Figure 2.17. Force recordings. A) The addressable circuit prototypes were able to independently stimulate the gastrocnemius and the tibialis anterior muscles generating controlled plantarflexion and dorsiflexion joint movements. B) The magnitude of the force exerted during the muscle contractions was modulated by varying the frequency of the *Stimulation bursts*.

2.4. Discussion

In the eAXON method, the implanted microstimulators electrically rectify innocuous HF current bursts flowing through the tissues so that LF currents capable of stimulation are generated locally through the device. In their simplest form, those microstimulators can consist of just a diode and two peripheral electrodes. However, communications, and in particular addressability, are a requirement if multiple targets must be stimulated independently in a controlled manner.

Here it has been demonstrated that addressable microstimulators that are based on the eAXON method are feasible. A derived, but relevant, outcome of this demonstration is that it is possible to power digital circuits in implants by means of the eAXON method. In particular, here it was shown that the bridge rectifier and the regulator provided enough dc power to supply a circuit that included a microcontroller and a few operational amplifiers. Therefore, the eAXON method is capable of powering implantable devices that lack bulky components such as coils and batteries.

The current limiters make the circuit behave as a peak current limiter for the half-rectified HF current. By limiting the magnitude of these half-rectified HF current, the circuit is capable of controlling the muscle recruitment during stimulation independently of the magnitude of the HF auxiliary current across the implant electrodes.

If mismatches appear between current limiters, a dc-blocking capacitor is capable of recovering the charge by passively discharging through the circuit and the tissues. The discharge time constant fits within a HF stimulation burst, and does not affect the maximum frequency of

stimulation F delivered by the implants. This passive charge balance approach has an important drawback: typical dc-blocking capacitors used in stimulators need to be large as they must integrate the total stimulation current [129]. This impedes further miniaturization of microstimulators. For the ultrathin version of the eAXONs, it is suggested to use an active charge-balance approach in which the control unit knows how much charge is delivered to the tissues through the current limiters. In this way, zero net-charge injection could be more precisely accomplished. Chapter 3 describes one possible active charge-balance approach for these microstimulators.

It has been *in vitro* demonstrated that the modulating signal generated by the external system is demodulated and decoded by the implant circuitry. To avoid communication errors between the external system and the implant prototypes, it is suggested to improve the reading process in future firmware versions. For example, as the Manchester code is self-clocking, the reading process of the control unit can be resynchronized in every bit.

It has been also *in vitro* demonstrated that the power consumption of the circuit prototype in-between stimulating bursts is low enough to avoid the microcontroller's reset. Thereby, no initialization processes is required as long as the sleep capacitor delivers 1.8 V to the microcontroller.

In vivo assays have shown that the circuit prototypes are able to perform independent stimulation of agonist and antagonist muscles in the rabbit's hind limb. Moreover it has been observed that the stimulation behavior seems to be equivalent to the one that would be obtained using regular LF pulses. This was the case of the custom made generator used to locate the motor points of the TA and GA muscles.

More complex stimulation patterns would be needed to improve muscular stimulation. This implies activating the implants sequentially, synchronically, or in overlapping periods of time. The electronic architecture proposed in here may be able to include these stimulation capabilities; only significant differences would appear in the modulating signal of the HF current and in the control unit's algorithm.

The above *in vivo* demonstration has been achieved by applying an amplitude modulated HF (1 MHz) voltage across two textile electrodes strapped around the animal's hind limb. The auxiliary HF current conductively powers the circuit prototypes, conveys information (address of the circuit to be activated) and it becomes the stimulation current when it is rectified through the circuits.

The stimulation systems described up to this point are open-loop systems: preprogrammed stimulation patterns are executed on command. By implementing uplink communications (from the microstimulators to the external system), it is possible to conceive closed-loop systems in which the stimulation signals are modulated in response to measurements

performed with the implants. For instance, the level of muscle contraction (e.g. by measuring the myoelectric activity or the pressure) or the joint angles (e.g. by performing magnetic field goniometry) are data that could be employed for performing more natural muscle recruitment patterns [47]. Uplink communications are explored as add-on functionality for this basic electronic architecture (Chapter 4).

2.5. Conclusion

It has been demonstrated that addressable stimulators based on the eAXON method are feasible. The powering and electrical stimulation method proposed is realizable and the circuit prototypes can perform controlled electrical neuromuscular stimulation of muscles in a vertebrate model. The circuit is able to passively balance the charge injected during stimulation. Contraction force can be modulated by varying the frequency of the stimulation bursts.

CHAPTER 3

Active charge-balance approach

Abstract – Neuromuscular electrical stimulators deliver voltage or current pulses to artificially trigger action potentials to restore motor function. Most electric current flowing through the body is carried by ions, while that delivered by electrical stimulators is composed of electrons. This implies that electrochemical reactions may occur at the electrode-tissue interface in order to transform electronic current into ionic current. Byproducts of these reactions can damage the electrodes and the tissues. This jeopardizes the safety of the patient and the effectiveness of electrical stimulation. One common strategy to minimize electrode and tissue damage is by ensuring zero net-charge injection using biphasic current waveforms generated by symmetrical sources. However, possible mismatches may appear between phases. Therefore, in order to completely ensure charge-balance a dc-blocking capacitor is generally used. This strategy has been used in the electronic architecture for the wireless addressable stimulators proposed in Chapter 2. As the total charge must be integrated in the dc-blocking capacitor during stimulation, the component must have a minimum capacitance to ensure voltage compliance. This implies that the dc-blocking capacitor can be too bulky for applications in which miniaturization is a must. As an alternative, here we present an active charge-balance approach based on the use of a digital charge quantifier, whose operation is inspired in the functioning of the tipping bucket rain gauge. The system monitors the charge applied by the stimulator, matching the amount of charge injected during the second half of the biphasic pulse with the amount charge injected during the first half of opposite polarity, thereby generating a biphasic current waveform that adapts itself to possible current limiter mismatches. In here we demonstrate the viability of the method by developing and testing a proof-of-concept prototype built with discrete components. The small monitoring capacitor (100 pF in the demonstrated proof-of-concept prototype) and the electronic components that are used for monitoring and compensating the charge injection can be easily integrated in the ultrathin implants based on ASICs envisioned for the eAXON method.

Part of the contents of this chapter is adapted from the following publication:

L. Becerra-Fajardo and A. Ivorra, “Charge Counter for Performing Active Charge-Balance in Miniaturized Electrical Stimulators,” in 6th European Conference of the International Federation for Medical and Biological Engineering SE - 64, vol. 45, I. Lacković and D. Vasic, Eds. Springer International Publishing, 2015, pp. 256–259.

3.1. Introduction

When implantable electrical stimulators are analyzed, it is possible to identify two elements that contribute drastically to their volume: the energy source to power the electronics, and the charge-balance mechanism used to prevent deleterious electrochemical effects such as electrode corrosion and tissue damage [106]. This has been extensively explained in Chapter 1, section 1.5.

The eAXON method, the electrical stimulation method proposed in [73] and demonstrated in this thesis, overcomes the challenge of the energy source size. It has the potential to allow ultrathin and flexible devices that act as rectifiers of high frequency (HF) current bursts (Chapter 1).

Regarding the charge-balance mechanism, it is common to use biphasic stimulation pulses based on symmetric sources of opposite polarity. This is a straightforward approach, as most of the charge injected in the first phase of the stimulation is recovered in the second phase, restoring the original voltage of the electrode-tissue interface. However, mismatches between cathodic and anodic pulses may appear, forcing the use of complementary charge-balance approaches. A very common strategy consists in the use of a bulky dc-blocking capacitor which is passively or actively discharged after the delivery of the pulse. This capacitor needs to be large as it must integrate the total stimulation current [129]. In other words, as for a given charge the capacitance is inversely proportional to the voltage between its terminals ($C = q/V$), a large capacitance is needed to minimize the voltage drop across the dc-blocking capacitor to ensure the stimulator's voltage compliance [130]. This can drastically affect the volume of the device, making it inconvenient for implantable devices that must ensure miniaturization. This is particularly problematic in the case of devices performing parallel stimulation (multiple electrodes delivering stimulating pulses as in retinal prostheses), as one dc-blocking capacitor is needed per electrode [129].

To overcome these limitations, other passive, semi-active and active charge-balance approaches have been explored to avoid the dc-blocking capacitor [131]. One technique, for example, uses switched discharge resistors at the stimulating electrodes [132]. Yet, a drawback of this method is the switching circuit, as a high voltage may be needed to operate the switch, and in many applications the implant cannot provide this high voltage control signal.

The technique described above has an important disadvantage: during operation, the stimulator does not know if the electrodes have been fully discharged to accomplish charge-balance. To overcome this limitation, active approaches based on feedback controlled charge balancing techniques have been also proposed. One technique balances the anodic and cathodic current sources dynamically, and after the biphasic pulse, the

electrode is shorted to ground to ensure that any residual charge error left on the electrode is recovered [133]. Yet, this shorting period of 1 ms limits stimulation frequency. Another active charge-balance approach uses feedback digital-to-analog converter (DAC) calibration to match the amplitude of biphasic symmetric current pulses [134]. However, the calibration circuit relies in two sensing capacitors that can add charge injection errors due to component tolerances. Other active charge-balance approach uses negative feedback self-calibration mechanisms with only one sampling capacitor to match the amplitudes of the two current sources [130]. One last active charge-balance approach uses pulse insertion to compensate the charge of the residual voltage left on the electrode after stimulation [135]. This technique requires a continuous monitoring of the voltage at the stimulation electrode, which is not feasible in other circuit topologies.

In Chapter 2, an electronic architecture was proposed to demonstrate addressable devices based on the eAXON method. That architecture uses biphasic current waveforms and a dc-blocking capacitor to prevent electrode and tissue damage. However, such dc-blocking capacitors are too large for the envisioned ultrathin implants based on ASICs. In here we propose an active charge-balance method for the electronic architecture described in Chapter 2 that avoids the use of this bulky component. The method consists in a circuit that continuously adapts the pulse width of an anodal phase by monitoring the charge injected by its preceding cathodal phase. This is accomplished using a single monitoring capacitor (< 100 pF) that is automatically discharged multiple times during the stimulation pulses, quantifying the charge injected during electrical stimulation. Compared to other approaches for active charge-balance, the proposed method minimizes complexity and component count, and may offer higher robustness due to its semi-digital architecture. In addition, it uses a small capacitor that can be integrated into the ASIC, or can be included in hybrid microcircuits.

3.2. Methods

3.2.1. Electronic architecture

The electronic architecture described in Chapter 2 essentially consists of two independent current limiters which deliver low frequency (LF) currents. To that basic architecture it is added an active charge-balance mechanism that monitors the charge injection during the two phases of the waveform. This mechanism is intended to compensate potential mismatches between the two sources. It consists of the following stages: 1- to monitor the charge injected during the cathodal phase using a small capacitor (e.g. 100 pF), and then 2- to match this charge during a pulse-width-adapted anodal phase, generating an asymmetric biphasic

waveform. In other words, we propose a system able to quantize and match the amount of charge injected in every phase of the biphasic waveform, avoiding the use of large capacitors.

The active charge-balance circuit architecture (Figure 3.1) consists of a monitoring capacitor that charges when an independent current limiter is enabled (as in the tipping bucket rain gauge [136]). The voltage in the capacitor is compared to a pair of thresholds, to control the amount of charge injected by the current limiter. The output of this window comparator is connected to a switch that shorts the monitoring capacitor, inducing its discharge. The two thresholds of the comparator guarantee that the switch remains in a stable state even if the monitoring capacitor's voltage varies rapidly with time, preventing unwanted rapid switching.

The output of the comparator is also a charge counter signal that is read by the control unit. The microcontroller sums and compares the amount of times the monitoring capacitor is automatically discharged in every phase of the stimulation, matching the charge injected in the anodic pulse with that previously injected in the cathodic pulse.

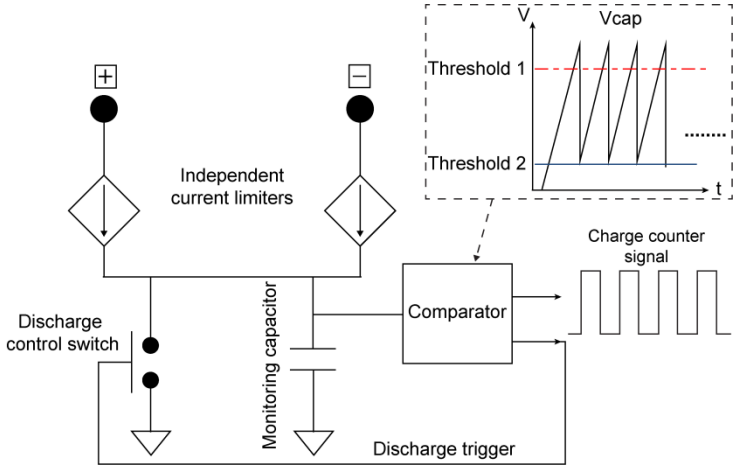

Figure 3.1. Proposed circuit architecture add-on for active charge-balance approach based on monitoring the electrical charge injection. The circuit automatically discharges a small monitoring capacitor, and generates a charge counter signal for the control unit. This unit quantizes and matches the amount of charge injected in every phase of the biphasic waveform, to accomplish active charge-balance.

The active charge-balance method proposed here is an add-on to the electronic architecture described in Chapter 2 (Figure 3.2). With this supplementary system, seven blocks can be identified in the architecture of the implant circuitry: 1- two electrodes that pick-up the HF current that flows through the tissues and that deliver LF currents for stimulation, 2- a full bridge rectifier and a regulation circuit, which electrically feed the

control unit, 3- an ASK demodulator, 4- a bridge switch that disconnects the regulation and the demodulator circuits from the bridge rectifier when the stimulating pulses are generated, 5- two switchable current limiters that generate biphasic currents, 6- a charge injection monitor consisting on a monitoring capacitor, a shorting switch and a counter/discharge signal, and 7- the control unit.

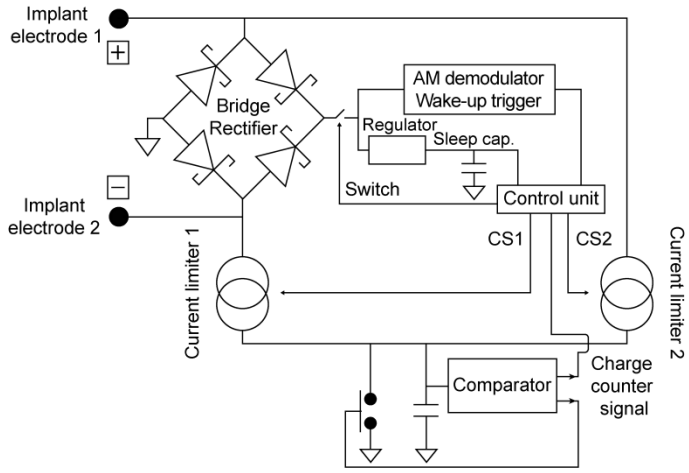

Figure 3.2. Circuit architecture proposed in Chapter 2 with the add-on active charge-balance approach based on a charge counter. The charge injection monitor controls the discharge switch and generates a counter signal that is read by the control unit. The control unit defines the duration of the anodic pulse according to the number of discharges generated by the charge monitor during the cathodic pulse.

3.2.2.Proof-of-concept demonstration

To implement the charge injection monitor, a dual precision operational amplifier (AD8606 by Analog Devices, Inc.) was used to generate the set and reset signals for the SR latch. The flip-flop was based on a couple of NOR gates with high speed switching characteristics (SN74LVC1G27 by Texas Instruments Inc.). The complementary output $\overline{Q}$ was used as a control signal for the shorting switch and as a counter signal for the control unit. Thresholds 1 and 2 (Figure 3.1) were set at 1.8 V and 1.2 V respectively. The discharge switch was designed using a NPN transistor (BC817−25LT1 by ON Semiconductor Corp.).

The proof-of-concept prototype was developed in a printed circuit board (PCB) breadboard using a 100 pF monitoring capacitor. The external system was configured to deliver HF bursts at a rate of 20 Hz. During each burst, the implantable device generates a biphasic asymmetric current pulse. At first, control signal 1 (CS1) activates a current limiter for 100 µs. This current limiter generates a cathodic current while charging the monitoring capacitor. During this pulse, the charge

counter circuit automatically discharges the monitoring capacitor, and generates a charge count signal that is read by the control unit. At the end of the pulse, the number of discharges is saved by the control unit to match it during the anodic pulse process. Between the cathodic and anodic pulse, an interphase dwell of 10 µs is included.

To generate the anodic pulse, the second current limiter is enabled by control signal 2 (CS2). The control unit reads the signal generated by the charge counter circuit, and matches the number of counts with that obtained in the cathodic pulse, therefore matching the charge injected by each phase of the stimulation.

The setup shown in Figure 3.3 was built to demonstrate the proof-of-concept circuit described above. The demonstrated circuit and a current probe for measurements are drawn in black and a simplified circuit for the rest of the system (i.e. external generator and tissue impedances) is represented in gray. The electrodes of the circuit are represented with nodes '+' and '-', and their impedances are neglected for simplicity. The resistances were chosen to coarsely represent muscle tissue impedances for a 3 cm long implant according to finite element method simulations (not reported here).

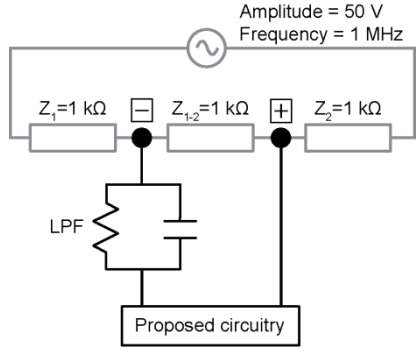

Figure 3.3. Setup for active charge-balance demonstration. The proposed circuitry is connected in series to a low-pass filter to record the delivered low frequency currents for stimulation. Muscle tissue impedances are coarsely represented by resistors.

To record the LF components of the currents delivered for electrical stimulation, the proposed circuit was connected in series to the parallel combination of a 10 Ω resistor and a 2.2 µF capacitor. This forms a RC low-pass filter (LPF) with a cutoff frequency of 7.2 kHz (Figure 3.3). The voltage drop across the LPF was recorded using a battery powered oscilloscope (TPS2014 by Tektronix, Inc.). The voltage across the monitoring capacitor, and the control signals that enable the current limiters were also recorded with the oscilloscope for offline evaluation.

3.3. Results

Figure 3.4-A shows CS1 and CS2, the control signals that enabled the current limiters to deliver cathodic and anodic current pulses respectively. The results show that the current limiters implemented were able to generate a LF current peak value of 2.7 mA in the cathodal phase and a peak value of 2.8 mA in the anodal phase.

The control unit generated a biphasic asymmetric current waveform, with a cathodic pulse duration of 100 μs, and an anodic pulse duration of 92.8 μs. The duration of this last pulse was adapted by the control unit in order to match the amount of charge injected by the first phase of the biphasic pulse.

In terms of the calculated charge injection, the circuit was able to inject over 0.22 μC in the cathodal phase of the stimulation (Figure 3.4-B). This charge was balanced during the anodal phase, as its pulse width was adapted using the charge counter circuit. The figure also shows the voltage across the monitoring capacitor, and its continuous charges and discharges. The number of discharges of the anodal phase matched those of the cathodal phase. A total of 40 discharges were recorded in every phase of the stimulating waveform.

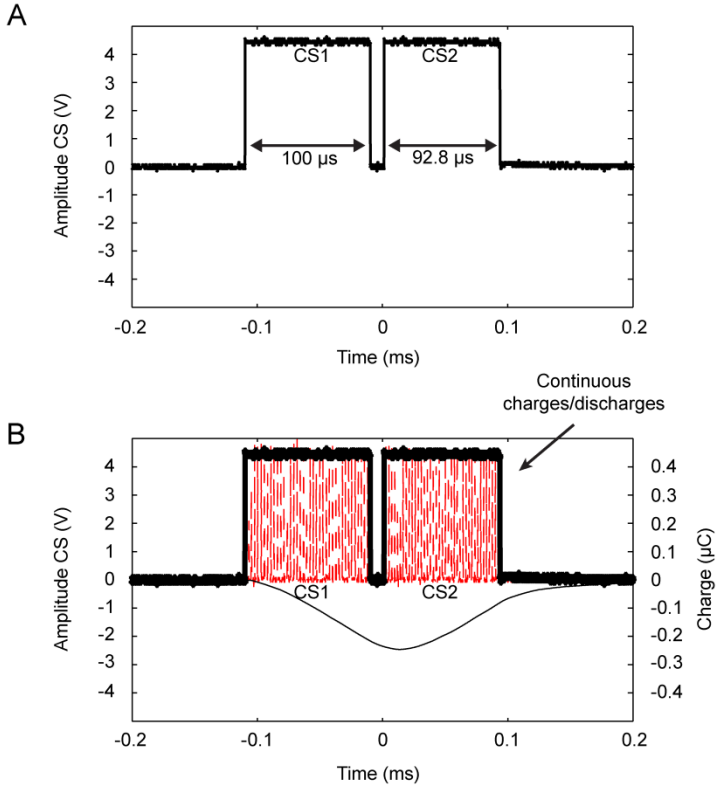

Figure 3.4. Proof-of-concept results. A) Control signal 1 (CS1) and control signal 2 (CS2). B) Calculated charge injection applied by the cathodic and anodic current pulses, and the continuous charges and discharges of the monitoring capacitor.

3.4. Discussion

Here we proposed and demonstrated an active charge-balance approach that avoids the need of large dc-blocking capacitors which are not easily integrated in ASICs. The proposed charge counter circuit is easily merged into the electronic architecture proposed for wireless addressable stimulators based on electronic rectification of high frequency current bursts – the eAXON method (Chapter 2).

It must be noted that in the proposed architecture the charge monitoring capacitor may act as a safety measure. If, for instance, the control unit fails and orders continuous delivery of LF current, this capacitor will block such delivery after a few microseconds. This increases tolerance to single fault conditions, which cannot be accomplished by other types of active charge-balance mechanisms.

The signals that control the switch that shorts the capacitor can be easily obtained by the rectified voltage acquired by the regulation circuit (Figure 2.1). This was a constraint when exploring other passive and

semi-active charge-balance mechanisms, as the discharge resistors at the stimulation electrodes proposed in [132].

The active charge-balance approach uses a capacitor to quantize the charge delivered during electrical stimulation. The monitoring circuit converts the charge accumulated in the monitoring capacitor into a digital signal that can be rapidly read by a control unit. This would not be possible using, for example, a shunt resistance. First, measuring current through this component would require an analog to digital conversion, which could be slower than the counter mechanism. Second, it does not offer the safety protection for single faults. And third, the capacitor is a much straightforward way to quantify the amount of charge injected during electrical stimulation, which is the main factor in charge-balance for preventing electrode and tissue damage.

The charge counter method demonstrated here is a useful method to accomplish zero net-charge injection in future ultrathin eAXONs. However, the approach is not very practical for the stimulators made of off-the-shelf components proposed in this thesis. The charge counter circuit is much more complex than the passive charge-balance approach based only on a dc-blocking capacitor (Chapter 2). The microcontrolled injectable stimulators aimed at in this thesis would require more discrete electronic components (other than the monitoring capacitor) that increase the implant's volume; and its development is much more complex due to the PCB routing and BGA package soldering. Additionally, some electronic components (e.g. microcontroller) are bigger than the dc-blocking capacitor, and so, the volume required for this passive charge-balance approach is not an inconvenient in this off-the-shelf components version. Hence, the active charge-balance add-on based on charge monitoring is suggested for the future ASIC architecture but it was not used in the injectable prototypes described in Chapter 5.

Chapters 2 and 3 have demonstrated two charge-balance approaches that accomplish zero net-charge injection. As explained in Chapter 1, electrode and tissue damage can be avoided by ensuring that all the charge delivered during electrical stimulation is recovered.

3.5. Conclusion

The active charge-balance approach proposed is able to quantify and match the amount of charge injected in every phase of the biphasic waveform, accomplishing zero net-charge injection. The method lacks large profile capacitors typical of dc-blocking capacitor methodologies, and can be easily integrated in the electronic architecture proposed for the ultrathin microstimulators based on the eAXON method.

CHAPTER 4

Bidirectional communications

Abstract – In the previous chapters it has been proposed and demonstrated a basic electronic architecture that works under the premise of electronic rectification of high frequency current bursts. This architecture includes advanced capabilities such as digital addressability. In here, we demonstrate that the proposed method also allows bidirectional communications between the implants and the external system that powers and governs them. This indicates that it will be possible to embed sensing capabilities that may be crucial for closed-loop neuroprosthetic systems. In the proof-of-concept prototypes developed here, it was implemented an uplink scheme based on amplitude modulation and Manchester encoding, in which the prototype delivers biphasic symmetric current pulses that are sensed by an external resistor. The obtained signal is filtered and processed by an electronic receiver. The results show that the proof-of-concept prototype is capable of sending information at a rate of 25 kBd, accomplishing a byte error rate of 6.7%.

Part of the contents of this chapter is adapted from the following publication:

L. Becerra-Fajardo and A. Ivorra, "Bidirectional communications in wireless microstimulators based on electronic rectification of epidermically applied currents," in Neural Engineering (NER), 2015 7th International IEEE/EMBS Conference on, 2015, pp. 545–548.

4.1. Introduction

Several efforts have been oriented to accomplish neural interfaces that are capable of performing distributed sensing and analysis of muscle activity, as well as neuromuscular stimulation. This would provide new resources to improve the diagnosis, treatment and management of neuromuscular related diseases and lesions.

We reported in Chapter 2 a basic electronic architecture for addressable wireless stimulators made of commercial components and based on the proposed eAXON method. These circuits were able to receive commands and generate controlled current pulses capable of stimulating the tibialis anterior and gastrocnemius muscle of an anesthetized rabbit. In other words, it was demonstrated that stimulation intensity control and downlink communications are feasible.

To use these addressable implants in a neural interface platform for closed-loop neuroprosthetic systems, it would be highly beneficial to include sensing features within the wireless implants. There are a few cases of microstimulators that include sensors [47]. BIONs have been an important development in this sense (Chapter 1, section 1.3.2) [24]. BIONs include sensing capabilities for biopotentials, pressure, temperature and angle/position [47]. These sensors can be used as the basis for an artificial proprioception system and to interpret commands from the patient. For instance, internal electromyogram signals can be sensed for detecting movement intention rather than employing an external joystick or a set of press buttons.

In this chapter we present a proof-of-concept prototype of a bidirectional communication link.

4.2. Methods

4.2.1. Uplink communications scheme

In Chapter 2, we presented the implementation of a downlink between an external system and the stimulators. We transmitted commands by means of amplitude-shift keying (ASK) using Manchester code, at a rate of 25 kBd on the auxiliary 1 MHz sinusoidal current. That is, the delivered high frequency (HF) current to power up the stimulators also included addresses and commands to control the devices. In response to those commands, the stimulators generated biphasic symmetric current pulses (200 + 200 μs) separated by an interphase dwell of 30 μs, at a repetition rate (i.e. stimulation frequency) defined by the external system that could vary between 40 and 120 Hz.

Figure 4.1 illustrates the external section of the uplink communication scheme proposed here. The external HF current generator is connected in series to a sensing resistor R_S, and to the external electrodes.

The implant electrodes pick up the HF current to power up the electronics and its control unit alternatively activates or deactivates the internal current limiters to generate a biphasic pulse at a frequency F_u. The activation of these current limiters causes an amplitude modulation of the rectified HF current across the implants which can be detected across the external sensing resistor R_S.

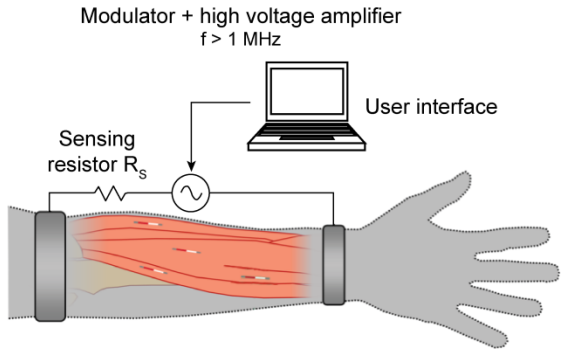

Figure 4.1. A sensing resistor R_S is connected in series with a high frequency generator for detecting the current signals generated by the implants.

In the proposed communications scheme, the frequency band for the ASK uplink must be low enough to differentiate itself from the auxiliary HF current used for powering an electrical stimulation; and high enough to avoid unwanted electrostimulation due to the delivery of LF currents [137]. Depending on their frequency of activation F_A, the currents generated by the implants could electrically stimulate motor neurons (F_A < 200 Hz), or could modulate the auxiliary HF currents for uplink that can be read in R_S (5 kHz < F_A < 100 kHz).

A constraint in the proposed bidirectional communication scheme is the possibility of causing electrochemical reactions at the electrode-tissue interface, which would cause electrode corrosion and tissue damage (explained in depth in Chapter 1) [17], [106]. These reactions are generally avoided using bipolar current pulses. The circuit's architecture proposed in [78] uses two independent current limiters that are able to apply biphasic symmetric current waveforms for stimulation. To perform uplink communications, we propose to use current waveforms with a half-phase period (HPT) of less than 50 µs (i.e. data rates ≥ 5 kBd) as shown in Figure 4.2. The proof-of-concept prototypes developed in this demonstration were programmed to perform uplink transmission using Manchester encoding at rates ranging from 5 to 25 kBd. These prototypes were implemented using the circuit architecture described in Chapter 2 [78], therefore the dc-blocking capacitor implemented in the

circuit as passive charge-balance approach protects the tissues if zero net-charge injection is not accomplished with the biphasic waveform.

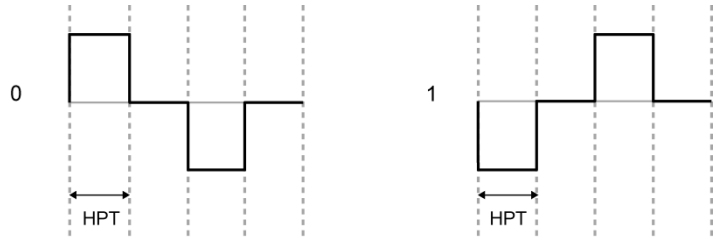

Figure 4.2. Schematic representation of bits '0' and '1' for the uplink. The circuit prototype generates biphasic symmetric pulses that ensures zero net-charge injection. The half-phase period (HPT) can range between 10 μs and 50 μs, corresponding to data rates ranging between 5 kBd and 25 kBd.

4.2.2. Receiver architecture

The external system used by the eAXON method (described in depth in Chapter 2) essentially consists in a signal generator that delivers amplitude modulated HF current (1 MHz). To read the information sent by the implant, here this generator is connected in series to a sensing resistor R_S (Figure 4.1). The LF currents generated by the circuitry of the prototypes cause a voltage drop across this resistor. An external receiver connected in parallel to the sensing resistor R_S (Figure 4.3) is triggered to capture, demodulate and decode this signal.

The architecture of the external receiver contains a RC low-pass filter that attenuates the HF components of the voltage. This low-pass filtered signal is captured by means of a data acquisition board (DAQ) and is digitally high-pass filtered so that low frequency interferences (e.g. power line) are attenuated. The signal is then transformed into rising and falling edges of the Manchester code, and an algorithm decodes these edges into '1' or '0' bits. A parity bit detector compares the parity bit sent by the circuit prototype against the parity bit calculated using the read data stream, to check for uplink errors.

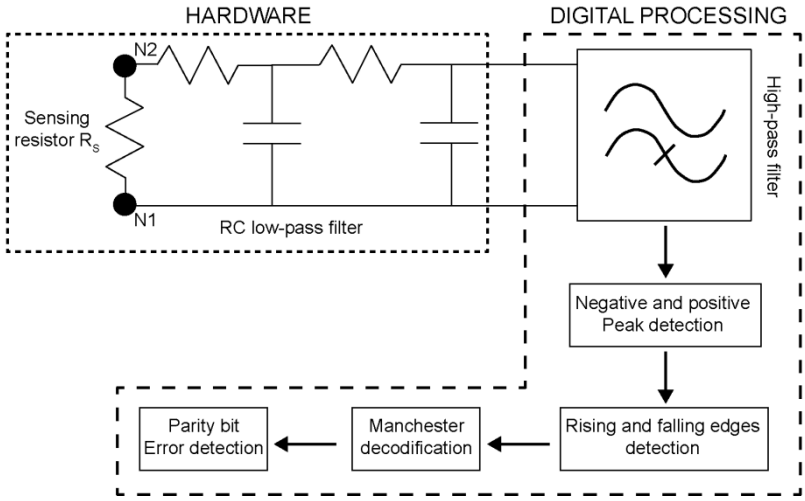

Figure 4.3. External receiver architecture. It consists of a hardware stage (sensing resistor R_S and a RC low-pass filter) followed by a digital processing stage (high-pass filter, peak detector, Manchester decoder and parity bit error detector).

4.2.3. *In vitro* demonstration

An *in vitro* setup was developed to demonstrate the capability of the system to perform bidirectional communications (Figure 4.4). An implant circuit prototype was connected to a custom-made bipolar probe which was inserted in a 2.5 cm diameter agar cylinder made from a 0.9% NaCl solution. The bipolar probe consisted of a 1.17 mm diameter coaxial cable (Filotex ET087059 by Nexans S.A.) whose core conductor was exposed 3 mm at its distal tip. A 3 mm wide stainless steel ring (Ø = 1.3 mm) was placed in contact with the shield conductor at a distance of 3 cm from the tip. The proximal tip of the coaxial cable was soldered to a bipolar jack connector that was plugged into the circuit prototypes.

The external generator and the sensing resistor R_S were electrically connected to the agar cylinder using two aluminum band electrodes that were placed at a distance of 12 cm. The whole external system consisted of: 1- a computer that generated a modulating signal for downlink communication and which performed the software tasks depicted in Figure 4.4 for uplink communication; 2- a function generator which generated a 1 MHz sinusoidal signal that was amplitude modulated using the modulating signal from the DAQ connected to the computer, and 3- a high voltage amplifier.

The sensing resistor R_S had a value of 100 Ω. This value was deemed to be low enough to avoid a high voltage drop, but high enough to allow the analog and digital processing of the uplink. The second order RC low-pass filter shown in Figure 4.3 was implemented using two 10 kΩ resistors and two 330 pF capacitors (cutoff frequency = 48.2 kHz). The

digital processing stage used a second order Butterworth high-pass filter with a cutoff frequency of 100 Hz. The sampling frequency of the DAQ was defined at 100 kHz.

The control unit inside the implant circuit prototype was configured to generate biphasic symmetric pulses (Figure 4.2) with a HPT value that varied from 10 to 50 µs in 10 µs steps, corresponding to data rates from a 25 kBd to 5 kBd respectively.

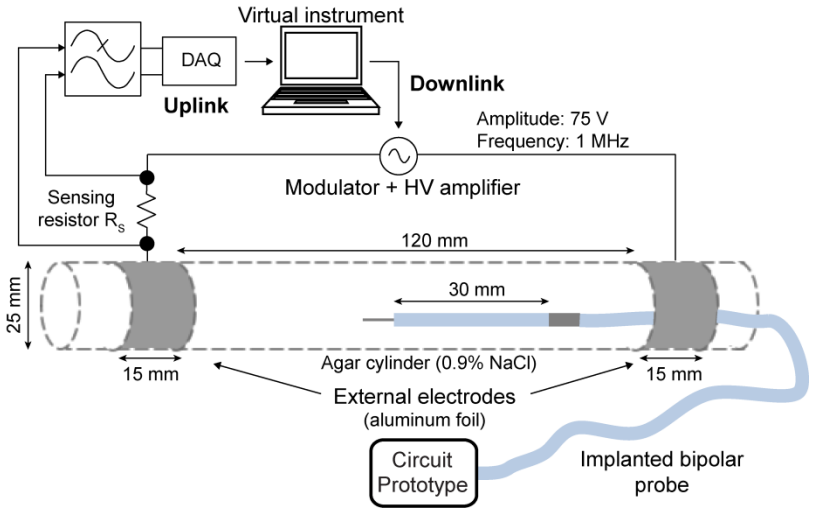

Figure 4.4. Experimental setup for bidirectional communications demonstration. The sensing resistor R_S is connected in series to the external system (modulator and high voltage amplifier) and to the external electrodes that are strapped around the agar cylinder. The external receiver filters the voltage across R_S, and an algorithm decodes the information and performs a parity bit error detection.

Both the modulating signal generation for the downlink communication, and the digital processing for demodulation and decoding in the uplink were implemented using a LabVIEW virtual instrument (National Instruments Corp.) running in a PC. It encoded a data stream of 8 bits and a parity bit, and sent this stream to the modulator using a DAQ board (NI-USB6216 by National Instruments Corp.). The 1 MHz carrier signal was generated and modulated by the function generator (AFG3022 by Tektronix, Inc.) and then amplified (WMA-300 by Falco Systems). The analog input of the DAQ board was used to acquire the filtered signal of the receiver for the uplink communication.

The demonstration trials consisted in using the virtual instrument to generate a byte, and sending it to the circuit prototype. Then, the circuit demodulated and decoded the information, and checked for errors using the parity bit. If there were no communication errors, the circuit prototype

sent the information back to the external system, and this information was demodulated and decoded by the external receiver (Figure 4.3). Finally, the decoded byte was compared to the originally sent byte.

The following section shows two sets of results: 1- those obtained using an external receiver implemented on a breadboard and the first version of the decoding algorithm (reported in [138]), and 2- those obtained using an external receiver implemented in a printed circuit board (PCB) and an upgraded version of the decoding algorithm.

4.3. Results

4.3.1. First prototype

An example of a filtered signal obtained by the DAQ is shown in Figure 4.5-A. The peaks identified by the demodulator are indicated with triangles. In this example, the control unit inside the implant circuit prototype was configured to transmit at a data rate of 6.25 kBd. Figure 4.5-B shows the demodulated bits obtained by the peak detection algorithm that runs in the virtual instrument.

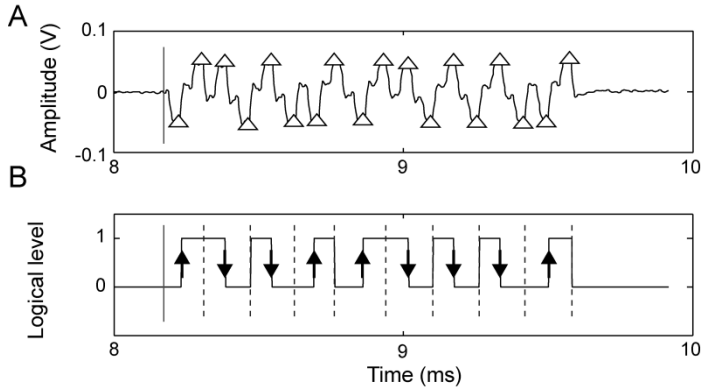

Figure 4.5. Example of signal demodulated at the external receiver. A) Filtered signal (data rate = 6.25 kBd). B) Rising and falling edge detection. The edges are indicated using up and down arrows, and correspond to the combination of local minima/maxima of the biphasic pulses generated by the circuit prototype.

Fifteen trials per half-phase period value were performed to evaluate the dependency of the demodulation and decoding methods proposed for the external system with the data rate used for the uplink. As the data rate increased from 5 to 25 kBd, the byte error rate (ByER) [138] increased from 0 to 33%. This was caused by the implemented external receiver rather than by the emitter: the receiver did not know the exact time when the prototype was sending information, and so, in multiple trials the receiver did not record parts of the data stream. Additionally, since the

filtered signal still had some HF noise, the local minima/maxima algorithm erroneously detected rising or falling edges, affecting the demodulation process. These drawbacks were solved by improving the triggering method of the receiver and the edge detection in the digital processing stage.

4.3.2. Upgraded external receiver

Having in mind the high byte error rate obtained with the demodulation method employed in the first prototype (reported in [138]), the uplink was updated to improve its efficiency. First, as stated in [127], the reading algorithm executed by the circuit prototype's control unit was upgraded to resynchronize in every bit. This minimizes the errors during the downlink, which is paramount for the bidirectional communications demonstration reported here. Second, the reading process of the external receiver was synchronized with the modulation process of the downlink. In this way, the uplink reading process would start when the modulating signal of the downlink process was modulated, avoiding losing data if the analog input of the DAQ board had reading delays. Third, the circuit prototype was programmed to perform the uplink transmission during the first and single burst of maximum amplitude delivered by the external system immediately after the *Synch&Data* communication stage (Chapter 2). This helped the uplink algorithm to identify when the uplink information was sent, without losing uplink bits. Furthermore, by establishing the start of the first burst as the trigger for the prototype's uplink transmission, the high amplitude burst time was reduced. This decreased the amount of HF current delivered to the tissues, minimizing the possibility of tissue heating during the uplink process. A fourth improvement was to reduce interferences by developing a PCB with ground plane for the external receiver hardware stage. This reduced the noise of the signal acquired by the DAQ board, and facilitated the decoding process.

The experimental setup shown in Figure 4.4 was implemented to evaluate the upgraded system. Figure 4.6 compares a signal, as obtained after the low-pass filter, using the first version of the external receiver (A), with that obtained using the upgraded receiver (B). An uplink data rate of 6.25 kBd was defined for both uplink processes. HF content is noticeable in signal A. This affects the peak detection algorithm, especially when higher data rates are used (e.g. 25 kBd). Additionally, the amplitude obtained in the upgraded receiver (signal B) is approximately half the amplitude of that obtained with the original receiver. This improves the efficiency of the system, since the high voltage amplifier must generate a lower HF amplitude than that required by the original uplink version.

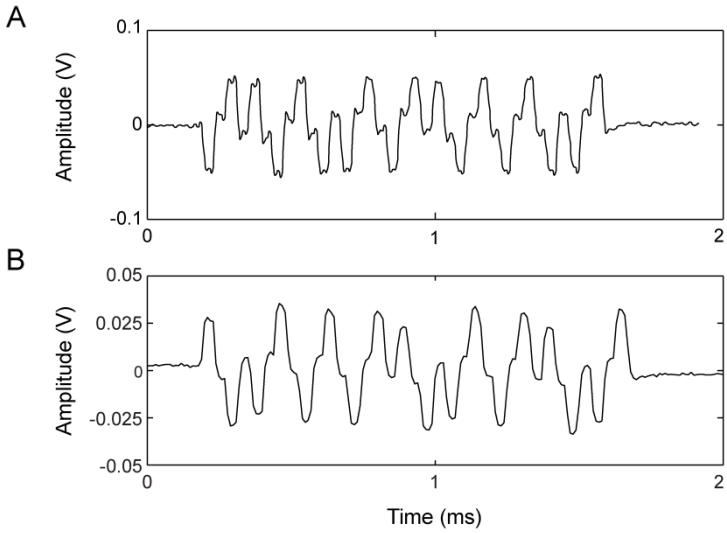

Figure 4.6. Comparison between A) signal resulting from the first external receiver and B) signal resulting from the upgraded external receiver. Both signals were generated by the implantable circuit prototype using a data rate of 6.25 kBd. The upgraded version has less noise content, improving the digital process.

Figure 4.7 shows a signal obtained with the upgraded receiver using a data rate of 25 kBd. All the positive and negative peaks, which correspond to '1' and '0' of the Manchester code, were detected by the receiver and marked with a triangle. The obtained filtered signal had an amplitude that was high enough for processing purposes (> 10 mV).

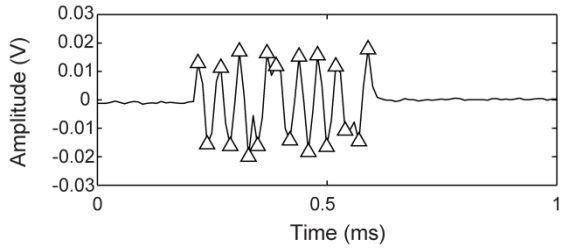

Figure 4.7. Signal obtained using the upgraded external receiver at a data rate of 25 kBd. Positive and negative peaks are detected by the algorithm, and decoding is performed accordingly.

The upgraded receiver improves the efficiency of the uplink process, as the byte error rate decreases significantly at high data rates. Table 4-1 compares the results obtained with the first and the improved uplink receivers. Fifteen trials were performed per HPT ranging from 10 μs to 50 μs at 10 μs steps (corresponding to data rates between 25 kBd and

5 kBd respectively). For the upgraded receiver, a byte error rate of 6.7% was accomplished for the 25 kBd rate, while a 0% error rate was accomplished for lower data rates.

Table 4-1. Results from trials with the first and the improved versions of the proof-of-concept external receiver

HPT (µs)	Data rate (kBd)	Byte error rate (%) for 15 trials	
		Original version	Improved version
10	25.0	33.3	6.7
20	12.5	6.7	0.0
30	8.3	0.0	0.0
40	6.3	0.0	0.0
50	5.0	0.0	0.0

4.4. Discussion

In the two *in vitro* evaluations presented here, we have demonstrated that it is possible to generate bidirectional communications for wireless microstimulators that are based on electronic rectification of epidermically applied HF current bursts – the eAXON method –. We have been able to send data from the external system to the implant circuit prototype (downlink), and then echo these data from the circuit back to the external system (uplink) using transmission rates ranging from 5 to 25 kBd.

We anticipate that the eAXON method will be able to provide much higher uplink data rates than those obtained in here. The data rate of both the first and improved uplink processes had to be limited by the maximum sampling frequency of the DAQ board and the speed of the control unit (i.e. microcontroller) of the implant circuit prototype that performed the echo task. This can be improved in the future ultrathin eAXONs based on ASICs.

The proof-of-concept system developed here for uplink demonstration may cause two phenomena that can be inconvenient in terms of safety: 1- tissue heating and 2- unwanted electrostimulation. Joule heating will occur because electric field bursts are generated in tissues by the implant during the data transmission. The duration of the burst depends on the data rate, while the number of bursts depends on the amount of bytes to transmit (in these demonstrations only one byte was transmitted). Therefore, tissue heating can be made negligible by limiting the half-phase period HPT used for the data transmission. The second phenomenon suggests further discussion: the proposed method uses the same waveforms to stimulate tissues and to transmit data and, therefore, unwanted electrostimulation could be expected to occur during uplink transmission. However, it is worth noting that the stimulation frequency is much lower than the uplink data transfer frequency. Hence, since the

threshold to elicit electrical stimulation in excitable tissues increases with frequency [137], the use of a much higher frequency for uplink communication avoids surpassing the threshold for electrostimulation. In other words, unwanted stimulation will be prevented by increasing the data rate (therefore increasing the current threshold for electrical stimulation). An alternative uplink communications scheme would avoid this issue: to simultaneously activate both current limiters so that load modulation is performed. In this case, the implant would not generate stimulation because no LF current would be injected into the tissues.

Bidirectional communications can be used, for instance, to test if the implantable devices are still functional (e.g. the device is effectively powered, can read information from the external system, and is capable of injecting LF current). However, it is far more relevant the possibility of adding sensing capabilities to the implant's electronic architecture to send information about the condition of the tissues and the neuromuscular stimulation process. For example, impedance measurement could be used to diagnose the electrode-tissue interface, while magnetic field sensors could be used to quantify the movement induced by neuromuscular stimulation. In this sense, the combination of sensing and uplink capabilities could enable the proposed implants not only to be used as stimulators, but also as wireless sensors for a neural interface platform. In this way, the miniaturized devices could detect movement intention for human machine interfaces [139]. This has been explored in motorized prostheses that are controlled with electromyography sensors implanted within the residual muscles of the patient [140]. Other approaches that can benefit from these devices consist in the control of prostheses using targeted muscle reinnervation (Chapter 1, section 1.7) [141]. Uplink capabilities could also enable a closed-loop control for a network of wireless microstimulators for neuroprostheses [142]. Adjusting the stimulation parameters using this feedback can represent a shift in the use of neuroprostheses, as it could improve functional benefit in the patient.

4.5. Conclusion

In here it has been demonstrated that the basic electronic architecture proposed for the implants in Chapter 2 is capable of modulating the auxiliary 1 MHz current coming from the external system, and this modulated signal can be read by an external receiver. Thereby, a wireless uplink connection can be created between the implantable circuits and external system. Trials were performed in which digital bytes were effectively sent to and echoed by the circuit prototype, demonstrating the bidirectional communication capabilities of the proposed system.

The wireless bidirectional communication system presented here is a first step towards the conceived concept of network of wireless microstimulators based on electronic rectification of HF current bursts.

With sensing capabilities, the wireless microdevices pave the way to the development of closed-loop neuroprosthetic systems.

CHAPTER 5

Injectable 2 mm thick microcontrolled stimulator: development and assays

Abstract – In Chapter 2 an electronic architecture for addressable rectifiers based on the eAXON method was proposed. All the electronic circuits that make up the addressable rectifier were described and evaluated. This electronic architecture paves the way to the development of ultrathin (Ø < 0.5 mm) addressable microstimulators based on application-specific integrated circuits (ASICs). Here we demonstrate that injectable and addressable stimulators based on this electronic architecture are feasible. To do so, we developed 2 mm thick cylindrical devices made of off-the-shelf components mounted on a rigid-flexible printed circuit board. The devices were enclosed in a silicone tube with two stainless steel electrodes at opposite ends. The injectable devices were tested *in vitro* to illustrate how they are powered by galvanic coupling. The implants were able to operate (e.g. power up, read and decode information modulated in the auxiliary HF current and enable the control signals for electrical stimulation) even if they were tilted 45º with respect to the delivered electric field. Additionally, the implants were tried in an animal model to demonstrate their ability to perform controlled electrical stimulation. They were deployed by injection into an antagonistic pair of muscles of an anesthetized rabbit using a 10 G catheter. Two textile electrodes were strapped around the animal's hind limb and were connected to the external system that delivered the high frequency current bursts for stimulation. The devices were addressed from the external system resulting in independent isometric contractions. Low frequency currents of 2 mA were delivered by the implants, inducing forces of ~ 1.2 N.

The content of this chapter is adapted from the following manuscript submitted for publication:

L. Becerra-Fajardo, M. Schmidbauer, and A. Ivorra, "Demonstration of 2 mm thick microcontrolled injectable stimulators based on rectification of high frequency current bursts," Under review, 2016.

5.1. Introduction

In Chapter 1 we described a novel powering and electrical stimulation method based on electronic rectification of epidermically applied HF current bursts that we coined “the eAXON method”. The method has the potential to accomplish a miniaturization level without precedents for implantable medical devices since the implants lack typical bulky parts as coils (used for inductive coupling) and batteries. The implants consist only of electronic components that can be implemented in a single integrated circuit or hybrid microcircuit connected to two electrodes at opposite ends of a flexible body.

We have already *in vivo* demonstrated flexible injectable devices (Ø = 1 mm) composed of a few passive components and which are capable of performing charge-balanced local electrical stimulation (Chapter 1, section 1.6) [111]. However, these simple stimulators lack a mechanism to independently address them. This feature is required if multiple devices are to be deployed to perform complex stimulation patterns for movement restoration.

In Chapter 2 we proposed a basic electronic architecture for addressable wireless stimulators which operate using the proposed eAXON method. Here we report the development and evaluation of microcontrolled injectable stimulators based on that electronic architecture. The implants are made only of commercially available components mounted on a rigid-flexible printed circuit board (rigid-flex PCB) which is housed in silicone tubing with two stainless steel electrodes at opposite ends. Their elongated body is capable of picking up enough HF current to power up their electronics and deliver currents capable of neuromuscular stimulation; and they are sufficiently thin to be deployed by injection (Ø = 2 mm). The injectable devices can be considered as low-cost intermediate proof-of-concept prototypes towards ultrathin (Ø < 0.5 mm) addressable implants based on application-specific integrated circuits (ASICs). To the best of our knowledge, the assayed implants are not only the first injectable and controllable devices based on off-the-shelf components but are also the first injectable devices powered only by galvanic coupling.

5.2. Methods

5.2.1. Electrical stimulation system

The stimulators consist in a narrow, elongated and semi-rigid tubular implant (Figure 5.2). The cylindrical structure houses an electronic circuit based only on off-the-shelf components. The circuit architecture and operation was detailed in Chapter 2 [78]. Figure 5.1 shows a simplified diagram of this architecture. Briefly, the implant electrodes pick up a portion of the HF current for powering the circuitry through a bridge

rectifier. A regulator circuit stabilizes the output from the bridge rectifier and supplies it to a digital control unit (CU), consisting in a microcontroller, and the rest of electronics of the implant. An amplitude demodulator extracts information from the same HF current, and sends it to the CU, which drives two current limiters that generate through the implant LF biphasic symmetric waveforms for stimulation. During these stimulation pulses, the bridge switch disconnects the regulation, demodulation and the wake-up trigger circuits from the bridge rectifier. In-between stimulation bursts, the CU is kept in a sleep mode to reduce power consumption so that it can be kept powered from the charge stored in a "sleep capacitor". When a burst is detected by the circuit, a wake-up trigger is generated and the CU activates to perform stimulation.

A few electronic components used in the external prototype described in Chapter 2 were replaced to ensure miniaturization. For example, the NPN BJT transistors were replaced with transistors that had a much smaller packaging (PBSS2515MB by NXP Semiconductors N.V.). The Schottky diodes were also replaced with smaller diodes that had a lower forward voltage (NSR02F30NXT5G by ON Semiconductor). As a result, the stimulator's CU activated with a lower voltage drop across the implant electrodes, improving the system's performance. The CU of the implantable stimulator still consists in the 1.555 × 1.403 mm ATtiny20 (ATTINY20-UUR by Atmel Corp.). It is an 8 bit, low-power microcontroller with software selectable power saving modes, critical to ensure that the device remains in a low-energy consumption mode in-between HF bursts.

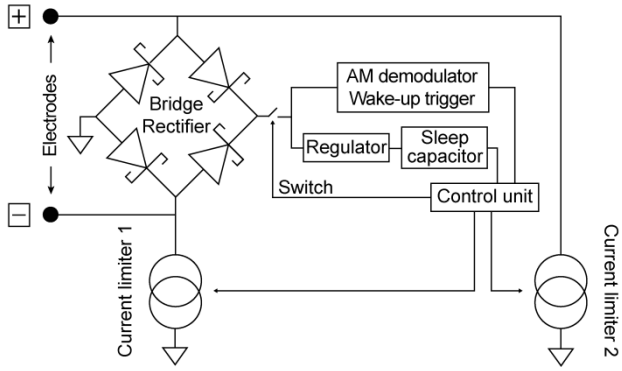

Figure 5.1. Simplified circuit architecture of the injectable stimulator. The complete circuit architecture is described in Chapter 2.

The components were assembled by soldering on the top and bottom layers of a 1.5 × 45 mm rigid-flex PCB manufactured under the IPC-6013 Type 4 specification (L. A. B. Circuits S. A.). This PCB was made up of 6 layers consisting of 2 sets of 2 layers of copper on a rigid substrate,

separated by 2 layers of copper placed over a flexible polyimide. To ensure flexibility, the PCB was divided in three rigid sections (average length of 13.7 mm) divided by two flexible sections (length = 2 mm).

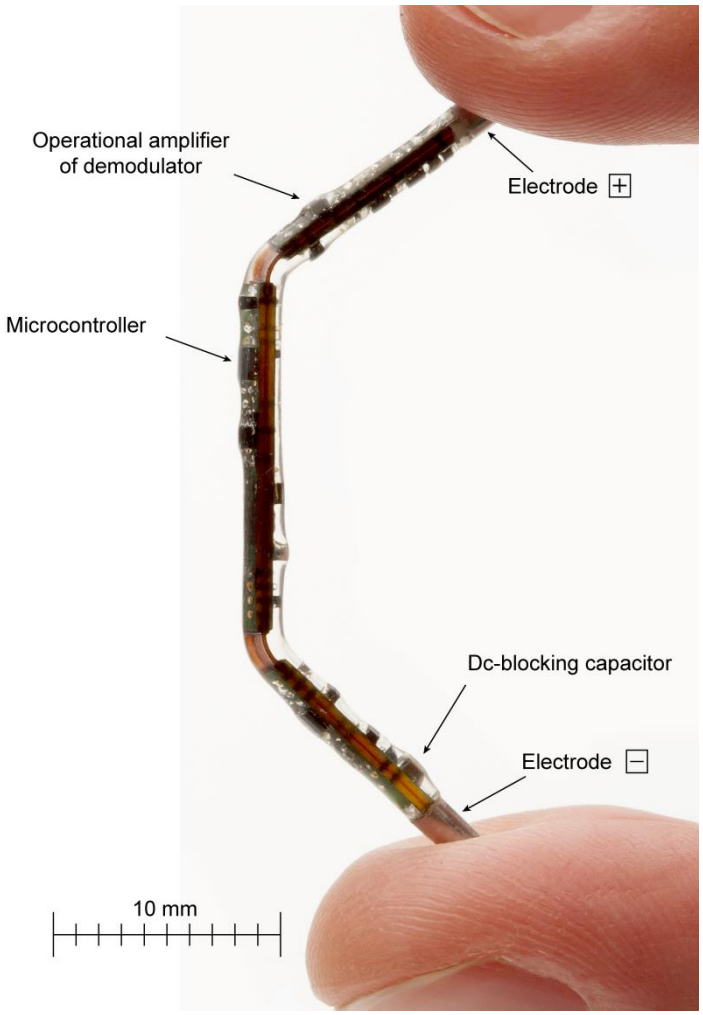

Figure 5.2. Microcontrolled injectable stimulator (Ø = 2 mm). The off-the-shelf components are soldered on a rigid-flexible PCB, and are enclosed in a silicone tube with two stainless steel electrodes at opposite ends.

The assembly process for the injectable stimulators, shown in Figure 5.3, can be summarized as follows. 1- Two components with ball grid array (BGA) packaging were soldered in an oven using the solder reflow temperature profile indicated by Atmel Corp. for the microcontroller. 2- The rest of the components were soldered using a

soldering iron, tweezers and a microscope. 3- The assembled circuit was gently inserted in a platinum cured silicone tube (721048 by Harvard Apparatus) that has a 1.9 mm outside diameter. 4- The tube was filled with a biocompatible silicone (MED-6015 by NuSil Technology) which has low viscosity when uncured. Each end of the PCB included a copper pad for the electrode assembly. After curing the silicone, the excess of silicone on the pads was removed to guarantee good electrical contact. 5- Using conductive epoxy (CW2400 by Chemtronics), the two copper pads were cold soldered to the inner end wall of 2 mm diameter stainless steel closed-end tubes cut to a length of 3.8 mm (Beijing ShengRuiKe Automation Equipment Co. Ltd). 6- Any empty spaces left by the epoxy in the pad-electrode union were filled with silicone.

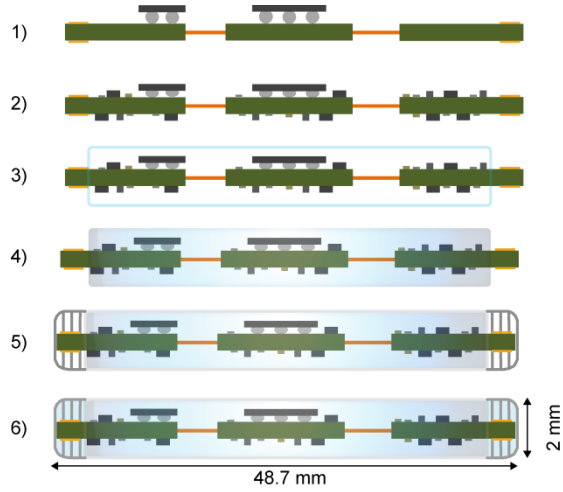

Figure 5.3. Assembly process for the injectable stimulators (not to scale). 1- The ball grid array components are first soldered using an oven. 2- The rest of the components are manually soldered. 3- The device is gently inserted in a silicone tube, and 4- is filled with silicone. 5- Electrode pads are cleaned and stainless steel electrodes (cups) are glued to them using conductive epoxy. 6- Silicone is injected in the empty spaces beneath the electrodes.

The external generator (Figure 5.4), including the hardware and the communication protocol, was described in depth in Chapter 2 [78]. In short, a computer generates a modulating signal using a data acquisition (DAQ) board. This signal modulates a 1 MHz sinusoidal voltage carrier, and the modulated signal is amplified and delivered across the target tissue using a pair of electrodes. For the *in vitro* assays, these electrodes consisted of aluminum plates. In the case of the *in vivo* experimentation, the external electrodes consisted of 3 cm wide bands made of silver-based

stretchable conductive fabric (MedTex P-180 by Statex) strapped around the rabbit's hind limb, as shown in Figure 5.8.

The communication protocol is also described in Chapter 2 [78]. The transmitted signal consists of a *Power up* stage, in which the circuit is powered and stabilized; a *Synch&Data* stage used for synchronization and for transmission of data (8 address bits followed by 1 parity bit) at a baud rate of 25 kBd; and the *Stimulation bursts*, a stage used to wake up the CU and perform the biphasic symmetric waveform for stimulation (e.g. 200 μs + 30 μs + 200 μs). The modulating signal uses Manchester coding, which offers two important advantages: 1- has no dc component, as required by the external system to avoid charge injection with the HF auxiliary current and 2- a clock signal can be recovered from the encoded data. This self-clocking feature allows that, during the decoding process, the CU resynchronizes in every bit.

5.2.2. *In vitro* setup to characterize dependence on implant orientation angle

The implant picks up a portion of the HF current and rectifies it internally to generate a dc voltage for powering its circuitry. This implies that a minimum voltage drop must be obtained across the implant electrodes for operation. Perfect alignment between the implant axis and the HF electric field would accomplish the maximum voltage gradient between electrodes. However, this ideal scenario may not be possible for two reasons: 1- physical implantation constraints and 2- relative rotation of the implant with respect to the external electrodes during normal operation.

To evaluate this, it was implemented an *in vitro* experimental setup (Figure 5.4) where the implants were placed at different angles with respect to the electric field. Two 7 cm × 2.5 cm aluminum plates acting as external electrodes (1.2 mm thick, 1050A) and connected to the external generator, were held parallel at a distance of 11 cm using two polycarbonate plates. A 1 cm × 1 cm grid made of cotton thread was sewed across the plates, 1.25 cm from the bottom of the structure. The structure was placed inside a 19 cm × 14 cm × 6.3 cm glass container filled up to 3 cm with saline (0.33% NaCl) with a conductivity of 0.5 S/m which approximately corresponds to the admittivity magnitude of skeletal muscle at 1 MHz [143].

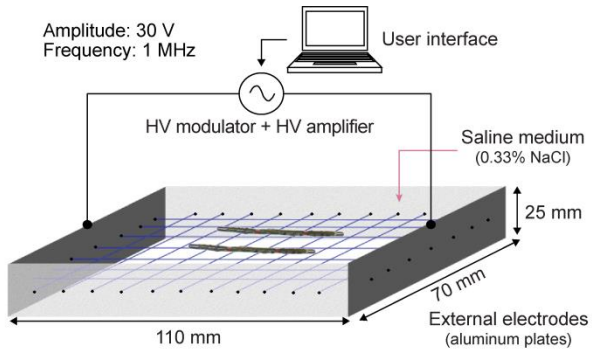

Figure 5.4. *In vitro* demonstration setup. Two aluminum external electrodes are held parallel and separated by two polycarbonate plates. The structure supports a regular grid made of cotton thread and is immersed into a glass container filled with saline. Four implants are placed over the grid. A user interface commands the modulation of a sinusoidal 1 MHz carrier, which is amplified and delivered through the external electrodes.

Up to four implants were laid on the grid and were wirelessly activated by the external generator. Multiple trials were performed in which the angle of the implants with respect to the plates and the distance between implants was varied. Each implant was programmed with its own address. In this *in vitro* study, in order to facilitate recognition of the implant activation, one current limiter inside the injectable device was replaced with a LED before the encapsulation process. Two thin wires connected to an oscilloscope (TPS2014 by Tektronix, Inc.) were placed in contact to the implant electrodes to record the voltage drop across a "dummy implant" that does not draw any current and a real implant that powers up but is not addressed by the external generator. Voltages were recorded for different tilts.

This *in vitro* setup was analyzed by means of a Finite Element Method (FEM) software platform (COMSOL Multiphysics). The 'Electric Currents' mode was used to perform a parametric study of electric potential at the electrodes of a dummy implant (Figure 5.5). The angle θ between the implant axis and the electric field was increased from 0º to 90º at 3º steps. Two 70mm × 25 mm aluminum plates acting as external electrodes were modeled parallel at a distance of 110 mm. An ac voltage with an amplitude (A) of 30 V was applied across them. The modeled dummy implant consists in an insulating tube (length = 41 mm, diameter = 2 mm, conductivity = 1×10^{-4} S/m, relative permittivity = 11.7) with two metallic cylinders at opposite ends (length = 3.8 mm, diameter = 2 mm, conductivity = 1×10^{4} S/m, relative permittivity = 1). The saline medium is modeled with a conductivity of 0.5 S/m and a relative permittivity of 1830 [143]. The software automatically generated a mesh of 7464 tetrahedral

elements. The implant electrodes were defined as probes, and the electric potential calculated during the parametric simulation was exported to a numerical computing software (Matlab, by Mathworks, Inc) for further graphical analysis.

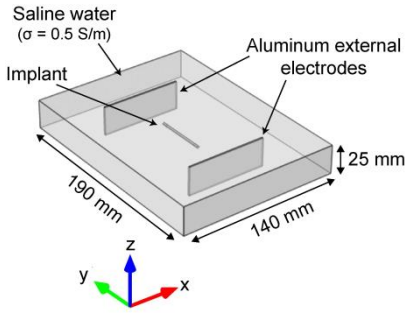

Figure 5.5. Geometry used in the FEM simulation. A parametric analysis was defined to rotate the implant in the xy plane, and record the electric potential of the implant electrodes. An ac voltage (A = 30 V) is applied across the external electrodes. The polycarbonate plates are not modeled for the sake of simplicity.

5.2.3. *In vivo* setup for demonstration

The *in vivo* demonstration included two different assays: 1- electrical measurements using a percutaneous bipolar probe implanted in the tibialis anterior (TA) muscle and connected to an implantable stimulator; and 2- force measurements using two implants deployed in the TA and gastrocnemius (GA) muscles of an anesthetized rabbit.

Animal handling

The animal procedure was approved by the Ethical Committee for Animal Research of the Barcelona Biomedical Research Park (CEEA-PRBB), application number: JMC 14-1606. One New Zealand White male rabbit weighting 4.46 kg was employed. For sedation and initial anesthesia, Dexmedetomidine (0.9 ml), Butorfanol (0.45 ml) and Ketamine (0.45 ml) were intramuscularly administered between 15 to 30 minutes prior to the preparation of the animal. Then, the right hind limb of the rabbit was shaved, from the head of the femur to the mid tarsus. In addition, a depilatory cream (Veet sensitive skin, by Reckitt Benckiser Group plc) was applied for 5 min and thoroughly rinsed. The animal was transferred to an anesthetic circuit using endotracheal intubation and anesthesia was maintained with Isoflurane (1-1.5%). Ringer's lactate (11 ml/h) was administered intravenously, and the animal was constantly monitored with a capnograph and pulse oximeter. A heating pad was employed during the entire session. At the end of the study, the animal was euthanized with an overdose of Thiobarbital sodium (8 ml IV).

Implantation procedure

The implantation procedure, inspired by the deployment system and sequence described in [47], is illustrated in Figure 5.6. At first, the target muscle was identified by palpation and the approximate site for deploying the implant (i.e. motor point) was located using anatomical cues. It was assumed that such motor point was close to the origin of the muscle. A 2.1 mm thick catheter (14 G, model 382268 by Becton, Dickinson and Company) was longitudinally introduced from the hock up to this end, resulting in an insertion depth of about 6 cm. The motor point of the muscle was verified using the tip of the catheter's needle as an exploration electrode and an Ag/AgCl gel electrode (model 2228 by 3M) placed on the thigh of the animal as a return electrode. A custom-made current generator delivered through the electrodes 1 to 6 mA biphasic symmetric pulses (pulse width = 200 μs) at 100 Hz. If the induced movement was deemed too weak or did not match the expected joint movement, the catheter was repositioned by inserting or extracting the catheter a few millimeters.

After the motor point was identified, the insertion point of the catheter was marked to avoid dislocation, and the needle was extracted. Then, the proximal end of the catheter was cut, and a 3.4 mm catheter (10 G, model 382287 by Becton, Dickinson and Company) used as dilator was gently slid down the 14 G catheter until a mark in the dilator matched the marked insertion point, indicating that both catheter tips were lined up. The 14 G catheter was gently extracted from the dilator (Figure 5.6-B), and a mark was placed on the dilator and skin to avoid dislocation.

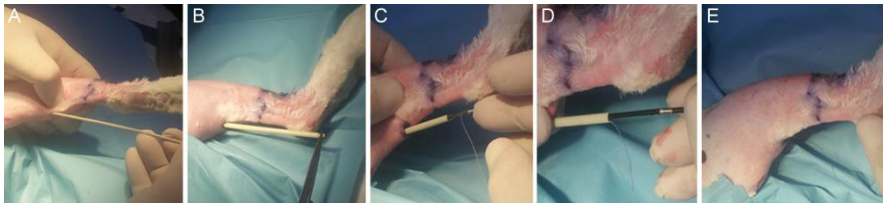

Figure 5.6. Implantation procedure. A) The approximate site for implant deployment was located by anatomical cues. A 14 G catheter was introduced towards the muscle's origin. The tip of the catheter's needle was used as an exploration electrode to locate the point of maximum excitability. For that, an electro-stimulator was connected across the catheter needle and an external return electrode, and the insertion depth of the catheter was adjusted until a strong contraction was noticed. B) The needle was extracted from the catheter, and a 10 G catheter was inserted to dilate the orifice. The 14 G catheter was extracted. C-D) The implant was inserted and pushed towards the identified motor point. E) The dilator was extracted and the external return electrode was detached. The surgical thread observed in C-E was tied to the implant to pull it out in case it was necessary to remove it for replacement.

At first, LF currents and voltage drop across the implant electrodes were measured using a bipolar probe connected to an injectable device (described below). The probe was inserted in the dilator until a mark on the probe lined up with the proximal end of the dilator, indicating that the tip of the probe was located by the identified motor point. The dilator was gently extracted, until both electrodes of the probe were in contact with the tissues, and the external measurements were performed. Then, the dilator was gently inserted back into the tissues, the marks were lined up assuring that its tip was in the motor point, and the probe was extracted.

A surgical thread was tied to the negative electrode ('-') of the implantable stimulator in case the stimulator had to be withdrawn after deployment. Then, the stimulator was introduced into the dilator (Figure 5.6-C), with the positive electrode ('+') facing the dilator's tip, and it was pushed towards the identified motor point using the custom-made probe (Figure 5.6-D). When a specific mark on the probe matched the proximal end of the dilator (assuring that the implant's positive electrode was in contact with the motor point), the dilator was cautiously withdrawn by holding firmly the probe, releasing the implant inside the muscle. Finally, the probe was removed, and the insertion point was treated (Figure 5.6-E). No bleeding was visible. The implantation procedure was carried out both in the TA and the GA muscles of the right hind limb of the rabbit.

Electrical measurements using the implanted bipolar probe

Before deploying a stimulator in the TA muscle, the operation of the injectable device was tested externally by connecting it to a percutaneous bipolar probe which was deployed at the motor point of the muscle where the stimulator would be later implanted. The probe consisted of a 1.8 mm diameter coaxial cable (50CX-41 by Temp-Flex Cable Inc.) whose core and shield conductors were contacted to two 3.8 mm long, 2 mm thick stainless steel electrodes separated by a 41 mm long fluorinated ethylene propylene (FEP) insulator. These dimensions are similar to those of the implantable stimulators. The distal electrode acted as the stimulation electrode whereas the proximal one acted as the return electrode. The probe was connected in series to the implant and to the parallel combination of a 10 Ω resistor and a 2.2 μF capacitor (low-pass filter LPF, cut-off frequency = 7.2 kHz) as shown in Figure 5.7. This setup allows recording the voltage drop across the implant electrodes and the LF components of the electric current flowing through the device using an oscilloscope (TPS2014 by Tektronix, Inc.).

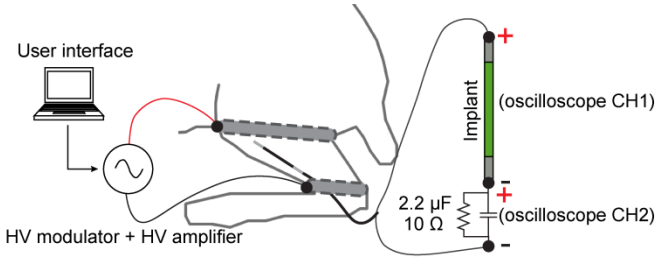

Figure 5.7. Electric measurement setup for the *in vivo* evaluation using a bipolar probe implanted in the tibialis anterior (TA) muscle and connected to the implant and a RC low-pass filter.

Force measurements

After the devices were deployed in the TA and GA muscles, isometric plantarflexion and dorsiflexion forces were recorded using a load cell (STC - 10kgAL-S by Vishay Precision Group, Inc.) mounted on a custom-made acrylic board (Figure 5.8). The animal was lying sideways, the hock was fixed to the horizontal surface using an atraumatic padded clamp and the foot was tied with clamps to the load cell. The force signal was recorded with a DAQ at a rate of 100 kHz using a signal conditioning electronic circuit that included a first order LPF with a cutoff frequency of 500 Hz.

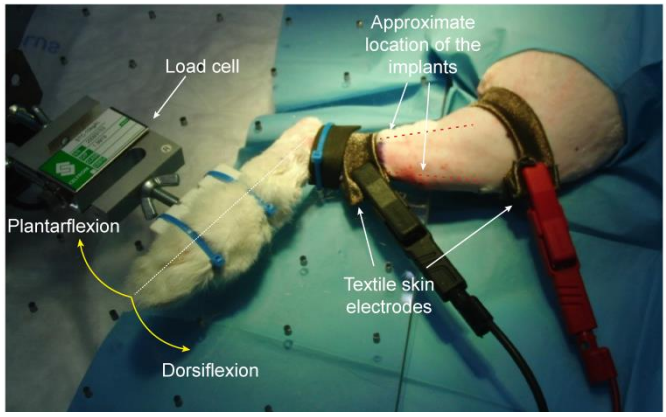

Figure 5.8. Isometric force measurement setup with implants deployed by injection (see Figure 5.6) into the TA and gastrocnemius (GA) muscles. The hock of the animal was fixed to a horizontal surface and the foot was fixed to a load cell. The textile electrodes were strapped around the hind limb and were connected to the external system.

5.3. Results

The developed injectable stimulator (length = 48.7 mm; Ø = 2.0 mm, mass = 0.4 g) is composed of a semi-rigid PCB enclosed in a silicone

tubing with two stainless steel electrodes at opposite ends (Figure 5.2). Its small diameter allows deployment using a catheter, and its length guarantees a sufficient voltage drop to electrically feed its electronic circuit and generate the LF currents required for stimulation.

5.3.1. *In vitro* and FEM results

Four implants were placed in the *in vitro* setup shown in Figure 5.4. They were powered and independently addressed using a HF bursts generator (f = 1 MHz, A = 30 V, distance between electrodes = 11 cm). The HF electric field magnitude in this scenario was 272 V/m. Two still frames of implants' activations for two different angles with respect to the electric field are shown in Figure 5.9. Frame A shows the activation of an implant aligned to the electric field applied by the external generator. Even though this implant is separated only 1 mm from another implant, the system is capable of powering and independently addressing that implant. Frame B shows the activation of an implant with a 45º angle with respect to the electric field. In this case, as reported in the simulations presented below, the amplitude of the ac voltage drop across the implant electrodes was expected to be about 7.7 V under the assumption that the implant did not draw any current (i.e. dummy implant). In reality, the voltage drop was 6.4 V as measured by contacting thin wires to the implant electrodes. This is enough to power the CU inside the injectable device and turn on the LED that shows the implant's activation. At larger angles the devices cannot be powered with this electric field magnitude. These results show that the injectable stimulators can be activated even if they are not perfectly aligned to the delivered electric field.

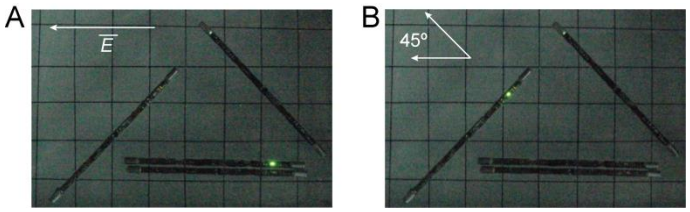

Figure 5.9. Pictures of addressed stimulators in *in vitro* setup. The implants activation is manifested by lighting LEDs. A) Even when the implants are placed close together, they independently operate. B) The implants can be powered and activated even if they are tilted 45º with respect to the applied field.

The FEM simulation results are shown in Figure 5.10-11. Figure 5.10 shows the amplitude of the ac electric potential generated by the external system and the corresponding electric field when the implant was tilted 10º. Figure 5.11-A shows the electric potential amplitude measured at the electrodes of the simulated dummy implant. The maximum voltage drop

amplitude across the implant electrodes is 11.1 V when the implant is perfectly aligned to the electric field (0º). For a tilt of 45º, the voltage drop is 7.7 V. These results indicate that, despite the implant electrodes are relatively large (length = 3.8 mm; Ø = 2.0 mm) the amplitude of the voltage drop across the implant electrodes can be approximated by the expression that would correspond to point electrodes:

$$\Delta V = d \cos\theta \left|\mathbf{E}_{peak}\right| \tag{5.1}$$

where θ is the tilt angle, d is the distance between implant electrodes, and $\left|\mathbf{E}_{peak}\right|$ is the peak electric field applied.

Figure 5.11-B shows the voltage drop obtained for the dummy implant in the FEM simulation, the approximation of Eq. 5.1 and the *in vitro* recordings; and that obtained with the real implant recorded in saline.

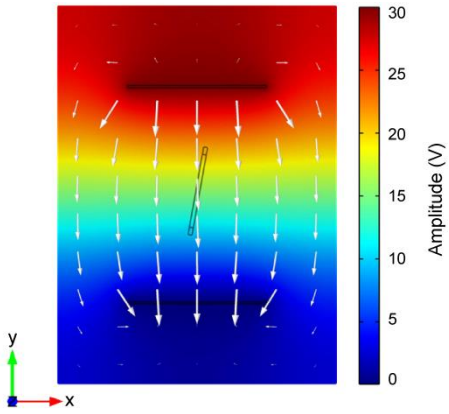

Figure 5.10. FEM simulation result of the amplitude of the ac electric potential (color scale) and of the electric field relative magnitude and direction (white arrows). It is simulated the delivery of an ac voltage (A = 30 V) across the external electrodes. A dummy implant is modeled at the center of the setup, and a parametric analysis is performed to evaluate the electric potential at the implant electrodes depending on its angle with respect to the applied field.

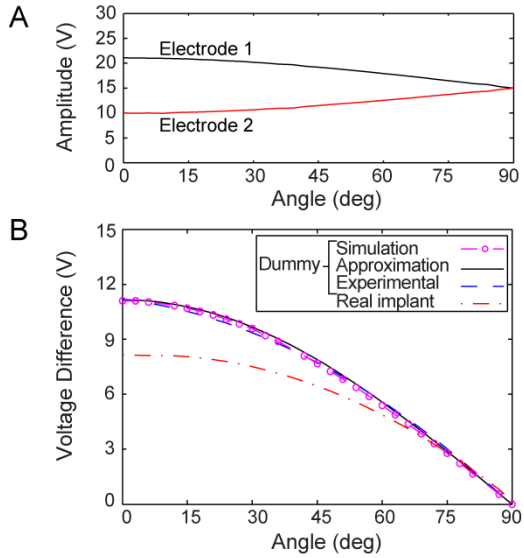

Figure 5.11. Electric potential across implant electrodes. A) Simulation results for the dummy implant electrodes. B) Comparison of the electric potential difference obtained for the dummy implant in the FEM simulation, the approximation of Eq. 5.1 and the *in vitro* recordings, with the real implant voltage drop recorded in saline.

5.3.2. *In vivo* results

Electrical and force measurements were performed to test the implants *in vivo*. Figure 5.12 shows the recorded LF current and the charge injection computed from it. The implant was programmed to and was able to apply biphasic LF currents with a magnitude of 2 mA and a duration of 200 µs + 200 µs with a dwell time of 30 µs. This implies that the implant's CU was able to decode the information sent through the HF signal and enable the current limiters to generate a biphasic symmetric current waveform. If a charge mismatch appeared at the end of the anodic (positive) current pulse, the dc-blocking capacitor of the implant passively balanced this charge in-between stimulating bursts. The bursts triggered a wake-up signal for the microcontroller to generate the stimulating waveforms, and the implant remained asleep between bursts, minimizing power consumption.

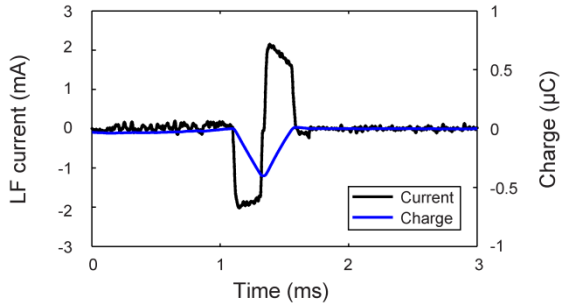

Figure 5.12. Low frequency current delivered by the implant in the tibialis anterior and the calculated charge injection. A dc-blocking capacitor balanced any charge mismatch occurring during the delivery of the biphasic symmetric current pulses.

The amplitude of the 1 MHz voltage applied across the external electrodes was 50 V during the *Stimulation bursts*. At these episodes, the voltage drop amplitude across the bipolar probe electrodes was 6.20 V when the probe was connected to the implant. According to the *in vitro* results and simulations reported above, this corresponds to a voltage drop of about 7.35 V under the assumption of a dummy implant and an estimated local field ($|\mathbf{E}_{peak}|$) of about 179 V/m. Figure 5.13 shows the estimated peak electric field at the location of the implant during the three stages of the protocol delivered by the external HF generator (*Power up*, *Synch&Data*, and *Stimulation bursts*) [78]. Both the generator and the implant were programmed so that the stimulation consisted of 5 biphasic waveforms at a frequency of 100 Hz. To do so, the generator had to deliver 5 bursts of 450 µs.

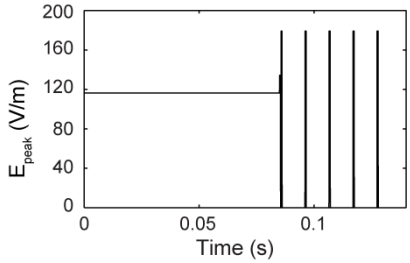

Figure 5.13. Estimated high frequency (HF) electric field magnitude at the location of the bipolar probe (and later the location of the implant) during the three stages of the HF signal (*Power up*, *Synch&Data*, *Stimulation bursts*).

After the electrical measurements, the probe was extracted and the devices were deployed by injection into the target tissues using a 10 G

catheter. Stiffness was not appreciated by palpation of the animal's hind limb probably thanks to the implants semi-rigidity.

Figure 5.14 shows the force recordings obtained by independently activating the two implanted stimulators. The user was able to wirelessly address the implants and control the stimulation frequency. Plantarflexion and dorsiflexion twitch contractions were induced with magnitudes of 0.96 and 1.20 N respectively (5 bursts, F = 80 Hz) as shown in Figure 5.14-A. The induced force could be modulated by varying the stimulation frequency (Figure 5.14-B).

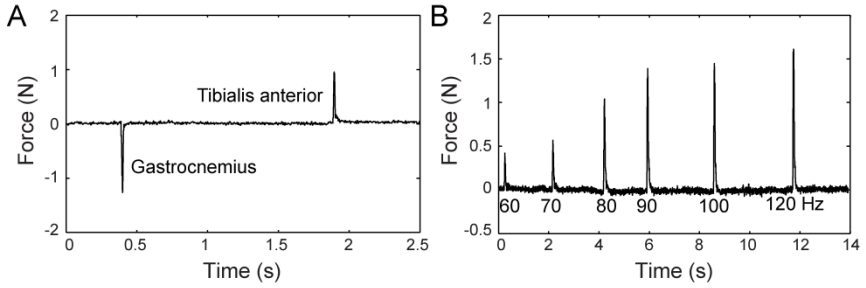

Figure 5.14. Force recordings. A) The user independently addressed one or the other implant to induce plantarflexion or dorsiflexion movements (F = 80 Hz), and B) defined the frequency of stimulation to modulate the force magnitude.

After the stimulation assays, X-ray images were taken of the hind limb of the animal where the implants were deployed (Figure 5.15). The integrity of the implants was preserved during the whole study (~ 5 h). After euthanasia, the implants were extracted, cleaned, inspected and electrically evaluated. It was verified that they were still fully functional in terms of addressability and stimulation capabilities.

Figure 5.15. X-ray images of the stimulators implanted in the tibialis anterior and gastrocnemius muscles. The '+' and '-' signs denote the positive and negative terminals of the stimulators.

5.4. Discussion

The microcontrolled injectable stimulators described here were able to perform neuromuscular stimulation by rectifying epidermically applied HF current bursts. The *in vivo* experiment showed that these prototypes are easily injected into muscle tissue through the lumen of a catheter without causing bleeding. This same catheter was employed to identify the target deployment site (motor point). Using a graphic interface that governed the modulation of the HF current bursts, the user defined which muscle to trigger and the repetition frequency of the bursts. This last parameter allowed gradual variation of the induced force, which is a common observation when conventional LF pulses are delivered for neuromuscular stimulation [128]. This suggests that, as hypothesized, the half-rectified HF currents delivered by the implants are equivalent in terms of excitatory behavior to conventional LF current pulses [78].

Galvanic coupling – which is the way the implants are energized here – has been extensively studied for intrabody communications [87]. However, the idea of using this approach as an energy source for implantable devices has not been explored thoroughly. This observation is corroborated in recent reviews on power approaches for implants in which galvanic coupling is not even mentioned [34], [37]. The reasons why other researchers were reluctant – or did not conceive – to use galvanic coupling for power can only be guessed. In our opinion, such reluctance mainly arises from not appreciating two facts. First, whereas moderate LF currents can be harmful, large HF currents can innocuously flow through the human body if applied as short bursts because they neither cause stimulation nor significant heating. Second, the implants can be shaped as

thin and flexible elongated bodies for picking up a sufficient voltage drop. Such implant conformation is highly beneficial in terms of minimal invasiveness, not only because it allows percutaneous deployment, but also because it minimizes tissue damage. That conformation is already massively used in clinical practice: in fact, thousands of women have been subdermally implanted with hormonal contraceptive implants which consist of a flexible rod that is about 4 cm long and 2 mm in diameter [144].

Galvanic coupling presents two drawbacks that were addressed in this study: 1- since the component of the electric field in the direction of the implant axis must be large enough for guaranteeing a sufficient voltage drop, some degree of alignment is required and 2- direct electrical contact between the external generator and the body tissues is necessary. The results show that even with a 45º tilt, the implants can activate, thereby alignment is not a stringent requirement. We have also *in vivo* demonstrated that gel-free textile electrodes perform an adequate contact for delivering the HF currents that enable the implants to operate. This is possible due to the low contact impedance that textile electrodes exhibit at high frequencies [145]. They could be easily embedded in garments for creating comfortable external systems.

The demonstrated implants consist only of off-the-shelf components mounted on a rigid-flex PCB. This use of low cost technologies suggests that these devices could be widely accessible for experimental studies. We anticipate that the tubular, flexible and small conformation of the implants will mitigate issues faced during implantation procedures and will boosts their use in practical scenarios where minimal invasiveness is a must. Aiming at further miniaturization, multiple strategies could be explored to improve the implants' design. The width of the PCB was mainly constrained by the size of the biggest component: the microcontroller. As electronic component manufacturers tend to offer further miniaturization, we anticipate that smaller similar implants will be feasible in the near future. This can also be applicable to other relatively large electronic components within the design. Furthermore, the implants' biggest passive component, the dc-blocking capacitor, could be avoided using other strategies to prevent dc currents such as the charge counter we demonstrated in [146] and presented in Chapter 3. The manufacturing capabilities of the PCB provider also constrained the implants' length. Aspects such as the minimum diameter of the annular ring in the internal layers (190 μm) and the minimum distance between conductors (125 μm) are likely to improve in the near future.

The demonstrated systems are only capable of electrical stimulation and do not possess sensing capabilities. In the near future, we plan to embed detection and quantification of electromyographic signals which could be picked up with the implant electrodes. These sensing capabilities

could, for instance, allow the implementation of artificial proprioception for closed-loop control [140]. We have already *in vitro* demonstrated bidirectional communications based on this electrical stimulation method (Chapter 4) [138].

5.5. Conclusions

The eAXON method allows the development of addressable neuromuscular stimulators made up only of commercial components, and which can be shaped as semi-rigid thin devices suitable for deployment by injection. In particular, the addressable implants reported here, composed of a relatively long (~5 cm) semi-rigid circuit enclosed in a silicone tube (Ø = 2 mm), were easily deployed into the target tissues through a 10 G catheter. Their operation was demonstrated in the hind limb of an anesthetized rabbit, accomplishing controlled and independent joint movements.

The HF currents that power the implants circuitry and that are transformed by them into LF currents capable of local stimulation can be delivered through textile skin electrodes without any need for gels or skin preparations aimed at improving the electrical contact. Need for alignment of the implants with the generated HF fields is not a stringent requirement. In here it was demonstrated that even with a 45º angle between the implant's axis and the electric field, the devices were powered and responded to activation requests by the external system.

By demonstrating an alternative to existing methods for power transfer/generation such as inductive coupling or batteries, these results pave the way to the development of sophisticated electronic implants unprecedented in terms of minimal invasiveness.

CHAPTER 6

Safety, power efficiency and portability analysis

Abstract – Since the eAXON method relies in the application of electric current to tissues, two adverse effects can occur with potentially harmful consequences for the health of the patient: unwanted stimulation and tissue heating. Additionally, as a significant amount of HF power is wasted by Joule heating, the method exhibits poor energy efficiency. In here numerical analyses are reported to evaluate how safe and portable a system based on the developed implant prototypes could be. Finite element method simulations using anatomically realistic arm and leg models are also included. The results obtained from this study indicate that a 1 MHz auxiliary current delivers peak *in situ* electric fields that would not generate unwanted electrostimulation during stimulation; and that the HF current bursts would generate specific absorption rates (1.9 W/kg) under the thresholds defined by international standards for tissue heating. The results from this study also indicate that, despite low power transfer efficiency (~ 0.05%), the power consumed by the external HF current generator is low enough (< 4 W) to grant the use of small portable batteries.

Part of the contents of this chapter is adapted from the following publications:

L. Becerra-Fajardo, M. Schmidbauer, and A. Ivorra, "Demonstration of 2 mm thick microcontrolled injectable stimulators based on rectification of high frequency current bursts," Under review, 2016.

L. Becerra-Fajardo, R. Garcia-Arnau, and A. Ivorra, "Injectable Stimulators Based on Rectification of High Frequency Current Bursts: Power Efficiency of 2 mm Thick Prototypes," in International Conference on NeuroRehabilitation (ICNR2016), 2016, p.

6.1. Introduction

In Chapter 5 we *in vivo* demonstrated 2 mm thick injectable microstimulators based on the eAXON method. We also *in vitro* demonstrated that the electronic architecture proposed for the implant is capable of modulating the high frequency (HF) current, in order to send information from the implant to the external system, accomplishing bidirectional communications (Chapter 4) [138].

According to the above, the implantable devices accomplished with the eAXON method could be used for electrical stimulation and for sensing purposes. However, the method presents two important issues we considered important to analyze for the case of the prototypes reported here: human exposure to radio frequency currents and low power efficiency.

International standards define unwanted electrostimulation and tissue heating as adverse health effects when there is human exposure to radio frequency currents. The exposure restrictions for unwanted electrostimulation apply to the frequency range up to 5 MHz, while exposure restrictions for tissue heating apply to frequencies between 100 kHz and 3 GHz [147]–[149]. The IEEE standard indicates so-called *basic restrictions* to avoid unwanted electrostimulation and tissue heating. The basic restrictions are defined as "the exposure restriction based on established adverse health effects that incorporate appropriate safety factors" [148].

The IEEE standard defines the unwanted electrostimulation threshold as the maximum allowed induced *in situ* electric field (rms) averaged over a 5 mm straight line segment with an averaging time of 0.2 s [148]. The standard indicates different thresholds for different body parts such as the brain, heart, and extremities. Since the eAXON method is mainly intended for restoration of motor function, we will focus on the extremities restrictions. The basic restriction sets a maximum electric field value rms of 2.1 V/m for frequencies below 3350 Hz [147], [148]. For frequencies above 3350 Hz and below 5 MHz, this electric field threshold value rms is defined by the expression:

$$\mathrm{E}_i = \mathrm{E}_0 \frac{f}{3350} \quad \mathrm{V/m} \tag{6.1}$$

where E_0 is the rheobase *in situ* field (2.1 V/m in extremities), and E_i is the maximum permissible induced *in situ* electric field value rms. The IEEE Std C95.6-2002, which establishes restrictions for exposures between 0 and 3 kHz, defines the maximum allowed induced *in situ* electric field value rms at 2.1 V/m [147], showing continuity between standards.

In terms of tissue heating due to human exposure to radio frequency currents, the standards specify a maximum threshold defined as the Specific Absorption Rate (SAR). It can be related to the electric field at a point by the expression:

$$\mathrm{SAR} = \frac{\sigma}{\rho}|\mathbf{E}_{\mathrm{rms}}|^2 \quad {}^{\mathrm{W}}/_{\mathrm{kg}} \tag{6.2}$$

where σ is the tissue electrical conductivity (S/m), ρ is the tissue mass density (kg/m^3), and $|\mathbf{E}_{\mathrm{rms}}|$ is the applied electric field rms magnitude (V/m) [148]. Both ICNIRP and IEEE standards specify different thresholds: 2 W/kg for head and trunk, and 4 W/kg for extremities exposure in the action level (i.e. general public); and 10 and 20 W/kg respectively for exposure in controlled environments. This maximum SAR is averaged over a 6 min period in a 10 g of tissue [149][148].

Figure 6.1 shows the relationship between unwanted electrostimulation and tissue heating. The developed implant prototypes described in Chapter 5 are addressed using 1 MHz current bursts delivered by the external system. According to international standards, this frequency may be high enough to avoid unwanted electrostimulation (E_i (rms) = 626 V/m). However, since the electric field magnitude delivered by the external system is high, the HF current bursts may surpass this maximum permissible induced *in situ* electric field. Additionally, as the frequency of the ac current bursts is larger than 100 kHz, it must also be evaluated in terms of tissue heating.

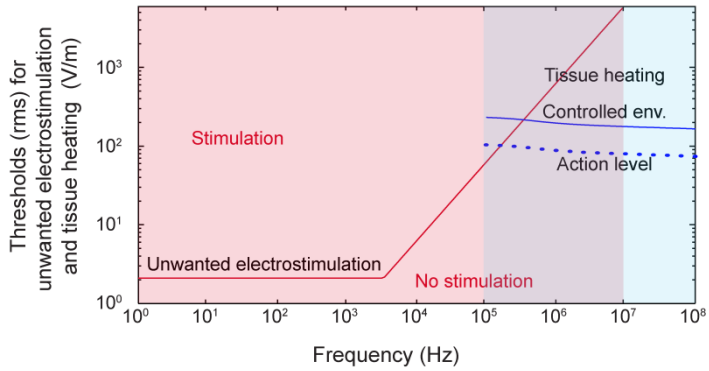

Figure 6.1. Relationship between frequency and adverse health effects based on the IEEE and ICNIRP safety standards for unwanted electrical stimulation and tissue heating in the extremities [147]–[149]. SAR is illustrated in terms of the $|\mathbf{E}_{\mathrm{rms}}|$ (Eq. 6.2), assuming the electrical conductivity of muscle and tissue density of 1000 kg/m^3. Frequencies between 100 kHz and 10 MHz should be evaluated for both adverse health effects.

Galvanic coupling, the basis of HF current conduction in the eAXON method, presents low levels of power efficiency due to the fact that most of the current is wasted as heat. This suggests further analysis since it could hamper the use of portable batteries in the external system. Nowadays, rechargeable portable batteries can deliver a specific energy of more than 100 Wh/kg. The battery industry will evolve significantly as batteries will have an important role in the development of sustainable products, such as electric vehicles and renewable energy plants. Yet, radical changes in the battery structure are needed to meet power requirements (e.g. lithium battery concept), and this will be challenging [150]. Therefore, the eAXON method should opt to rely on technologies available nowadays, and so, the portability analysis is a must in this step of our research.

6.2. Methods

6.2.1. Numerical analysis of the auxiliary HF current

The numerical analysis evaluates the stimulation protocol and variations of it plausible in neuromuscular stimulation scenarios. The auxiliary HF current, which embeds a modulated signal, has three stages: *Power up*, Synchronization and Data transfer (*Synch&Data*); and *Stimulation bursts* (Chapter 2). For simplicity, in this chapter the first two stages are combined into a single stage called *Initialization*.

A numerical analysis was performed to illustrate that the delivered HF current bursts can be safe in terms of unwanted electrostimulation and tissue heating. According to safety standards, both adverse effects that are potentially harmful for health depend on the root mean square (rms) value of the applied electric field $|\mathbf{E}_{\mathrm{rms}}|$. However, the averaging time used to find the rms differs between both adverse effects: 0.2 s for unwanted electrostimulation, and 6 min for tissue heating.

For a sinusoidal signal, the applied electric field $|\mathbf{E}_{\mathrm{rms}}|$ defined over the interval $\mathrm{T}_1 \leq t \leq \mathrm{T}_2$ can be expressed as:

$$|\mathbf{E}_{\mathrm{rms}}| = \sqrt{\frac{1}{\mathrm{T}_2 - \mathrm{T}_1} \int_{\mathrm{T}_1}^{\mathrm{T}_2} \left|\mathbf{E}_{\mathrm{peak}}(t)\right|^2 dt} \tag{6.3}$$

Assuming that in the interval between T_1 and T_2 the external system only initializes the implants once (*Power up* stage), sends information for one address (*Synch&Data*) and uses the remaining time to transmit stimulation bursts, the $|\mathbf{E}_{\mathrm{rms}}|$ could be expressed as:

$$|\mathbf{E}_{\mathrm{rms}}| = \sqrt[2]{\frac{\int \left|\mathbf{E}_{\mathrm{peak}}^{Power\ up}(t)\right|^2 dt + \int \left|\mathbf{E}_{\mathrm{peak}}^{Synch\&Data}(t)\right|^2 dt + \int \left|\mathbf{E}_{\mathrm{peak}}^{Stim}(t)\right|^2 dt}{\mathrm{T}_2 - \mathrm{T}_1}} \quad (6.4)$$

In the prototypes developed in this thesis, the *Power up* stage has a duration of 85 ms, and a k_1 relative amplitude with respect to the applied peak field during the stimulation stage ($|\mathbf{E}_{\mathrm{peak}}|$). The *Synch&Data* stage sends 12 bits (3 syncronization bits, 8 data bits and 1 parity bit) at a rate of 25 kBd, with a k_2 relative amplitude with respect to the applied field $|\mathbf{E}_{\mathrm{peak}}|$. A 200 µs, zero amplitude slot is used for processing purposes. Having these values in mind, the terms of Eq. 6.4 can be rewritten in terms of $\mathbf{E}_{\mathrm{peak}}(t)$ as:

$$\int \left|\mathbf{E}_{\mathrm{peak}}^{Power\ up}(t)\right|^2 dt = \int_0^{85\ ms} \left|k_1 \mathbf{E}_{\mathrm{peak}}(t)\right|^2 dt \quad (6.5)$$

$$\int \left|\mathbf{E}_{\mathrm{peak}}^{Synch\&Data}(t)\right|^2 dt = \int_{85\ ms}^{85\ ms + 12 \cdot \frac{1}{25000}} \left|k_2 \mathbf{E}_{\mathrm{peak}}(t)\right|^2 \mathrm{D}_{S\&D}\ dt + \int_{85.48\ ms}^{85.48\ ms\ +200\ \mu s} 0\ dt \quad (6.6)$$

$$\int \left|\mathbf{E}_{\mathrm{peak}}^{Stim}(t)\right|^2 dt = \int_{0.08568}^{r_t} \left|\mathbf{E}_{\mathrm{peak}}(t)\right|^2 \mathrm{D}_{\mathrm{Sb}}\ dt \quad (6.7)$$

where r_t is the time available to apply stimulation bursts during the evaluated interval ($\mathrm{T}_2 - \mathrm{T}_1 - 0.08568$), $\mathrm{D}_{\mathrm{S\&D}}$ is the duty cycle during *Synch&Data* (equal to 0.5 due to Manchester encoding), and D_{Sb} is the duty cycle during the stimulation phase, and is defined as:

$$\mathrm{D}_{\mathrm{Sb}} = \mathrm{F}\ (2\ \ pulse_{width} + 50\mu s) \quad (6.8)$$

where F is the stimulation frequency.

As explained in [78], $k_1$and k_2 of Eq. 6.5 and Eq. 6.6 are specified to be equal to 0.65 and 0.75, as the former relative amplitude is capable of initializing the implantable circuitry, while the latter compensates the discharge of the capacitors during the low levels of the *Synch&Data* stage and the processing slot.

The user interface of the external generator is capable of defining the frequency of stimulation (F) and the pulse width of the biphasic symmetric current waveform before generating the HF current bursts. Then, the rms value of the electric field will depend on both stimulation parameters.

6.2.2. Models for computing power efficiency

To analyze the power efficiency and the portability of the injectable prototypes, the resulting current delivered by the external electrodes was used to calculate the power applied by the external system. This power depends on the rate of *Initialization* stages and that of *Stimulation bursts* as defined in the communication protocol reported in Chapter 2 [78].

To perform the numerical analysis, we customized a high-resolution anatomical model from a 34 year old male which was developed for electromagnetic studies [151]. It consists of three regions: bone tissue, muscle tissue and "other tissues". This last region corresponds to the skin, subcutaneous adipose tissue and fat. One lower extremity and one upper extremity were extracted from this anatomical model. For each limb, the three regions were decimated and converted into solid geometries [152]. These resulting geometries were imported into a finite element method (FEM) software package (COMSOL Multiphysics 4.4) for performing electrical simulations using the 'Electric Currents' application mode.

Table 6-1 reports the dielectric properties of the simulated materials for the explored frequencies: 1 MHz for HF currents delivered by the external system, and 100 Hz for the LF current delivered by the implant during stimulation. In the case of "other tissues", a weighted average between those reported for fat, skin and subcutaneous adipose tissue was selected [153].

In the case of the lower limb, two superficial electrodes were modeled around the leg (Figure 6.2) and two 2 mm thick dummy implants were modeled inside the tibialis anterior (TA) and gastrocnemius (GA) muscles. The dummy implants simply consist in an insulating tube (length = 41 mm, Ø = 2 mm) with two metallic cylinders at opposite ends (length = 3.8 mm, Ø = 2 mm). The software automatically generated a mesh of 407,300 tetrahedral elements.

Table 6-1. Dielectric properties of materials

Tissue	1 MHz		100 Hz	
	Conductivity σ (S/m)	Relative permittivity ε_r	Conductivity σ (S/m)	Relative permittivity ε_r
Bone (cortical) [154]	0.024	145	0.081	2.17×10^5
Muscle [154]	0.503	1840	0.267	9.33×10^6
Other tissues [154]	0.049	285.6	0.040	5.22×10^5
Electrodes	1×10^4	1	1×10^4	1
Insulating tube	1×10^{-4}	12	1×10^{-4}	12

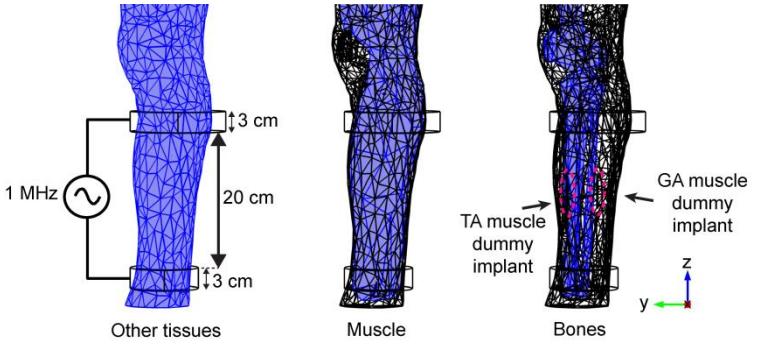

Figure 6.2. Lower limb model used in the simulations, corresponding to a male adult. Two external electrodes are modeled around the leg, and two dummy implants are modeled in the tibialis anterior (TA) and gastrocnemius (GA) muscles.

In the case of the upper limb, two superficial electrodes were modeled around the upper arm, as shown in Figure 6.3. The dummy implants were modeled in the triceps and biceps brachii. The software automatically generated a mesh of 439,117 tetrahedral elements.

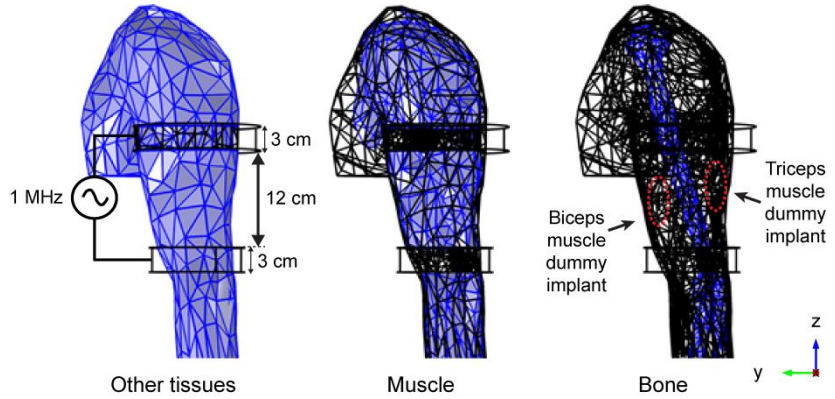

Figure 6.3. Arm model, corresponding to a male adult. The external electrodes are modeled strapped around the upper arm. Two dummy implants are modeled in the triceps and biceps brachii.

A parametric analysis was performed for the arm and leg models to evaluate the injectable prototypes (Chapter 5) in terms of power efficiency and portability. The amplitude of the external voltage was increased from 0 to 100 V at 10 V steps. The implant electrodes were defined as voltage probes, and the resulting electric potential was exported to another computing software (Matlab, by Mathworks, Inc) for further numerical and graphical analysis (e.g. power calculation depending on frequency of stimulation).

6.3. Results

6.3.1. Auxiliary high frequency currents

Unwanted electrostimulation

The IEEE standard specifies that at 1 MHz the maximum *in situ* electric field $|\mathbf{E}_{\mathrm{rms}}|$ for preventing unwanted electrostimulation must be lower than 626 V/m at the extremities (Eq. 6.1). We have previously reported in Chapter 5 that, as found in *in vivo* assays, the local field magnitude ($|\mathbf{E}_{\mathrm{peak}}|$) required to allow implant operation is about 179 V/m [127]. Then, from Eq. 6.5-6.7 we can calculate the average $|\mathbf{E}_{\mathrm{rms}}|$ during a time interval $T_2 - T_1$ equal to 0.2 s (averaging time specified by the IEEE standard for unwanted electrostimulation) using stimulation frequencies ranging from 40 to 200 Hz, and pulse widths of 100 and 200 μs (Table 6-2). The maximum $|\mathbf{E}_{\mathrm{rms}}|$ obtained is 86.2 V/m (F = 200 Hz, pulse width of 200 μs). Therefore, the HF bursts can be considered as safe in terms of unwanted electrostimulation.

Table 6-2. Calculated $|\mathbf{E}_{rms}|$ (V/m) – unwanted electrostimulation

Pulse width (μs)	F (Hz)	E_{rms} 0.2 s (V/m)
100	40	77.2
	80	78.4
	120	79.5
	160	80.7
	200	81.8
200	40	78.1
	80	80.2
	120	82.3
	160	84.2
	200	86.2

Figure 6.4 shows the dependency of the applied HF electric field with the frequency of stimulation (i.e. controlled stimulation performed by the implantable devices) when evaluating in terms of unwanted electrostimulation. As stimulation frequency increases, the averaged $|\mathbf{E}_{\mathrm{rms}}|$ increases. However, the safety threshold for a frequency of 1 MHz is much higher than the obtained averaged *in situ* electric field.

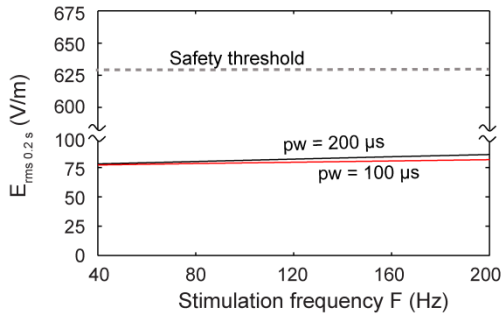

Figure 6.4. Safety standards compliance for unwanted electrostimulation. $|\mathbf{E}_{\mathrm{rms}}|$ averaged over 0.2 s for different stimulation pulse widths and frequencies, and the safety threshold.

Tissue heating

In terms of tissue heating during stimulation, Table 6-3 shows the $|\mathbf{E}_{\mathrm{rms}}|$ value averaged over a time interval $T_2 - T_1$ equal to 1 s, for different pulse widths and frequencies according to Eq. 6.4. Figure 6.5 shows the local SAR obtained for each $|\mathbf{E}_{\mathrm{rms}}|$. A muscle density ρ of 1000 kg/m^3 [155] and conductivity σ of 0.5 S/m at 1 MHz [143] are assumed.

Table 6-3. Calculated $|E_{rms}|$ (V/m) – tissue heating

Pulse width (μs)	F (Hz)	E_{rms} 1 s (V/m)
100	40	38.1
	80	41.7
	120	45.1
	160	48.2
	200	51.2
200	40	41.0
	80	47.0
	120	52.3
	160	57.1
	200	61.6

In the worst case scenario analyzed here in which the external HF generator triggers a 200 Hz stimulation with a pulse width of 200 μs, the computed SAR is about 1.90 W/kg, much lower than the 4 W/kg threshold defined as the maximum localized SAR for the extremities in the action level (i.e. general public). International standards indicate that this SAR threshold has to be averaged for a 6 min period [148], [149]. However, it seems unlikely that any stimulation system will be continuously performing stimulation at 200 Hz for this period of time. Therefore, the safety margins may be considerably larger than the values shown in Figure 6.5.

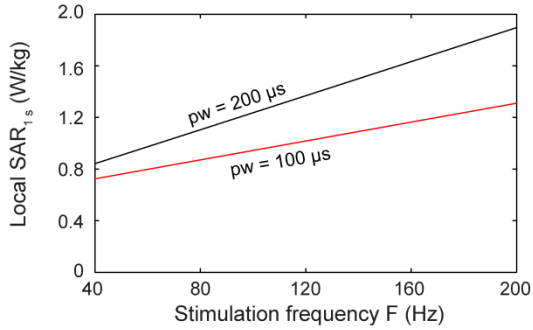

Figure 6.5. Safety standards compliance for tissue heating during electrical stimulation. Local SAR averaged over 1 s for different stimulation pulse widths and frequencies. The obtained SAR is much lower than the 4 W/kg threshold established for exposure in the extremities (action level).

6.3.2. Power efficiency and Portability analyses

Lower limb

Figure 6.6-A shows the voltage amplitude across the implants electrodes with respect to the amplitude applied by the external electrodes at the

lower limb. As reported in Chapter 5, a minimum voltage amplitude of 7.35 V across the dummy implant electrodes is required for implant operation [127]. This, according to the simulation, corresponds to 57 V and 68 V applied by the external system to activate the GA and TA implants respectively. Figure 6.7 shows the electric potential amplitude in the cross sectional area of the implants deployed into the TA and GA muscles when 70 V are applied by the external system.

If the implants were to be used for continuous stimulation, assuming that the system had to be initialized each second, the power would range between 2.7 and 4 W depending on the frequency of stimulation (Figure 6.6-B).

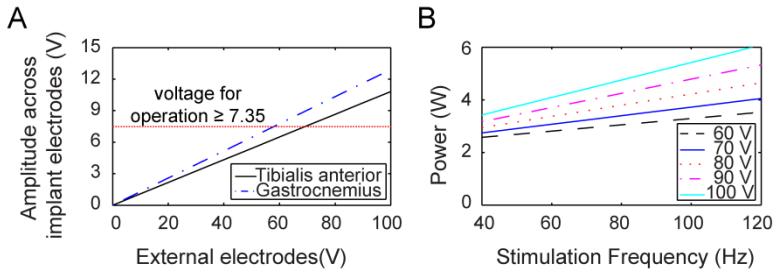

Figure 6.6. Parametric simulation results for the lower limb. A) Voltage amplitude across implant electrodes for different voltages applied by the external system. B) Power consumption of the external system when the implants are used for continuous stimulation, modeling different input voltages and stimulation frequencies (i.e. bursts frequency).

For each stimulation burst, the implants deliver a biphasic current pulse with an amplitude of about 2 mA through an impedance of about 500 Ω (muscle tissue impedance measured across the implant electrodes in the lower limb using the FEM model). Hence the instantaneous power delivered by the implants is about 2 mW. At a stimulation frequency of 100 Hz, assuming that the implants are required to stimulate continuously (A= 70 V), the required HF power would be 3.7 W (Figure 6.6-B), which implies an efficiency of 0.05%.

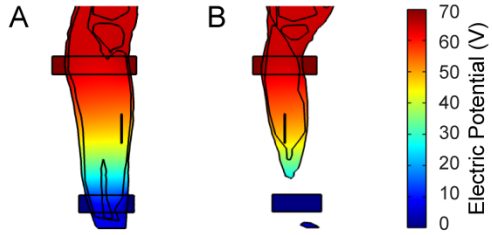

Figure 6.7. Electric potential at yz planes where the implants are deployed when 70 V are applied by the external system at the lower limb. A) Plane through implant at tibialis anterior and B) gastrocnemius muscles.

Upper limb

Figure 6.8-A shows the voltage amplitude across the implant electrodes located at the biceps and triceps brachii, with respect to the voltage applied by the external system at the external electrodes. As the minimum voltage for operation of the dummy implant is 7.35 V, the external system should deliver at least 40 V to operate the dummy implants. Figure 6.9 shows the electric potential in the cross sectional area where the dummy implants are located. Assuming that the system is initialized every second (A = 40 V), the HF power consumption would range between 1.1 and 2 W, depending on the frequency of stimulation (Figure 6.8-B).

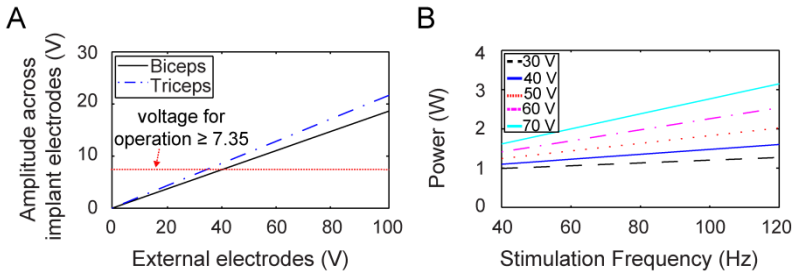

Figure 6.8. Parametric simulation results for the upper limb. A) Voltage amplitude across the implants electrodes for different voltages applied by the external system. B) Power consumption of the external system when the implants are used for continuous stimulation, modeling different input voltages and stimulation frequencies (i.e. bursts frequency).

In terms of power efficiency during electrical stimulation, the muscle tissue impedance across the implant electrodes is approximately 300 Ω when located in the upper arm. If the implant delivers biphasic current pulses of about 2 mA, the instantaneous power delivered by the device is about 1.2 mW. Assuming the continuous operation of the implant and a stimulation frequency of 100 Hz (A= 40 V), the HF power required to

electrically feed the implants and generate LF current for stimulation is 1.48 W (Figure 6.8-B). Therefore, the efficiency of the system for a 100 Hz electrical stimulation at the triceps and biceps brachii is 0.08%.

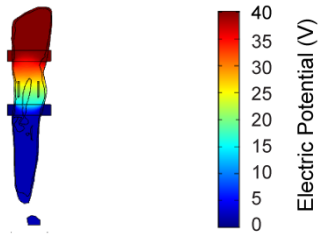

Figure 6.9. Electric potential at the yz plane where the implants are deployed when 40 V are applied by the external system at the upper limb.

6.4. Discussion

The numerical analysis shows that the equivalent electric field delivered by the external generator is safe in terms of unwanted electrostimulation and tissue heating. Both the calculated $|\mathbf{E}_{\mathrm{rms}}|$ and the local SAR comfortably comply with IEEE standards.

To make the system safer in terms of unwanted electrostimulation, it is suggested to increase the frequency used by the auxiliary HF current generator. For example, if a 5 MHz ac current is used, the threshold for unwanted electrostimulation in extremities would raise to a rms value of 3134 V/m. Then, the HF current would only be a concern for tissue heating. However, in the particular case of the external system used in this thesis, the bandwidth of the high voltage amplifier (WMA 300 by Falco Systems) limits the amplification of this HF current frequency. Hence, the HF current frequency could only be increased by replacing such high voltage amplifier.

Despite it was simulated an extreme and almost implausible scenario in which the implants described in this thesis must continuously apply stimulation pulses at 100 Hz at the lower and upper limb, this study shows that the power drawn by the external generator described in Chapter 2 would be below 4 W. This indicates that, although the eAXON method exhibits a very poor energy efficiency as most of the HF currents delivered to tissues are lost in Joule heating, it will be possible to use existing rechargeable portable batteries (> 100 Wh/kg) in the external generator to drive the network of injectable devices demonstrated in this thesis. Thus, not only the implants can be minimally invasive but also the external systems can be comfortable as they may consist in a small electronic unit wired to superficial electrodes, which may be embedded in a garment using conductive textiles [78].

6.5. Conclusions

In here we numerically demonstrate that, according to the IEEE standards, the injectable devices demonstrated in this thesis are safe in terms of unwanted electrostimulation. We have also demonstrated that, according to ICNIRP and IEEE standards, the HF currents delivered by the external system proposed in Chapter 2 for stimulation are safe in terms of tissue heating. This is explained basically as the external system delivers HF currents (avoiding unwanted electrostimulation) applied in short bursts (avoiding tissue heating).

Because of its intended functionality, a FES system based on the eAXON method must be portable. In here we demonstrate that even with a low power efficiency, the power required for operation can be supplied by existing portable batteries.

CHAPTER 7

Conclusions

7.1. General conclusions

In this thesis, it has been demonstrated that epidermically applied HF current bursts can be used to power miniaturized implantable devices and perform local electrical stimulation of excitable tissues by means of electronic rectification. In particular, it has been demonstrated that this method, referred to in this thesis as the *eAXON method*, allows the development of 2 mm thick microcontrolled injectable neuromuscular stimulators built only with off-the-shelf components. This goal was accomplished by:

- Proposing a basic electronic architecture for the addressable implant which can be implemented with small commercially available discrete components. The proposed circuitry picks up high frequency current and rectifies it into low frequency current for powering and performing electrical stimulation.
- Proposing add-ons that complement the proposed electronic architecture. The first add-on corresponds to the development of an active charge balance approach for future ultrathin ASIC based implants. The second add-on corresponds to a method to perform bidirectional communications, contributing to the development of closed-loop control for neuroprosthetic systems.
- Developing an implantable prototype based only on off-the-shelf components mounted on a rigid-flexible printed circuit board. The prototype was encapsulated in silicone tubing with two stainless steel electrodes at opposite ends. The device performs charge-balanced electrical stimulation of excitable tissues, and responds to commands amplitude modulated on the auxiliary HF current.
- Demonstrating that the high frequency current bursts delivered by the external system to operate the implants are safe in terms of tissue heating and unwanted electrostimulation according to safety standards, and that the external system that provides this high frequency current could employ portable batteries.

7.2. Overview

Chapter 1 described the eAXON method and explained how high frequency current bursts can be used to power up implantable electronic devices by means of galvanic coupling. The cell membrane and the intracellular and extracellular media behave as a low-pass filter. This phenomenon gives rise to the eAXON method, as the high frequency currents can be used to power up an implantable stimulator, and these currents can be rectified by the implant to generate low frequency currents capable of neuromuscular electrical stimulation. The method proposed was compared with other powering approaches for implantable stimulators, showing that the eAXON method avoids the use of bulky

components such as coils and batteries, paving the way to miniaturized electrical stimulators for neuroprostheses. Furthermore, it was reported why the external system that delivers high frequency current bursts to tissues is convenient in terms of ease of use. This is explained as only two external textile electrodes are required and could be easily embedded in garments.

In Chapter 2 it is described an electronic architecture for an injectable stimulator based on the eAXON method. It is made only of commercially available components. *In vitro* assays were carried out to evaluate how the information that is amplitude modulated on the high frequency current is demodulated by the implantable circuit. Additionally, the power saving mode of the control unit was evaluated to demonstrate that the implantable device could operate even if the external system provided the high frequency current in the form of bursts. *In vivo* assays were performed in an anesthetized rabbit. It was demonstrated that the circuit prototypes are capable of delivering enough low frequency current for neuromuscular stimulation. As the devices act as peak current limiters for the half-rectified HF current (i.e. they behave as current-controlled stimulators), they do not strongly depend on load impedance. The biphasic symmetric current waveforms were passively balanced using a dc-blocking capacitor, avoiding electrode corrosion and active tissue damage in the electrode-tissue interface. The *in vivo* assays demonstrated that the electronic architecture proposed accomplishes independent electrical stimulation, as the implant prototypes can be wirelessly addressed by the external system and can selectively stimulate one muscle or another.

In Chapter 3 an active charge-balance approach for future ultrathin implants based on ASICs is reported. The method consists of a monitoring capacitor that is automatically discharged by a digital charge quantifier. The control unit counts the amount of discharges, to match the discharges made in the anodal phase of the biphasic waveform, with those made in the previous cathodal phase. Then, the anodic pulse duration is adjusted by the number of discharges generated by the circuit during the preceding cathodic pulse. This results in a biphasic asymmetric current waveform for stimulation. The operation of the charge counter for balancing injected charge is inspired in the functioning of the tipping bucket rain gauge. This active charge-balance add-on avoids the use of bulky capacitors, as those used for dc-blocking in passive charge-balance approaches. Thereby, it contributes to the development of future ASIC-based ultrathin implants that rectify high frequency current bursts for electrical stimulation.

Chapter 4 illustrates how the eAXON method also allows bidirectional communications between the implants and the external system. This will enable proprioception-like sensing capabilities that may be crucial for closed-loop neuroprosthetic systems. To generate the

uplink, the implants deliver biphasic symmetric current waveforms with a frequency which is low enough as to not interfere with the high frequency current delivered by the external system. These Manchester encoded currents amplitude-modulate the high frequency current, and are externally sensed, filtered, demodulated and decoded by a receiver consisting of a sensing resistor, low-pass filters and a decoding algorithm.

Chapter 5 reports the development and testing of an injectable device based on the electronic architecture proposed in Chapter 2. A cylindrical, semi-rigid, 2 mm thick implant was accomplished. This cylindrical body conformation allows ease of implantation using a percutaneous injection. Additionally, the semi-rigidity of the device helps it settle down in tissues smoothly. The implant housing is composed of biocompatible materials. The devices were deployed using a 10 G catheter into the tibialis anterior and gastrocnemius muscles of an anesthetized rabbit. They were addressed using the external high frequency current generator proposed. The injectable devices generated locally low frequency currents to independently stimulate the target muscles. The external system, via the user interface, was capable of defining the frequency of stimulation and the stimulation intensity.

Chapter 5 reports finite element method simulations and *in vitro* assays to test the ability of the eAXON method to power the developed injectable prototypes by means of galvanic coupling. In this sense, it was evaluated how the angle between the prototypes' axis and the electric field delivered by the external system affects the voltage picked up by the implant electrodes. The results demonstrated that even with a 45º tilt, the injectable prototypes can power up by galvanic coupling and deliver enough low frequency current for stimulation. This paves the way to use galvanic coupling as a remote wireless powering approach for implantable devices, especially those intended to accomplish high level of miniaturization.

Chapter 6 demonstrates that the high frequency current bursts delivered by the external system proposed in this thesis are safe in terms of unwanted electrostimulation and tissue heating according to the IEEE standards. The chapter also reports finite element method simulations in high-resolution anatomical body parts, demonstrating that the proposed external system can be made portable, which is a must to ensure patient comfort in motor neuroprostheses.

7.3. Future perspective and directions

In this thesis it has been reported the development and assay of 2 mm thick microcontrolled injectable stimulators based on what we refer to as the *eAXON method*. No drawbacks were identified that should prevent the method from being applied to the development of ultrathin eAXON implants made of ASICs (Figure 7.1). Hopefully, in the near future it will

be possible to develop ultrathin implants for patients suffering from paralysis.

The electronic architecture proposed in this thesis can be improved in several ways. First, taking advantage of the bidirectional communications capabilities of the electrical stimulation method proposed, the electronic architecture could include sensing circuits to provide information to the external system. This information could include the integrity of the electrode-tissue interface, the muscular activation generated by the implantable stimulator, and the intentions of the patients to move a specific part of his or her body, as in the case of patients that have a minimum control over their extremities, or in the case of targeted muscle reinnervation.

Second, the architecture has proven to accomplish the goals proposed in terms of electrical stimulation by using stimulation parameters as pulse duration and frequency to modulate force. However, as explained in Chapter 1, shorter pulses increase the spatial selectivity of stimulation, reduce the power requirements for stimulation, and reduce the possibility of electrode corrosion or tissue damage. Furthermore, the stimulation frequency should be defined high enough to accomplish summation of muscle twitches, but low enough to avoid fatigue. Therefore, the electronic architecture proposed could be more efficient modulating force by varying the magnitude of the stimulus pulse. This implies that the circuit could include different current limiters to deliver different current magnitudes, improving the stimulation patterns.

The proposed communication protocol is capable of addressing one implant for every *Power up* stage delivered by the external system. This is not practical if the implants are intended for more complex recruitment patterns, as multiple *Power up* stages could foment tissue heating. Further work has been done in this sense to activate multiple implants using a single *Power up* stage. Recently, we have developed an upgraded downlink communication protocol to activate two implants simultaneously, sequentially, or in overlapping periods of time. This work has been part of a Master thesis project developed by a student from Technical University of Munich [156]. Further research on this topic is proposed to control at least 8 implantable devices using a single initialization process (one *Power up* stage).

Future research is proposed to improve the implant's housing for acute (i.e. hours and days) and chronic (weeks or months) assays. For instance, is it proposed to improve hermeticity to protect the electronic components from corrosion and damage, and to protect the rigid-flexible PCB, which is very susceptible to humidity. It is also proposed to change the material of the implant electrodes. Nowadays, the prototypes use stainless steel electrodes. However, electrodes based on platinum are more suitable for implantable electrical stimulators as they are more resistant to

corrosion. The union between the electrode and the implant's housing (e.g. the silicone tubing) could be improved to help accomplish hermeticity.

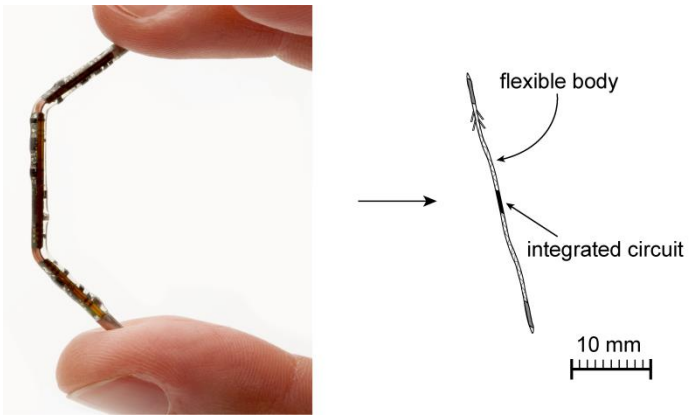

Figure 7.1. The microcontrolled injectable stimulators developed and demonstrated in this thesis are a proof-of-concept for the development of ultrathin eAXONs based on a single integrated circuit.

References

[1] NIH; American Heart Association; The Centers for Disease Control and Prevention, “Heart Disease and Stroke Statistics At a Glance,” 2015.

[2] WHO, “Spinal cord injury, Fact sheet N°384,” 2013.

[3] S. M. Gomez-Amaya, M. F. Barbe, W. C. de Groat, J. M. Brown, G. F. Tuite, J. Corcos, S. B. Fecho, A. S. Braverman, and M. R. Ruggieri, “Neural reconstruction methods of restoring bladder function.,” *Nat. Rev. Urol.*, vol. 12, no. 2, pp. 100–18, Feb. 2015.

[4] A. A. Freehafer, “Tendon transfers to improve grasp in patients with cervical spinal cord injury.,” *Paraplegia*, vol. 13, no. 1, pp. 15–24, May 1975.

[5] P. H. Peckham and K. L. Kilgore, “Challenges and Opportunities in Restoring Function After Paralysis,” *Biomed. Eng. IEEE Trans.*, vol. 60, no. 3, pp. 602–609, 2013.

[6] D. R. Moore and R. V Shannon, “Beyond cochlear implants: awakening the deafened brain,” *Nat Neurosci*, vol. 12, no. 6, pp. 686–691, Jun. 2009.

[7] NIH National Institutes of Health, “FACT SHEET - Cochlear Implants,” 2010.

[8] K. Mathieson, J. Loudin, G. Goetz, P. Huie, L. Wang, T. I. Kamins, L. Galambos, R. Smith, J. S. Harris, A. Sher, and D. Palanker, “Photovoltaic retinal prosthesis with high pixel density,” *Nat Phot.*, vol. 6, no. 12, p. 872, Dec. 2012.

[9] A. C. Ho, M. S. Humayun, J. D. Dorn, L. da Cruz, G. Dagnelie, J. Handa, P.-O. Barale, J.-A. Sahel, P. E. Stanga, F. Hafezi, A. B. Safran, J. Salzmann, A. Santos, D. Birch, R. Spencer, A. V Cideciyan, E. de Juan, J. L. Duncan, D. Eliott, A. Fawzi, L. C. Olmos de Koo, G. C. Brown, J. A. Haller, C. D. Regillo, L. V Del Priore, A. Arditi, D. R. Geruschat, and R. J. Greenberg, “Long-Term Results from an Epiretinal Prosthesis to Restore Sight to the Blind.,” *Ophthalmology*, vol. 122, no. 8, pp. 1547–54, Aug. 2015.

[10] L. Greenemeier, “FDA Approves First Retinal Implant,” *Nature*, Feb. 2013.

[11] S. Salmons, “Skeletal Muscle,” in *Neuroprosthetics: Theory and Practice*, K. Horch and G. S. Dhillon, Eds. World Scientific Publishing Co Pte Ltd, 2004, pp. 158–183.

[12] P. H. Peckham and J. S. Knutson, “Functional Electrical Stimulation for Neuromuscular Applications,” *Annu. Rev. Biomed. Eng.*, vol. 7, no. 1, pp. 327–360, 2005.

[13] G. S. Brindley, “The first 500 patients with sacral anterior root stimulator implants: general description,” *Paraplegia*, vol. 32, no. 12, pp. 795–805, 1994.

[14] J. H. Burridge, M. Haugland, B. Larsen, R. M. Pickering, N. Svaneborg, H. K. Iversen, P. B. Christensen, J. Haase, J. Brennum, and T. Sinkjaer, “Phase II trial to evaluate the ActiGait implanted drop-foot stimulator in established hemiplegia.,” *J. Rehabil. Med.*, vol. 39, no. 3, pp. 212–8, Apr. 2007.

[15] W. W. L. Glenn and M. L. Phelps, “Diaphragm Pacing by Electrical Stimulation of the Phrenic Nerve.,” *Neurosurgery*, vol. 17, no. 6, 1985.

[16] A. DiMarco, “Diaphragm pacing in patients with spinal cord injury,” *Top. Spinal Cord Inj. Rehabil.*, vol. 5, no. 1, pp. 6–20, 1999.

[17] D. M. Durand, W. M. Grill, and R. Kirsch, “Electrical Stimulation of the Neuromuscular System,” in *Neural Engineering SE - 5*, B. He, Ed. Springer US, 2005, pp. 157–191.

[18] K. Kilgore and R. F. Kirsch, “Upper and lower extremity motor neuroprostheses,” in *Neuroprosthetics: Theory and Practice*, K. Horch and G. S. Dhillon, Eds. World Scientific, 2004, pp. 844–877.

[19] A. Prochazka, “Neural Prostheses for Neurotrauma,” in *Translational Neuroscience: Fundamental Approaches for Neurological Disorders*, H. M. Tuszynski, Ed. Boston, MA: Springer US, 2016, pp. 457–478.

[20] E. Hultman, H. Sjöholm, I. Jäderholm-Ek, and J. Krynicki, “Evaluation of methods for electrical stimulation of human skeletal muscle in situ,” *Pflügers Arch. Eur. J. Physiol.*, vol. 398, no. 2, pp. 139–141, Jul. 1983.

[21] J. E. Hall and A. C. Guyton, *Guyton and Hall Textbook of Medical Physiology*. Elsevier, 2015.

[22] M. J. Kane, P. P. Breen, F. Quondamatteo, and G. ÓLaighin, “BION microstimulators: A case study in the engineering of an electronic implantable medical device,” *Med. Eng. Phys.*, vol. 33, no. 1, pp. 7–16, 2011.

[23] D. R. Merrill, R. Davis, R. Turk, and J. H. Burridge, “A Personalized Sensor-Controlled Microstimulator System for Arm Rehabilitation Poststroke. Part 1: System Architecture,” *Neuromodulation Technol. Neural Interface*, vol. 14, no. 1, pp. 72–79, Jan. 2011.

[24] G. E. Loeb, R. A. Peck, W. H. Moore, and K. Hood, “BION™ system for distributed neural prosthetic interfaces,” *Med. Eng. Phys.*, vol. 23, no. 1, pp. 9–18, 2001.

[25] W. M. Grill, “Electrical stimulation of the peripheral nervous system: biophysics and excitation properties,” in *Neuroprosthetics: Theory and Practice*, K. Horch and G. S. Dhillon, Eds. World Scientific, 2004, pp. 319–341.

[26] J. T. Mortimer and N. Bhadra, “Chapter 11 - Fundamentals of Electrical Stimulation,” in *Neuromodulation*, P. H. P. Elliot S. Krames A. Hunter Peckham and Ali R. Rezai Elliot S. Krames and A. R. Rezai, Eds. San Diego: Academic Press, 2009, pp. 109–121.

[27] M. E. Llewellyn, K. R. Thompson, K. Deisseroth, and S. L. Delp, “Orderly recruitment of motor units under optical control in vivo,” *Nat. Med.*, vol. 16, no. 10, pp. 1161–1165, Sep. 2010.

[28] P. Feiereisen, J. Duchateau, and K. Hainaut, “Motor unit recruitment order during voluntary and electrically induced contractions in the tibialis anterior,” *Exp. Brain Res.*, vol. 114, no. 1, pp. 117–123, Mar. 1997.

[29] A. C. Hughes, L. Liang Guo, and S. P. DeWeerth, “Interleaved multichannel epimysial stimulation for eliciting smooth contraction of muscle with reduced fatigue,” in *Annual International Conference of the IEEE Engineering in Medicine and Biology Society*, 2010, pp. 6226–6229.

[30] L. Z. P. Maneski, N. M. Malešević, A. M. Savić, T. Keller, and D. B. Popović, “Surface-distributed low-frequency asynchronous stimulation delays fatigue of stimulated muscles,” *Muscle Nerve*, vol. 48, no. 6, pp. 930–937, Dec. 2013.

[31] D. McDonnall, G. A. Clark, and R. A. Normann, “Interleaved, multisite electrical stimulation of cat sciatic nerve produces fatigue-resistant, ripple-free motor responses,” *IEEE Trans. Neural Syst. Rehabil. Eng.*, vol. 12, no. 2, pp. 208–215, 2004.

[32] R. A. Normann, B. R. Dowden, M. A. Frankel, A. M. Wilder, S. D. Hiatt, N. M. Ledbetter, D. A. Warren, and G. A. Clark, “Coordinated, multi-joint, fatigue-resistant feline stance produced with intrafascicular hind limb nerve stimulation,” *J. Neural Eng.*, vol. 9, no. 2, p. 026019, Apr. 2012.

[33] P. H. Peckham and D. M. Ackermann, “Chapter 18 - Implantable Neural Stimulators,” in *Neuromodulation*, San Diego: Academic Press, 2009, pp. 215–228.

[34] A. Ben Amar, A. B. Kouki, and H. Cao, “Power Approaches for Implantable Medical Devices.,” *Sensors*, vol. 15, no. 11, pp. 28889–914, 2015.

[35] M. Rasouli and L. S. J. Phee, “Energy sources and their development for application in medical devices.,” *Expert Rev. Med. Devices*, vol. 7, no. 5, pp. 693–709, Sep. 2010.

[36] C. L. Schmidt and P. M. Skarstad, “The future of lithium and lithium-ion batteries in implantable medical devices,” *J. Power Sources*, vol. 97, pp. 742–746, 2001.

[37] A. Kim, M. Ochoa, R. Rahimi, and B. Ziaie, “New and Emerging Energy Sources for Implantable Wireless Microdevices,” *IEEE Access*, vol. 3, pp. 89–98, 2015.

[38] C. Meng, O. Z. Gall, and P. P. Irazoqui, “A flexible super-capacitive solid-state power supply for miniature implantable medical devices.,” *Biomed. Microdevices*, vol. 15, no. 6, pp. 973–83, Dec. 2013.

[39] L. B. Wingard, C. H. Shaw, and J. F. Castner, “Bioelectrochemical fuel cells,” *Enzyme Microb. Technol.*, vol. 4, no. 3, pp. 137–142, 1982.

[40] J. W. Spickler, N. S. Rasor, P. Kezdi, S. N. Misra, K. E. Robins, and C. LeBoeuf, “Totally self-contained intracardiac pacemaker,” *J. Electrocardiol.*, vol. 3, no. 3, pp. 325–331, 1970.

[41] C. Dagdeviren, B. D. Yang, Y. Su, P. L. Tran, P. Joe, E. Anderson, J. Xia, V. Doraiswamy, B. Dehdashti, X. Feng, B. Lu, R. Poston, Z. Khalpey, R. Ghaffari, Y. Huang, M. J. Slepian, and J. A. Rogers, “Conformal piezoelectric energy harvesting and storage from motions of the heart, lung, and diaphragm.,” *Proc. Natl. Acad. Sci. U. S. A.*, vol. 111, no. 5, pp. 1927–32, Feb. 2014.

[42] P. P. Mercier, A. C. Lysaght, S. Bandyopadhyay, A. P. Chandrakasan, and K. M. Stankovic, “Energy extraction from the biologic battery in the inner ear.,” *Nat. Biotechnol.*, vol. 30, no. 12, pp. 1240–3, Dec. 2012.

[43] W. J. Heetderks, “RF powering of millimeter- and submillimeter-sized neural prosthetic implants.,” *IEEE Trans. Biomed. Eng.*, vol. 35, no. 5, pp. 323–7, May 1988.

[44] G. E. Loeb, C. J. Zamin, J. H. Schulman, and P. R. Troyk, “Injectable microstimulator for functional electrical stimulation,” *Med. Biol. Eng. Comput.*, vol. 29, no. 6, pp. NS13–NS19, Nov. 1991.

[45] B. Ziaie, M. D. Nardin, A. R. Coghlan, and K. Najafi, “A single-channel implantable microstimulator for functional neuromuscular stimulation,” *Biomed. Eng. IEEE Trans.*, vol. 44, no. 10, pp. 909–920, 1997.

[46] B. Smith, Z. Tang, M. W. Johnson, S. Pourmehdi, M. M. Gazdik, J. R. Buckett, and P. H. Peckham, “An externally powered, multichannel, implantable stimulator-telemeter for control of paralyzed muscle.,” *IEEE Trans. Biomed. Eng.*, vol. 45, no. 4, pp. 463–75, Apr. 1998.

[47] J. H. Schulman, “The Feasible FES System: Battery Powered BION Stimulator,” *Proc. IEEE*, vol. 96, no. 7, pp. 1226–1239, 2008.

[48] B. Smith, T. J. Crish, J. R. Buckett, K. L. Kilgore, and P. H. Peckham, “Development of an implantable networked neuroprosthesis,” in *Conference Proceedings. 2nd International IEEE EMBS Conference on Neural Engineering, 2005.*, 2005, pp. 454–457.

[49] J. S. Ho, A. J. Yeh, E. Neofytou, S. Kim, Y. Tanabe, B. Patlolla, R. E. Beygui, and A. S. Y. Poon, "Wireless power transfer to deep-tissue microimplants," *Proc. Natl. Acad. Sci.*, pp. 7974–7979, May 2014.

[50] J. S. Ho, S. Kim, and A. S. Y. Poon, "Midfield Wireless Powering for Implantable Systems," *Proc. IEEE*, vol. 101, no. 6, pp. 1369–1378, Jun. 2013.

[51] K. L. Montgomery, A. J. Yeh, J. S. Ho, V. Tsao, S. Mohan Iyer, L. Grosenick, E. A. Ferenczi, Y. Tanabe, K. Deisseroth, S. L. Delp, and A. S. Y. Poon, "Wirelessly powered, fully internal optogenetics for brain, spinal and peripheral circuits in mice," *Nat Meth*, vol. 12, no. 10, pp. 969–974, Oct. 2015.

[52] B. C. Towe, P. J. Larson, and D. W. Gulick, "A microwave powered injectable neural stimulator," in *Engineering in Medicine and Biology Society (EMBC), 2012 Annual International Conference of the IEEE*, 2012, pp. 5006–5009.

[53] A. vander (André) Vorst, A. Rosen, and Y. (Youji) Kotsuka, *RF/microwave interaction with biological tissues*. John Wiley & Sons, 2006.

[54] D. Freedman, M. Sahin, and B. Towe, "Wireless Microstimulators," in *Encyclopedia of Computational Neuroscience SE - 605-3*, D. Jaeger and R. Jung, Eds. Springer New York, 2014, pp. 1–11.

[55] P. J. Larson and B. C. Towe, "Miniature ultrasonically powered wireless nerve cuff stimulator," in *2011 5th International IEEE/EMBS Conference on Neural Engineering*, 2011, pp. 265–268.

[56] D. W. Gulick and B. C. Towe, "Method of locating ultrasound-powered nerve stimulators.," *Annu. Int. Conf. IEEE Eng. Med. Biol. Soc.*, vol. 2012, pp. 887–90, Jan. 2012.

[57] D. W. Gulick and B. C. Towe, "Characterization of simple wireless neurostimulators and sensors.," *Annu. Int. Conf. IEEE Eng. Med. Biol. Soc.*, vol. 2014, pp. 3130–3, Jan. 2014.

[58] B. C. Towe, P. J. Larson, and D. W. Gulick, "Wireless ultrasound-powered biotelemetry for implants," in *2009 Annual International Conference of the IEEE Engineering in Medicine and Biology Society*, 2009, pp. 5421–5424.

[59] J. Charthad, M. J. Weber, T. C. Chang, and A. Arbabian, "A mm-Sized Implantable Medical Device (IMD) With Ultrasonic Power Transfer and a Hybrid Bi-Directional Data Link," *IEEE J. Solid-State Circuits*, vol. 50, no. 8, pp. 1741–1753, Aug. 2015.

[60] A. Auricchio, P.-P. Delnoy, C. Butter, J. Brachmann, L. Van Erven, S. Spitzer, T. Moccetti, M. Seifert, T. Markou, K. Laszo, and F. Regoli, "Feasibility, safety, and short-term outcome of

leadless ultrasound-based endocardial left ventricular resynchronization in heart failure patients: results of the wireless stimulation endocardially for CRT (WiSE-CRT) study.," *Europace*, vol. 16, no. 5, pp. 681–8, May 2014.

[61] H. Liu, T. Zhao, W. Jiang, R. Jia, D. Niu, G. Qiu, L. Fan, X. Li, W. Liu, B. Chen, Y. Shi, L. Yin, and B. Lu, "Flexible Battery-Less Bioelectronic Implants: Wireless Powering and Manipulation by Near-Infrared Light," *Adv. Funct. Mater.*, vol. 25, no. 45, pp. 7071–7079, Dec. 2015.

[62] A. Abdo, M. Sahin, D. S. Freedman, E. Cevik, P. S. Spuhler, and M. S. Unlu, "Floating light-activated microelectrical stimulators tested in the rat spinal cord.," *J. Neural Eng.*, vol. 8, no. 5, p. 056012, Oct. 2011.

[63] A. Abdo and M. Sahin, "Feasibility of Neural Stimulation With Floating-Light-Activated Microelectrical Stimulators," *Biomed. Circuits Syst. IEEE Trans.*, vol. 5, no. 2, pp. 179–188, 2011.

[64] E. Ç. Seymour, D. S. Freedman, M. Gökkavas, E. Ozbay, M. Sahin, and M. S. Unlü, "Improved selectivity from a wavelength addressable device for wireless stimulation of neural tissue.," *Front. Neuroeng.*, vol. 7, p. 5, Jan. 2014.

[65] M. Sahin and V. Pikov, "Wireless Microstimulators for Neural Prosthetics," *Crit. Rev. Biomed. Eng.*, vol. 39, no. 1, pp. 63–77, 2011.

[66] G. E. Loeb, R. A. Peck, J. Singh, Y.-H. Kim, S. Deshpande, L. L. Baker, and J. T. Bryant, "Mechanical loading of rigid intramuscular implants.," *Biomed. Microdevices*, vol. 9, no. 6, pp. 901–910, 2007.

[67] G. E. Loeb, F. J. R. Richmond, and L. L. Baker, "The BION devices: injectable interfaces with peripheral nerves and muscles," *Neurosurg. Focus*, vol. 20, no. 5, pp. 1–9, 2006.

[68] H. Kaplan and G. Loeb, "Design and Fabrication of an Injection Tool for Neuromuscular Microstimulators," *Ann. Biomed. Eng.*, vol. 37, no. 9, pp. 1858–1870, 2009.

[69] G. E. Loeb, F. J. R. Richmond, W. H. Moore, and R. A. Peck, "Design and fabrication of hermetic microelectronic implants," in *1st Annual International IEEE-EMBS Special Topic Conference on Microtechnologies in Medicine and Biology. Proceedings*, 2000, pp. 455–459.

[70] Boston Scientific Corporation, "Boston Scientific Announces Acquisition of Advanced Bionics Corporation," Valencia, California, 2004.

[71] G. E. Loeb, L. Zhou, K. Zheng, A. Nicholson, R. A. Peck, A. Krishnan, M. Silka, J. Pruetz, R. Chmait, and Y. Bar-Cohen, "Design and testing of a percutaneously implantable fetal

pacemaker.,” *Ann. Biomed. Eng.*, vol. 41, no. 1, pp. 17–27, Jan. 2013.

[72] L. Zhou, A. N. Vest, R. H. Chmait, Y. Bar-Cohen, J. Pruetz, M. Silka, K. Zheng, R. Peck, and G. E. Loeb, “A percutaneously implantable fetal pacemaker.,” *Annu. Int. Conf. IEEE Eng. Med. Biol. Soc.*, vol. 2014, pp. 4459–63, Jan. 2014.

[73] A. Ivorra, “Remote Electrical Stimulation by Means of Implanted Rectifiers,” *PLoS One*, vol. 6, no. 8, p. e23456, 2011.

[74] A. Ivorra and L. Becerra-Fajardo, “Wireless Microstimulators Based on Electronic Rectification of Epidermically Applied Currents: Safety and Portability Analysis,” in *18th IFESS Annual Conference*, 2013, pp. 213–216.

[75] D. Holder, “Appendix A. Brief introduction to bioimpedance,” in *Electrical Impedance Tomography: Methods, History and Applications*, D. S. Holder, Ed. Taylor & Francis, 2007, pp. 411–422.

[76] J. Santos-Sacchi, “On the frequency limit and phase of outer hair cell motility: effects of the membrane filter.,” *J. Neurosci.*, vol. 12, no. 5, pp. 1906–16, May 1992.

[77] J. P. Reilly, *Applied bioelectricity: from electrical stimulation to electropathology*. New York: Springer-Verlag, 1998.

[78] L. Becerra-Fajardo and A. Ivorra, “In Vivo Demonstration of Addressable Microstimulators Powered by Rectification of Epidermically Applied Currents for Miniaturized Neuroprostheses,” *PLoS One*, vol. 10, no. 7, p. e0131666, Jul. 2015.

[79] A. Ivorra and L. Becerra-Fajardo, “Flexible Thread-like Electrical Stimulation Implants Based on Rectification of Epidermically Applied Currents Which Perform Charge Balance,” in *Replace, Repair, Restore, Relieve – Bridging Clinical and Engineering Solutions in Neurorehabilitation SE - 67*, vol. 7, W. Jensen, O. K. Andersen, and M. Akay, Eds. Springer International Publishing, 2014, pp. 447–455.

[80] R. Davis, T. Houdayer, B. Andrews, and A. Barriskill, “Paraplegia: Prolonged Standing Using Closed-Loop Functional Electrical Stimulation and Andrews Ankle-Foot Orthosis,” *Artif. Organs*, vol. 23, no. 5, pp. 418–420, May 1999.

[81] Y. Palti, “Stimulation of muscles and nerves by means of externally applied electrodes.,” *Bull. Res. Counc. Isr. Sect. E. Exp. Med.*, vol. 10, pp. 54–6, Jun. 1962.

[82] J. C. Schuder and H. Stoeckle, “The Silicone Diode as a Receiver for Electrical Stimulation of Body Organs.,” *ASAIO J.*, vol. 10, no. 1, 1964.

[83] M. Oberle, “Low power systems-on-chip for biomedical

applications." ETHZ, 2002.
[84] M. S. Wegmueller, S. Huclova, J. Froehlich, M. Oberle, N. Felber, N. Kuster, and W. Fichtner, "Galvanic Coupling Enabling Wireless Implant Communications," *IEEE Trans. Instrum. Meas.*, vol. 58, no. 8, pp. 2618–2625, Aug. 2009.
[85] Y. Song, Q. Hao, K. Zhang, M. Wang, Y. Chu, and B. Kang, "The Simulation Method of the Galvanic Coupling Intrabody Communication With Different Signal Transmission Paths," *IEEE Trans. Instrum. Meas.*, vol. 60, no. 4, pp. 1257–1266, Apr. 2011.
[86] M. A. Callejón, J. Reina-Tosina, L. Roa, and D. Naranjo, "A Distributed-Parameter Approach to Model Galvanic and Capacitive Coupling for Intra-body Communications," in *Wireless Mobile Communication and Healthcare SE - 1*, vol. 83, K. Nikita, J. Lin, D. Fotiadis, and M.-T. Arredondo Waldmeyer, Eds. Springer Berlin Heidelberg, 2012, pp. 1–8.
[87] M. Seyedi, B. Kibret, D. T. H. Lai, and M. Faulkner, "A survey on intrabody communications for body area network applications.," *Biomed. Eng. IEEE Trans.*, vol. 60, no. 8, pp. 2067–79, Aug. 2013.
[88] Z. Tang, R. J. Sclabassi, C. Sun, S. A. Hackworth, J. Zhao, X. T. Cui, and M. Sun, "Transcutaneous battery recharging by volume conduction and its circuit modeling.," in *Annual International Conference of the IEEE Engineering in Medicine and Biology Society*, 2006, vol. 1, pp. 644–7.
[89] S. A. Hackworth, "Design, optimization, and implementation of a volume conduction energy transfer platform for implantable devices," University of Pittsburgh, 2010.
[90] L. S. Gan, A. Prochazka, T. D. Bornes, A. A. Denington, and K. M. Chan, "A new means of transcutaneous coupling for neural prostheses.," *IEEE Trans. Biomed. Eng.*, vol. 54, no. 3, pp. 509–17, Mar. 2007.
[91] L. S. Gan, E. Ravid, J. A. Kowalczewski, J. L. Olson, M. Morhart, and A. Prochazka, "First permanent implant of nerve stimulation leads activated by surface electrodes, enabling hand grasp and release: the stimulus router neuroprosthesis.," *Neurorehabil. Neural Repair*, vol. 26, no. 4, pp. 335–43, May 2012.
[92] W. M. Grill and J. T. Mortimer, "The effect of stimulus pulse duration on selectivity of neural stimulation.," *IEEE Trans. Biomed. Eng.*, vol. 43, no. 2, pp. 161–6, Feb. 1996.
[93] P. H. Gorman and J. T. Mortimer, "The Effect of Stimulus Parameters on the Recruitment Characteristics of Direct Nerve Stimulation," *Biomed. Eng. IEEE Trans.*, vol. BME-30, no. 7, pp. 407–414, 1983.
[94] W. M. Grill and R. F. Kirsch, "Neuroprosthetic applications of electrical stimulation.," *Assist. Technol.*, vol. 12, no. 1, pp. 6–20,

Jan. 2000.
[95] N. A. Maffiuletti, “Physiological and methodological considerations for the use of neuromuscular electrical stimulation,” *Eur. J. Appl. Physiol.*, vol. 110, no. 2, pp. 223–234, 2010.
[96] K. T. Ragnarsson, “Functional electrical stimulation after spinal cord injury: current use, therapeutic effects and future directions.,” *Spinal Cord*, vol. 46, no. 4, pp. 255–74, Apr. 2008.
[97] M. Sawan, Y. Laaziri, F. Mounaim, E. Elzayat, J. Corcos, and M. M. Elhilali, “Electrode-tissues interface: modeling and experimental validation.,” *Biomed. Mater.*, vol. 2, no. 1, pp. S7–S15, Mar. 2007.
[98] D. Tyler and K. H. Polasek, “Electrodes for the neural interface,” in *Neuromodulation*, vol. 9, E. S. Krames, P. Peckham, and A. R. Rezai, Eds. Academic Press San Diego, 2009, pp. 181–213.
[99] D. R. Merrill, M. Bikson, and J. G. R. Jefferys, “Electrical stimulation of excitable tissue: design of efficacious and safe protocols.,” *J. Neurosci. Methods*, vol. 141, no. 2, pp. 171–98, Feb. 2005.
[100] D. R. Merrill, “The electrochemistry of charge injection at the electrode/tissue interface,” in *Implantable Neural Prostheses 2*, Springer, 2010, pp. 85–138.
[101] W. Franks, I. Schenker, P. Schmutz, and A. Hierlemann, “Impedance characterization and modeling of electrodes for biomedical applications.,” *IEEE Trans. Biomed. Eng.*, vol. 52, no. 7, pp. 1295–302, Jul. 2005.
[102] A. Uranga del Monte, *Desarrollo de un estimulador eléctrico integrado implantable para el control de la micción en lesionados medulares*. PhD Dissertation Thesis, Universitat Autònoma de Barcelona, 2001.
[103] M. Ghovanloo and K. Najafi, “A compact large voltage-compliance high output-impedance programmable current source for implantable microstimulators.,” *IEEE Trans. Biomed. Eng.*, vol. 52, no. 1, pp. 97–105, Jan. 2005.
[104] Y. Onuki, U. Bhardwaj, F. Papadimitrakopoulos, and D. J. Burgess, “A Review of the Biocompatibility of Implantable Devices: Current Challenges to Overcome Foreign Body Response,” *J. Diabetes Sci. Technol.*, vol. 2, no. 6, pp. 1003–1015, Nov. 2008.
[105] T. Stieglitz, “Electrode materials for recording and stimulation,” in *Neuroprosthetics: Theory and Practice*, vol. 2, World Scientific, 2004, pp. 475–516.
[106] S. F. Cogan, “Neural Stimulation and Recording Electrodes,” *Annu. Rev. Biomed. Eng.*, vol. 10, no. 1, pp. 275–309, 2008.
[107] P. H. Peckham, J. Van Der Meulen, and J. Reswick, “Electrical

Activation of Skeletal Muscle by Sequential Stimulation," in *The Nervous System and Electric Currents - Proceedings of the Third Annual National Conference of the Neuro-Electric Society*, N. L. Wulfsohn and A. Sances, Eds. Boston, MA: Springer US, 1970.

[108] K. Yoshida and K. Horch, "Reduced fatigue in electrically stimulated muscle using dual channel intrafascicular electrodes with interleaved stimulation," *Ann. Biomed. Eng.*, vol. 21, no. 6, pp. 709–714, Nov. 1993.

[109] R. Nguyen, K. Masani, S. Micera, M. Morari, and M. R. Popovic, "Spatially distributed sequential stimulation reduces fatigue in paralyzed triceps surae muscles: a case study.," *Artif. Organs*, vol. 35, no. 12, pp. 1174–80, Dec. 2011.

[110] A. C. Hughes, L. Guo, and S. P. Deweerth, "Interleaved multichannel epimysial stimulation for eliciting smooth contraction of muscle with reduced fatigue.," *Annu. Int. Conf. IEEE Eng. Med. Biol. Soc.*, vol. 2010, pp. 6226–9, Jan. 2010.

[111] A. Ivorra, L. Becerra-Fajardo, and Q. Castellví, "In vivo demonstration of injectable microstimulators based on charge-balanced rectification of epidermically applied currents," *J. Neural Eng.*, vol. 12, no. 6, p. 66010, 2015.

[112] L. Becerra-Fajardo, R. Garcia-Arnau, and A. Ivorra, "Injectable Stimulators Based on Rectification of High Frequency Current Bursts: Power Efficiency of 2 mm Thick Prototypes," in *International Conference on NeuroRehabilitation (ICNR2016)*, 2016, p. Accepted.

[113] C. E. Bouton, A. Shaikhouni, N. V. Annetta, M. A. Bockbrader, D. A. Friedenberg, D. M. Nielson, G. Sharma, P. B. Sederberg, B. C. Glenn, W. J. Mysiw, A. G. Morgan, M. Deogaonkar, and A. R. Rezai, "Restoring cortical control of functional movement in a human with quadriplegia," *Nature*, vol. 533, p. 247, Apr. 2016.

[114] N. Rogers, "Brain implant helps quadriplegic play Guitar Hero," *Science AAAS*, 2016.

[115] D. Graupe and H. A. C. Bazo, "Thoracic Level Complete Paraplegia–Walking Performance, Training and Medical Benefits with the PARASTEP FES System," *Int J Phys Med Rehabil*, vol. 3, no. 298, 2015.

[116] J. Hausdorf and H. Ring, "The Effect of the Ness L300 Neuroprosthesis on Gait Stability and Symmetry," *J. Neurol. Phys. Ther.*, vol. 30, no. 4, 2006.

[117] S. Khamis, R. Martikaro, S. Wientroub, Y. Hemo, and S. Hayek, "A functional electrical stimulation system improves knee control in crouch gait," *J. Child. Orthop.*, vol. 9, no. 2, pp. 137–143, 2015.

[118] J. Hoffer, M. Baru, S. Bedard, E. Calderon, G. Desmoulin, P. Dhawan, G. Jenne, J. Kerr, M. Whittaker, and T. Zwimpfer,

"Initial results with fully implanted NeurostepTM FES system for foot drop," in *10th Annual Conference of the International FES Society*, 2005.

[119] A. R. Buick, J. Kowalczewski, R. G. Carson, and A. Prochazka, "Tele-Supervised FES-Assisted Exercise for Hemiplegic Upper Limb.," *IEEE Trans. Neural Syst. Rehabil. Eng.*, vol. 24, no. 1, pp. 79–87, Jan. 2016.

[120] "Myndmove neuroprostheses." [Online]. Available: http://www.myndtec.com/myndmove.

[121] J. Spensley, "STIMuGRIP; a new hand control implant.," *Annu. Int. Conf. IEEE Eng. Med. Biol. Soc.*, vol. 2007, p. 513, Jan. 2007.

[122] A. Ivorra, J. Sacristán, and A. Baldi, "Injectable Rectifiers as Microdevices for Remote Electrical Stimulation: an Alternative to Inductive Coupling," in *World Congress on Medical Physics and Biomedical Engineering May 26-31, 2012, Beijing, China SE - 415*, vol. 39, M. Long, Ed. Springer Berlin Heidelberg, 2013, pp. 1581–1584.

[123] L. Becerra-Fajardo and A. Ivorra, "Proof of Concept of a Stimulator Based on AC Current Rectification for Neuroprosthetics," in *Congreso Anual Sociedad Española de Ingeniería Biomédica CASEIB*, 2012, p. pp76.

[124] L. Becerra-Fajardo and A. Ivorra, "Towards addressable wireless microstimulators based on electronic rectification of epidermically applied currents," in *Annual International Conference of the IEEE Engineering in Medicine and Biology Society*, 2014, pp. 3973–3976.

[125] C. van den Honert and J. T. Mortimer, "The response of the myelinated nerve fiber to short duration biphasic stimulating currents," *Ann. Biomed. Eng.*, vol. 7, no. 2, pp. 117–125, Mar. 1979.

[126] R. R. Riso, F. K. Mosallaie, W. Jensen, and T. Sinkjaer, "Nerve cuff recordings of muscle afferent activity from tibial and peroneal nerves in rabbit during passive ankle motion," *IEEE Trans. Rehabil. Eng.*, vol. 8, no. 2, pp. 244–258, 2000.

[127] L. Becerra-Fajardo, M. Schmidbauer, and A. Ivorra, "Demonstration of 2 mm thick microcontrolled injectable stimulators based on rectification of high frequency current bursts," *Under Rev.*, 2016.

[128] T. Kesar, L.-W. Chou, and S. A. Binder-Macleod, "Effects of stimulation frequency versus pulse duration modulation on muscle fatigue.," *J. Electromyogr. Kinesiol.*, vol. 18, no. 4, pp. 662–71, Aug. 2008.

[129] M. Ortmanns, "Charge Balancing in Functional Electrical Stimulators: A Comparative Study," in *2007 IEEE International*

Symposium on Circuits and Systems, 2007, pp. 573–576.
[130] S. Guo and H. Lee, "Biphasic-current-pulse self-calibration techniques for monopolar current stimulation," in *2009 IEEE Biomedical Circuits and Systems Conference*, 2009, pp. 61–64.
[131] M. Ghovanloo and K. Najafi, "A wireless implantable multichannel microstimulating system-on-a-chip with modular architecture.," *IEEE Trans. Neural Syst. Rehabil. Eng.*, vol. 15, no. 3, pp. 449–57, Sep. 2007.
[132] M. Sivaprakasam, M. S. Humayun, and J. D. Weiland, "A variable range bi-phasic current stimulus driver circuitry for an implantable retinal prosthetic device," *IEEE J. Solid-State Circuits*, vol. 40, no. 3, pp. 763–771, Mar. 2005.
[133] Ji-Jon Sit and R. Sarpeshkar, "A Low-Power Blocking-Capacitor-Free Charge-Balanced Electrode-Stimulator Chip With Less Than 6 nA DC Error for 1-mA Full-Scale Stimulation.," *IEEE Trans. Biomed. Circuits Syst.*, vol. 1, no. 3, pp. 172–83, Sep. 2007.
[134] E. K. F. Lee and A. Lam, "A Matching Technique for Biphasic Stimulation Pulse," in *2007 IEEE International Symposium on Circuits and Systems*, 2007, pp. 817–820.
[135] K. Sooksood, T. Stieglitz, and M. Ortmanns, "An active approach for charge balancing in functional electrical stimulation.," *IEEE Trans. Biomed. Circuits Syst.*, vol. 4, no. 3, pp. 162–70, Jun. 2010.
[136] B. Instrument, "Tipping bucket automated precipitation gauge," 2016. [Online]. Available: http://belfortinstrument.com/wp-content/uploads/2013/09/TIPPING-BUCKET-AUTOMATED-PRECIPITATION-GAUGE.pdf.
[137] J. P. Reilly, "Peripheral nerve stimulation by induced electric currents: Exposure to time-varying magnetic fields," *Med. Biol. Eng. Comput.*, vol. 27, no. 2, pp. 101–110, Mar. 1989.
[138] L. Becerra-Fajardo and A. Ivorra, "Bidirectional communications in wireless microstimulators based on electronic rectification of epidermically applied currents," in *Neural Engineering (NER), 2015 7th International IEEE/EMBS Conference on*, 2015, pp. 545–548.
[139] D. Farina, N. Ning Jiang, H. Rehbaum, A. Holobar, B. Graimann, H. Dietl, and O. C. Aszmann, "The Extraction of Neural Information from the Surface EMG for the Control of Upper-Limb Prostheses: Emerging Avenues and Challenges," *IEEE Trans. Neural Syst. Rehabil. Eng.*, vol. 22, no. 4, pp. 797–809, Jul. 2014.
[140] D. R. Merrill, J. Lockhart, P. R. Troyk, R. F. Weir, and D. L. Hankin, "Development of an implantable myoelectric sensor for advanced prosthesis control.," *Artif. Organs*, vol. 35, no. 3, pp. 249–52, Mar. 2011.
[141] T. A. Kuiken, G. Li, B. A. Lock, R. D. Lipschutz, L. A. Miller, K.

A. Stubblefield, and K. B. Englehart, “Targeted muscle reinnervation for real-time myoelectric control of multifunction artificial arms.,” *JAMA*, vol. 301, no. 6, pp. 619–28, Feb. 2009.

[142] D. Borton, S. Micera, J. del R. Millán, and G. Courtine, “Personalized neuroprosthetics.,” *Sci. Transl. Med.*, vol. 5, no. 210, p. 210rv2, Nov. 2013.

[143] S. Gabriel, R. W. Lau, and C. Gabriel, “The dielectric properties of biological tissues: III. Parametric models for the dielectric spectrum of tissues,” *Phys. Med. Biol.*, vol. 41, no. 11, pp. 2271–2293, Nov. 1996.

[144] P. D. Blumenthal, K. Gemzell-Danielsson, and M. Marintcheva-Petrova, “Tolerability and clinical safety of Implanon.,” *Eur. J. Contracept. Reprod. Health Care*, vol. 13 Suppl 1, pp. 29–36, Jun. 2008.

[145] L. Beckmann, C. Neuhaus, G. Medrano, N. Jungbecker, M. Walter, T. Gries, and S. Leonhardt, “Characterization of textile electrodes and conductors using standardized measurement setups.,” *Physiol. Meas.*, vol. 31, no. 2, pp. 233–47, Feb. 2010.

[146] L. Becerra-Fajardo and A. Ivorra, “Charge Counter for Performing Active Charge-Balance in Miniaturized Electrical Stimulators,” in *6th European Conference of the International Federation for Medical and Biological Engineering SE - 64*, vol. 45, 2015, pp. 256–259.

[147] “IEEE Standard for Safety Levels With Respect to Human Exposure to Electromagnetic Fields, 0-3 kHz.” p. 0_1–, 2002.

[148] “IEEE Standard for Safety Levels with Respect to Human Exposure to Radio Frequency Electromagnetic Fields, 3 kHz to 300 GHz,” pp. 1–238, Apr. 2006.

[149] “Guidelines for limiting exposure to time-varying electric, magnetic, and electromagnetic fields (up to 300 GHz). International Commission on Non-Ionizing Radiation Protection.,” *Health Phys.*, vol. 74, no. 4, pp. 494–522, Apr. 1998.

[150] B. Scrosati and J. Garche, “Lithium batteries: Status, prospects and future,” *J. Power Sources*, vol. 195, no. 9, pp. 2419–2430, 2010.

[151] A. Christ, W. Kainz, E. G. Hahn, K. Honegger, M. Zefferer, E. Neufeld, W. Rascher, R. Janka, W. Bautz, J. Chen, B. Kiefer, P. Schmitt, H.-P. Hollenbach, J. Shen, M. Oberle, D. Szczerba, A. Kam, J. W. Guag, and N. Kuster, “The Virtual Family—development of surface-based anatomical models of two adults and two children for dosimetric simulations,” *Phys. Med. Biol.*, vol. 55, no. 2, pp. N23–N38, Jan. 2010.

[152] R. Garcia-Arnau, “Implementación de modelos anatómicos humanos para simulaciones electromagnéticas en COMSOL Multiphysics.” Bachelor’s Thesis - Universitat Pompeu Fabra,

Barcelona, 2016.
[153] M. Parazzini, S. Fiocchi, E. Rossi, A. Paglialonga, and P. Ravazzani, “Transcranial direct current stimulation: estimation of the electric field and of the current density in an anatomical human head model.,” *IEEE Trans. Biomed. Eng.*, vol. 58, no. 6, pp. 1773–80, Jun. 2011.
[154] C. Gabriel and S. Gabriel, “Compilation of the Dielectric Properties of Body Tissues at RF and Microwave Frequencies.,” 1996.
[155] A. Ibrahiem, C. Dale, W. Tabbara, and J. Wiart, “Analysis of the Temperature Increase Linked to the Power Induced by RF Source,” *Prog. Electromagn. Res.*, vol. 52, pp. 23–46, 2005.
[156] M. Schmidbauer, “Upgrading Communications for Microstimulators based on Electronic Rectification of Epidermally Applied Currents.” Master Thesis - Technische Universität München, 2016.

List of Publications

International Journal Articles:

1. L. Becerra-Fajardo, M. Schmidbauer, and A. Ivorra, "Demonstration of 2 mm thick microcontrolled injectable stimulators based on rectification of high frequency current bursts," Under review, 2016.
2. A. Ivorra, L. Becerra-Fajardo, and Q. Castellví, "In vivo demonstration of injectable microstimulators based on charge-balanced rectification of epidermically applied currents," J. Neural Eng., vol. 12, no. 6, p. 66010, 2015.
3. L. Becerra-Fajardo and A. Ivorra, "In Vivo Demonstration of Addressable Microstimulators Powered by Rectification of Epidermically Applied Currents for Miniaturized Neuroprostheses," PLoS One, vol. 10, no. 7, p. e0131666, Jul. 2015.

Conference Proceedings:

1. L. Becerra-Fajardo and A. Ivorra, "Bidirectional communications in wireless microstimulators based on electronic rectification of epidermically applied currents," in Neural Engineering (NER), 2015 7th International IEEE/EMBS Conference on, 2015, pp. 545–548.
2. L. Becerra-Fajardo and A. Ivorra, "Charge Counter for Performing Active Charge-Balance in Miniaturized Electrical Stimulators," in 6th European Conference of the International Federation for Medical and Biological Engineering SE - 64, vol. 45, 2015, pp. 256–259.
3. L. Becerra-Fajardo and A. Ivorra, "Towards addressable wireless microstimulators based on electronic rectification of epidermically applied currents," in Annual International Conference of the IEEE Engineering in Medicine and Biology Society, 2014, pp. 3973–3976.
4. A. Ivorra and L. Becerra-Fajardo, "Flexible Thread-like Electrical Stimulation Implants Based on Rectification of Epidermically Applied Currents Which Perform Charge Balance," in Replace, Repair, Restore, Relieve – Bridging Clinical and Engineering Solutions in Neurorehabilitation SE - 67, vol. 7, W. Jensen, O. K. Andersen, and M. Akay, Eds. Springer International Publishing, 2014, pp. 447–455.
5. A. Ivorra and L. Becerra-Fajardo, "Wireless Microstimulators Based on Electronic Rectification of Epidermically Applied Currents: Safety and Portability Analysis," in 18th IFESS Annual Conference, 2013, pp. 213–216.

6. L. Becerra-Fajardo and A. Ivorra, “Proof of Concept of a Stimulator Based on AC Current Rectification for Neuroprosthetics,” in Congreso Anual Sociedad Española de Ingeniería Biomédica CASEIB, 2012, p. pp76.

International Conference Abstracts:

1. L. Becerra-Fajardo, R. Garcia-Arnau, and A. Ivorra, “Injectable Stimulators Based on Rectification of High Frequency Current Bursts: Power Efficiency of 2 mm Thick Prototypes,” in Conference on NeuroRehabilitation (ICNR2016), 2016, p. Accepted as oral presentation.

Acknowledgements

First, I will like to express my gratitude to Antoni Ivorra. He gave me the chance to do my master thesis project in neuroprostheses, and then offered me the possibility to continue with this challenging project for my PhD. He has been always available for scientific discussions and current events talks. Thanks for trying to teach me how to be a scientist, for your infinite patience, and for many laughs.

I will like to thank the Department of Information and Communication Technologies for the PRC fellowship and the two travel grants that I received. I am especially grateful with the members of the Secretariat. Their help in all the processes (academic, economic, contractual, etc.) has been exceptional. You make our lives easier.

I am also grateful with the people from the Biomedical Electronics Research Group for their enjoyable company, their help during difficult times, and their cigarette breaks.

I will like to acknowledge my friends: those that are here, those that are back home, and especially those that are wondering around the world. They have given me the support I needed during these years. Soccer, Gchat and Skype have been excellent scenarios to forget about my thesis project when I required it, laugh about our experiences and come back recharged of energy and good vibe. Thanks to Alex for giving me thousands of reasons to smile every day and for making me feel at home. Your support has been invaluable, and you are just awesome. Thanks to life for giving me such amazing people to travel with, and off course, for giving me the opportunity to do so. The world is ours.

Last but not least, I will like to express infinite gratitude to my family, who have supported all my decisions, who give me strength to carry on, and who give me the reasons to keep fighting for my dreams. Mom, this is my very best present for you. Gracias!

Biography

Laura Becerra-Fajardo was born in Bogotá, Colombia, in December 1983. She studied at Colegio Los Nogales and graduated in the summer of 2002. From 2002 to 2008, Laura studied Electronic Engineering at Universidad Nacional de Colombia, benefited with a PAES (best high school graduates 2002) scholarship. In 2007, Laura traveled to Argentina to study biomedical engineering insight courses as exchange student at Universidad de Buenos Aires. Between 2008 and 2010, Laura worked as Technology professional and coordinator in Maloka, and as research assistant at Pontificia Universidad Javeriana. In 2010, she started a M.Sc. in Biomedical Engineering at Universitat de Barcelona and Universitat Politècnica de Catalunya, benefited with a Colfuturo PCB scholarship. After graduation in 2012, she joined the Biomedical Electronics Research Group at Universitat Pompeu Fabra as a PhD student, benefited with a PRC fellowship.